Thin-film metal hydrides for solar energy applications

by

Trygve Tveiterås Mongstad

Submitted in partial fulfillment

for the degree of Philosophiae Doctor

June, 2012

Department of Physics

Faculty of Mathematics and Natural Sciences

University of Oslo

Series of dissertations submitted to the
Faculty of Mathematics and Natural Sciences, University of Oslo
No. 1217

ISSN 1501-7710

Cover: Inger Sandved Anfinsen.
Printed in Norway: AIT Oslo AS.

Produced in co-operation with Akademika publishing.
The thesis is produced by Unipub merely in connection with the
thesis defence. Kindly direct all inquiries regarding the thesis to the copyright
holder or the unit which grants the doctorate.

“We probably could have saved ourselves,
but we were too damned lazy to try very hard.
…and too damn cheap”

Kurt Vonnegut, 1991

Abstract

Thin-film metal hydrides may become important solar energy materials in the future. This thesis demonstrates interesting material properties of metal hydride films, relevant for applications as semiconducting materials for photovoltaic (PV) solar cells and for regulation of light using smart window technology.

The work presented here has comprised an experimental study, focusing on three different materials: Magnesium hydride (MgH_2), magnesium nickel hydride (Mg_2NiH_4) and yttrium hydride (YH_x). Reactive sputter deposition was used to prepare the metal hydride film samples. This synthesis method is relatively uncommon for metal hydrides. Here, the first demonstration of reactive sputtering synthesis for YH_x and Mg_2NiH_4 is given. Different challenges in forming single-phase, pure metal hydrides were identified: MgH_2 could not be deposited without 3-16% metallic Mg present in the films, and YH_x was found to react strongly to oxygen (O) during the deposition process. On the other hand, Mg_2NiH_4 films formed easily and apparently without major metallic clusters and with low O content.

Mg_2NiH_4 is a semiconductor with an optical band gap that is suitable for PV solar cells. This study has showed that films with promising electrical and optical properties can be synthesized using reactive co-sputtering of Mg and Ni. Using optical methods, the band gap for the as-deposited samples was estimated to 1.54-1.76 eV, depending on the Mg-Ni composition. The as-deposited films were amorphous or nanocrystalline, but could be crystallized into the high-temperature fcc struc-

ture of Mg_2NiH_4 using heat treatment at 523 K. The band gap of the crystalline films was 2.1-2.2 eV, depending on the composition.

A pronounced photochromic reaction to visible and UV light was observed for transparent yttrium hydride (T-YH_x) samples. The optical transmission was reduced when the samples were illuminated, and the original optical transmission was restored when the samples were kept under dark conditions. Photochromism at normal conditions had not been reported earlier for any metal hydride. In fact, the reactively deposited films of YH_x presented interest at many levels: Two electronic states could be obtained: black, conductive YH_x (B-YH_x), and transparent, insulating YH_x (T-YH_x). The T-YH_x samples were found to have a surprisingly high content of O, and the crystal structure of the compound differed slightly from earlier known structures in the Y-O-H system. The crystal structure of the T-YH_x films was very similar to the known structure of YH_2, but at the same time the optical and electronic properties resembled those known for YH_3.

Preface

This project was initiated at the Department for Solar Energy at Institute for Energy Technology (IFE), led by my supervisor Dr. Smagul Karazhanov, former head of department Dr. Arve Holt and researcher Dr. Alexander Ulyashin. A combination of experience with computer simulation of materials and research of new materials and concepts for solar cells germinated the idea of utilizing metal hydrides in semiconductor electronics, especially solar cells. Project funding for an experimental study was granted through the NANOMAT program of the Research Council of Norway, and the experimental work was commenced in 2007, two years before I started in my Ph.D. position in 2009.

The project was innovative, and in my work I experienced the pros and cons of starting up a new activity. I had one foot in the field of solar cell technology, one foot in the field of metal-hydride science and one foot in the field of thin-film deposition technology. It is awkward to advance on three feet, but this spread made me get to know a lot of interesting and talented people from different disciplines. It has been challenging and motivating to try to establish interest for this project, a project that has seemed to reside in the vacuum between the established research fields. I hope that our results and ideas will be used in the future both by researchers from our own group and from the international materials science community.

Contact

Science is about collaboration and communication. I am sure that many important details have been lost in the writing of this thesis, and I therefore encourage you as a reader to contact me if you have any questions,

comments or ideas concerning what I have presented here. If you cannot reach me in any other way, please try my permanent electronic address: *trygvetv@gmail.com*.

Acknowledgements

I have enjoyed the three years of my Ph.D. studies at IFE. I am grateful for the opportunity to work these years together with a great group of colleagues. Countless interesting discussions about results and methods have been rewarding for me and my academic development. However, it is on a personal level my colleagues have contributed the most – during the long and diverting coffee breaks, the "solar beers", social and work-related trips to different cabins and on the travels to several conferences in Norway, the rest of Europe and the USA. The scientific work has been hard, I have spent a lot of time working alone, so, without the social motivation of my colleagues it would have been a tough time.

I have had the pleasure of having help from as much as three supervisors. They have all helped me in different ways: Dr. Smagul Karazhanov, my main supervisor and a researcher at IFE Sol, has been a great inspiration for me with his ambitious and visionary view of science. I am deeply grateful for his permanent positive attitude, and for our almost daily scientific discussions. Dr. Charlotte Platzer-Björkman was my second supervisor. She had already worked in the metal hydride project at IFE Sol for half a year as a post doc. when I started in my position, and her experience gave me a flying start. We worked side-by-side during my first five months, before she went back to continue her work as a Lecturer at Uppsala University. Learning from her experimentalist way of thinking provided great help for me in my later work. I also gained from her sharp insight through several meetings in Uppsala, where she also brought me in contact with a number of world level researchers from Uppsala University. My third supervisor, Dr. Bjørn Hauback, from the

Physics department of IFE, is the most experienced of my supervisors. He has been particularly important for me in establishing contact with scientists in the international metal hydride research field. I also greatly appreciate his contributions to my scientific papers, which he helped lift to a higher level through extensive feedback in the writing process.

I would like to express my gratitude for the experimental collaborations I have had with Dr. Chang Chuan You and Dr. Josefine Selj, both from my own department. Each of these collaborations resulted in one of the scientific publications included in this thesis.

Apart from my supervisors and my colleagues at the Department for Solar Energy, I have enjoyed the sharing of experience with researchers at the Physics and Energy Systems departments at IFE. Our project has profited substantially from the knowledge from the metal hydride field that these two departments have obtained through decades of research practice. I would like to especially thank Dr. Jan Petter Mæhlen from Energy Systems, who took part in bi-weekly project meetings and participated in much of the experimental work I have presented in this thesis.

Collaboration with several international research partners has contributed to increased quality of the scientific work. Most importantly, I would like to thank the staff of the "Materials for Energy Conversion and Storage" group at TU Delft in the Netherlands. I thank Professor R. Griessen (VU Amsterdam) and Professor B. Dam (TU Delft) for interesting discussions and especially Professor Dam for welcoming me in the laboratories of his group at TU Delft. I greatly appreciated working together with H. Schreuders, L. Mooij and Y. Pivak in experimental work during my stay in Delft in October 2010. Further, I would like to thank

Dr. F. Cousin from Laboratoire Leon Brillouin in France for his help and suggestions with regards to neutron reflectometry. I also thank Professor G. Possnert and Dr. M. Wolff at Uppsala University for help with measurements of the composition of my samples.

Finally, I would like to thank my sweet and lovable wife, Leiry. She has taken me through the hard times, and helped me being confident about my own work and results in periods of doubt. We have also had many interesting discussions regarding my work, even with our very different academic backgrounds. In an academic discussion, it is not necessarily the relevance of the academic experience and the prior knowledge which determines the outcome, but rather the level of interest and dedication from the parts.

Trygve Mongstad
Kjeller, June 2012

Contents

List of abbreviations

AFM	Atomic force microscopy
B-YH_x	Black yttrium hydride
CE	Common era
DC	Direct current
DFT	Density functional theory
EDS	Energy dispersive X-ray spectroscopy
ESRF	European Synchrotron Radiation Facility
fcc	Face-centered cubic
GDP	Gross domestic product
GI-XRD	Grazing incidence X-ray diffraction
hcp	Hexagonal close-packed
IFE	Institute for Energy Technology
IPCC	Intergovernmental Panel on Climate Change
IR	Infrared
n-SLD	Neutron scattering length density
NR	Neutron reflectometry
NRA	Neutron reaction analysis
PV	Photovoltaic
RBS	Rutherford back-scattering
RF	Radio frequency
RGA	Residual gas analyzer
SEM	Scanning electron microscopy
SLD	Scattering length density
SMN	Centre for Materials Science and Nanoscience
SNBL	The Swiss-Norwegian Beamline (at ESRF, Grenoble)

TEM	Transmission electron microscopy
TU Delft	Delft University of Technology
T-YH_x	Transparent yttrium hydride
UiO	University of Oslo
UV	Ultraviolet
XPS	X-ray photoelectron spectroscopy
XRD	X-ray diffraction
XRR	X-ray reflectometry

List of publications

Paper I: C. Platzer-Björkman, T. Mongstad, S. Zh. Karazhanov, J. P. Mæhlen, E. S. Marstein and A. Holt. *Reactive sputtering of magnesium hydride thin films for photovoltaic applications.* Materials Research Society Symposium Proceedings 1210 (2010), 1210-Q03-15

Paper II: C. Platzer-Björkman, T. Mongstad, J. P. Mæhlen, A. Baldi, S. Zh. Karazhanov and A. Holt. *Deposition of magnesium hydride thin films using radio frequency reactive sputtering*. Thin Solid Films 519 (2011), 5949-5954.

Paper III: T. Mongstad, C. Platzer-Björkman, S. Zh. Karazhanov, A. Holt, J. P. Mæhlen, B. C. Hauback. *Transparent yttrium hydride films prepared by reactive sputtering*. Journal of Alloys and Compounds S509[1] (2011), S812-S816.

Paper IV: T. Mongstad, C. Platzer-Björkman, J. P. Mæhlen, L. P. A. Mooij, Y. Pivak, B. Dam, E. S. Marstein, B. C. Hauback and S. Zh. Karazhanov. *A new thin film photochromic material: Oxygen-containing yttrium hydride*. Solar Energy Materials and Solar Cells 95 (2011), 8-11.

Paper V: T. Mongstad, C. C. You, A. Thøgersen, J. P. Mæhlen, C. Platzer-Björkman, B. C. Hauback and S. Zh. Karazhanov. *$Mg_yNi_{1-y}(H_x)$ thin films deposited by magnetron co-sputtering*. Journal of Alloys and Compounds 527 (2012), 76-83.

Paper VI: J. H. Selj, T. Mongstad, B. C. Hauback and S. Zh. Karazhanov, *The dielectric functions and optical band gaps of thin films of*

[1] Proceedings of the 12th International Symposium on Metal-Hydrogen Systems, Fundamentals and Applications, Moscow 2010.

amorphous and cubic crystalline $Mg_{\sim 2}NiH_{\sim 4}$. Thin Solid Films 520 (2012), 6786-6792.

Paper VII: T. Mongstad, C. Platzer-Björkman, J. P. Mæhlen, B. C. Hauback and S. Zh. Karazhanov. *Surface oxide on thin films of yttrium hydride studied by neutron reflectometry*. Applied Physics Letters 100 (2012), 191604.

1 Introduction

1.1 The challenges related to energy

We are living on a marvelous planet. During its 4.55 billion years of history it has developed from a dusty chunk of rock-covered lava into a splendidly diversified planet consisting of different climates, eco-systems and with an incredible variation in life forms. The planet will continue this development, and, if we could look into the future, I am certain that anyone of us would be astonished about what we would see. This might be positive or negative, but the fact is that we are now entering a situation where the way we live our lives within the next decades and centuries can have ruinous consequences for the future of our planet, its variation of nature and its beauty.

We, the humanity, differ from all the other life forms on Earth in our extraordinary ability to develop knowledge and technology in a cumulative way. Through efficient communication and collaborative effort we use the knowledge of our ancestors and peers as building blocks for our own knowledge. This has proved extremely efficient, and has fueled a close to exponential growth in our knowledge and technology that in turn has led to an incredible increase in global population, economy, resource consumption and atmospheric emissions (Figure 1). At certain points in time, this development has been so aggressive that it has caused grave and permanent changes in localized eco-systems, like the ecological collapse on the Easter Island [1]. Over the last century, the human growth has been so strong that it has started to affect the eco-system of our entire planet [2].

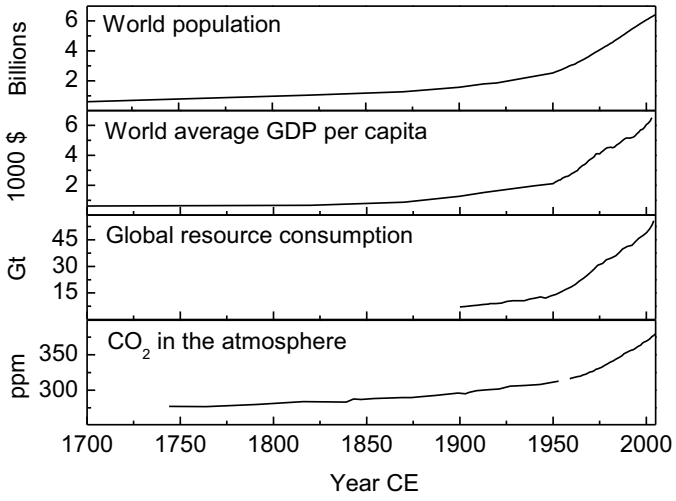

Figure 1 – Human growth and the consequences in the years 1700-2005 CE: World population (data from [3]), world average GDP per capita (data from [3]), total global resource consumption in Giga-tons (adapted from [4]) and CO_2 concentration in the atmosphere (data from [5]).

The main challenge for us who are living in the 21st century is now to stabilize the relation between the humanity and the planet. This means that we have to make a turn in our development towards more sustainable solutions with which the planet and humanity can co-exist for thousands or millions of years. If we continue on the track we are on now, the Earth will look totally different within a couple of centuries, with a serious reduction in the variety in life forms that exists today [2], [6], [7].

Some of the most grave and global consequences of human growth are today related to how we extract and use energy. We need energy for producing food, for transportation, for housing, for well-being and entertainment. This energy has since the start of the industrial revolution mainly been harvested from the Earth's buried resources of fossil energy.

These resources are limited, and they contribute to a substantial transport of carbon from below the ground and into the atmosphere. The release of carbon in the form of carbon dioxide (CO_2) and its accumulation in the atmosphere results in an increase in the average temperature of the surface and atmosphere of the Earth. There is today broad general agreement among climate-specialized scientists when it comes to the causes of global warming and the possible grave consequences of anthropogenic greenhouse gas emissions, thoroughly reviewed in the fourth assessment report of the Intergovernmental Panel on Climate Change (IPPC) [8], [9]. The problem of anthropogenic global warming is also closely connected to the environmental and economic consequences of the consumption and subsequently the depletion of the fossil fuel resources.

There are several ways to deal with the problems related to energy consumption. There are two main paths: The first is to change how we *produce* energy[2]; we need to find sources that can provide us with a secure supply for a long time without disturbing the balance of the planet and depleting the resources of future generations. The second is to change how we *manage* energy; we can reduce the amount of energy we use by calling attention to energy use and by implementing smarter solutions for energy management. The subjects of this thesis are related to both of these paths, and might thus lead to the development of new and more sustainable energy technology.

[2] Or to speak in more correct physical terms; How we convert energy. According to physical laws, it is not possible to produce energy "from nothing", we can only convert it from one form to another.

1.2 Electricity from solar cells

Renewable energy today covers 13.3 % of the world's energy consumption [10]. We need to achieve close to 100% coverage to secure sustainable existence of humanity. Fortunately, there is a great potential for development for all renewable energy sources, of which solar energy represents by far the greatest potential. The sunlight that reaches the Earth carries close to 10 000 times the energy that the global human civilization consumes at our current rate[3].

Solar energy can be harvested in the form of *heat* in solar thermal systems, or one can use PV solar cells to convert the solar energy into *electricity*. The latter is the most relevant for this thesis, so I will not go through more details on solar thermal energy. To understand the scientific motivation for this work, it is important to understand the basics of how a solar cell works. This understanding is based on the nature of light and how light is absorbed in semiconductors. I will therefore give a brief introduction to these two subjects, without going into details.

Light

The energy from the sun is irradiated to our planet in the form of electromagnetic waves – light. The energy of the light is divided in tiny packs of energy, called photons. The energy of each photon E_{ph} is directly related to the wavelength λ of the electromagnetic waves through the relation

[3] The human energy consumption rate is approximately 1.5×10^{13} W, or ~2 kW per person in average. The sunlight that hits the Earth is equivalent to the solar energy flux (the solar constant) S = 1361 W/m^2 times the area of the cross-section of the Earth $A = \pi R^2 = \pi$ (6371 km)^2: $S \times A = 1.7 \times 10^{17}$ W.

$$E_{ph} = h\nu = hc/\lambda,$$

where h is Plancks constant, ν is the frequency and c is the speed of light. Photon energy is generally measured in electron-volts, eV, and wavelength in nano-meters, nm. The photon energy, or the wavelength, also represents color, as demonstrated in Figure 2. A typical red laser pointer emits light with a wavelength of around 650 nm, corresponding to a photon energy of 1.9 eV. The sun radiates light containing photons of different energies going from the low-energy infrared (IR) to the high-energy ultraviolet (UV).

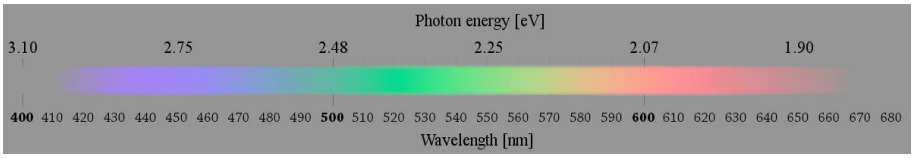

Figure 2 – A presentation of photon energy and wavelength for visible light of different colors. Adapted from [11].

Semiconductors

A semiconductor is a material that has an electrical resistivity in between that of a metal and that of an insulator. Semiconductor technology constitutes the core of almost all modern electronic devices, e.g. computers would have been impossible to produce in the way we know them without semiconductors. The semiconducting material most commonly used in electronics is silicon (Si).

A photon that hits a semiconductor will be absorbed in the material if it has more energy than what is known as the *band gap* energy, E_g, of the semiconductor. The absorbed energy of a photon will knock an electron out of its place and leave behind a *"hole"* in the lattice. In a solar cell, a configuration of different layers of semiconductors manages to

separate this electron from the hole and utilize the energy that it has received in an external electric circuit.

1.2.1 Solar cell technologies

All solar cell technologies are based on semiconductors. An introduction to the different solar cell technologies is available in many books – for an overview I recommend the book *Solar Cells: Materials, Manufacture and Operation* by Markvart and Castaner [12].

Silicon solar cells

The Si wafer-based solar cell was the first solar cell technology to be developed with a reasonable efficiency, and is still the dominating technology in commercial solar cells. The manufacturing process starts with the purification of Si from quartz. High-purity Si is then cast into large blocks or a large single crystal is pulled from a melt, and subsequently cut in thin wafers of dimensions of typically 15 × 15 cm^2 with a thickness of around 200 μm. The solar cell is produced from the wafer by going through a multi-step industrial process into a final solar cell. The most important steps are emitter doping, antireflection coating, passivation and metallization. A sketch of a typical Si solar cell is showed in Figure 3(a).

Thin-film solar cells

The most important thin-film PV technologies are copper-indium-gallium-selenium(sulfur) (CIGS), cadmium telluride (CdTe) and amorphous silicon (a-Si). The production process of thin-film solar cells differs from the silicon solar cells in that all the active materials are deposited onto a substrate, in very thin layers of only a few μm. The substrate itself is normally not an active component in the structure. As an exam-

ple, an outline of a typical CdTe solar cell is given in Figure 3(b). The thin-film technologies consume much less material than wafer-based solar cells because the semiconductor layers are about 100 times thinner, and the free choice of substrate and deposition method leaves room for substantial savings in the production. Therefore, the CdTe technology was first to cross the "magic" cost limit of 1 $\$/W_{peak}$ in 2009 [13], and thin-film solar cells are today cheaper than Si wafer based solar cells[4].

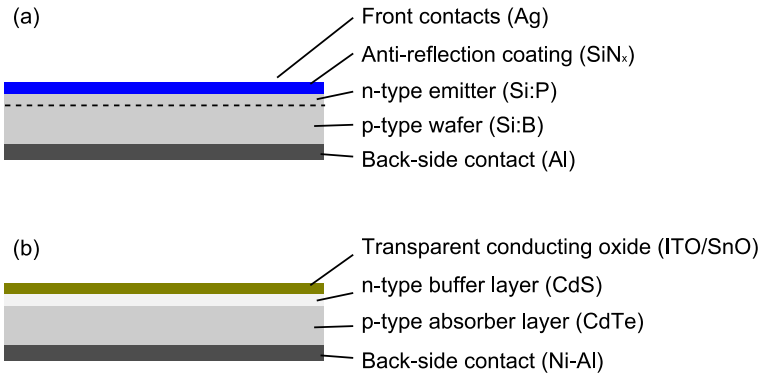

Figure 3 – Outline of the cross-section of two different solar cell technologies. (a) A typical wafer-based Si solar cell and (b) a typical thin film CdTe solar cell.

Challenges for the existing PV technologies

Even though the existing technologies for solar cells have proved to be strong and there has been an incredible growth in the production and sales of solar cells over the last decade, there are some challenges for the

[4] According to *Solarbuzz Module Pricing* March 2012 update, the lowest retail prices for multi-crystalline Si solar cell modules was 0.78 €/Wp, comparing to 0.62 €/Wp as the lowest retail price for thin-film modules. Because the efficiency of thin film solar modules is generally lower, the cost of the total system may draw a different picture and Si solar cells have therefore preserved a high market share.

existing technologies. Wafer-based Si solar cells consume a lot of material due to the unnecessary thick wafers, and around half of the material is wasted in the casting and sawing processes. For the thin-film technologies of CIGS and CdTe, the low abundance and extraction rates of the elements In and Te are expected to put a limit on the production of 13-38 GW_p/year for each technology within the next 10 years[5] [14]. Amorphous silicon solar cells suffer from severe photo-degradation and other factors which have so far limited the attainable efficiency of this technology. The record efficiencies for Si, CIGS, CdTe and a-Si solar cells under solar illumination are currently 25.0%, 19.6%, 16.7% and 10.1%, respectively [15]. The efficiencies of commercial solar modules are substantially lower than these numbers.

Multi-junction solar cells

The maximum theoretical efficiency of a solar cell based on a single semiconductor is given by the band gap of the semiconductor. This limit is known as the Shockley-Queisser limit [16]. Figure 4 shows the efficiency limit for solar cells under sunlight illumination, as a function of the band gap of the light-absorbing semiconductor. Several concepts for going beyond this limit have been suggested and some have also been demonstrated. The most well-established is the multi-junction solar cell, also called tandem solar cell, which combines several layers of semiconductors with different band gaps. Each layer absorbs a certain wavelength range of the sunlight. The record efficiency for multi-junction solar cells, under concentrated sunlight, is currently 43.5% [15]. Such high

[5] In 2011, the total installations of new solar cells amounted to a capacity of 27 GW_p. With a growth rate of 30% per year, the total demand for installations in 2020 will be at 300 GW_p.

efficiency cells are however extremely costly due to high processing costs and expensive materials. High-efficiency multi-junction solar cells are today based on Ge/InGaAs/GaInP or similar material stacks.

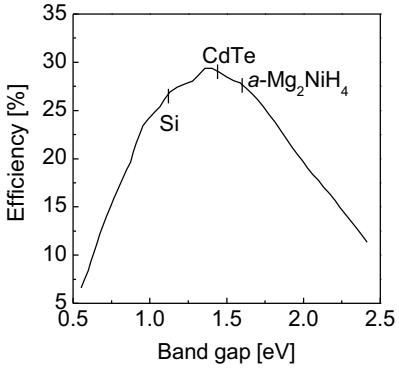

Figure 4 – Solar cell efficiency limit for the solar spectrum (Air Mass 1.5) as a function of the band gap of the light-absorbing semiconducting material. The band gaps of Si, CdTe and a-Mg_2NiH_4 have been indicated. Figure adapted from [17], adding the band gap of a-Mg_2NiH_4.

1.3 Energy saving with smart windows

In the EU and USA, energy consumption in buildings accounts for close to 40% of the total energy consumption [18]. The energy consumption in buildings is steadily increasing, especially in more southern countries. In all types of buildings and all environments, most of the energy which is consumed in buildings is used for heating, ventilation, cooling and indoor lightning.

One way of controlling the heat transfer and natural lightning in buildings, and thereby reduce the energy consumption, is to deploy smart windows. Smart windows make use of *chromogenic materials*, materials that allow variation of the transmittance of light and IR radiation. Studies

have shown that smart windows based on such technologies outnumber the energy performance of static windows that only make use of static spectrally selective coatings and insulation layers [19]. It is especially in hot climates with high needs for cooling during daytime that smart windows can save substantial amounts of energy, by reflecting or absorbing solar energy that would otherwise excessively heat the building.

Different chromogenic reactions have the potential to be useful in smart windows:

- *Photochromism* [20], changing in the optical properties as a response to illumination. Photochromic windows would typically reduce the optical transmission when sunlight is shining directly on the window, while maintaining the view under indirect daylightning and in dark. The principle of a window with a photochromic film applied for optical regulation is demonstrated in Figure 5.
- *Thermochromism* [20], changing the optical properties as a response to temperature. Thermochromic materials can react to hot conditions by reducing optical transmission, while permitting passive solar heating and visual view at low temperatures.
- *Electrochromism* [21], changing the optical properties as a response to an applied electric field. The optical properties can be controlled automatically or manually.
- *Gasochromism* [22], an optical reaction to exposure to certain gases. Gasochromic materials could in principle work similarly as the electrochromic materials.

Electrochromic and gasochromic materials are the most versatile because they can be controlled intentionally. On the negative side for

electrochromic and gasochromic materials, the installation of the windows is complicated because of the need for a connection to control infrastructure for operation, and they are little worth if not operated in the right manner.

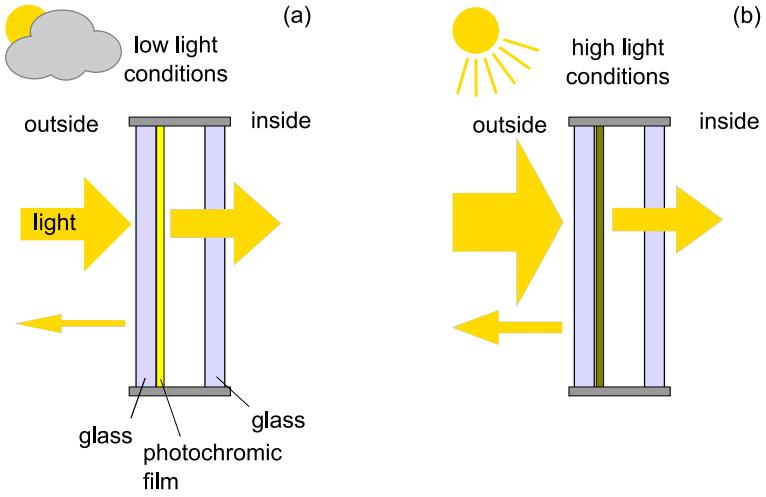

Figure 5 – The working principle of a double layer glass window with a photochromic film under (a) low and (b) high light conditions. The light transmission and reflection is demonstrated by the weight of the arrows.

1.4 The materials – metal hydrides

Metal hydrides are compounds formed by reactions of metals with hydrogen (H). A wide variety of metal hydrides have been demonstrated, comprising almost all metals and many different metal alloys. The metal hydrides have over the last decades received substantial attention due to the possibility of reversibly storing H with high density in metals. This could be a favorable way of storing energy in a future society where H_2 might become a common energy carrier. H_2 is promising as an energy carrier for example for transportation, because it has approximately three times higher chemical energy per mass compared to gasoline [23], and

because water is the only combustion product. One of the challenges for H_2 as an energy carrier is the storage, as the amount of H_2 necessary for driving 400 km in a car would occupy around 45 m^3 at atmospheric pressure [23]. Hydrogen storage in metal hydrides is a solution to reduce this volume [24], and well-known metal hydrides have a volumetric H density that is even higher than that of liquid H_2 [23]. It is also relevant to consider metal-hydride-based energy storage systems for stationary purposes, especially in systems based on intermittent renewable energy sources like solar or wind energy [25].

There are large variations in the physical and chemical properties of metal hydrides. There is also normally a large difference in the properties of the parent metal and the metal hydride. The crystal structure is often changed, and other material properties can be completely different. The strongest demonstration of the great difference in optical properties is the invention of the metal hydride switchable window, that was reported by Huiberts et al. in 1996 [26] (See Figure 8, page 27).

In this work, we have used reactive sputter deposition to synthesize films of three different types of metal hydrides: MgH_2, Mg-Ni-H and YH_x.

1.4.1 Magnesium hydride

Magnesium hydride, MgH_2, is one of the classics among the metal hydrides. It is considered one of the most interesting materials for hydrogen storage, because of the high gravimetric capacity of 7.6 wt% H in MgH_2 and the possibility of absorbing and desorbing H reversibly [27]. However, the problems of high operation temperature and slow kinetics has proved a difficult barrier to pass for hydrogen storage in MgH_2 [27]. The problems can be circumvented by nano-structuring and adding catalytic

agents, and one of the currently largest commercial projects within solid-state H_2 storage is using MgH_2 [28].

The electronic band gap of MgH_2 is reported to be 5.6 eV [29], which means that it should be insulating and transparent to visible light. Transparent films have indeed been obtained when hydrogenating Pd-capped Mg [29], but *in-situ* deposition by activated reactive evaporation was reported to give films that only were partly transparent for visible light [30]. This discrepancy was explained by the presence of approximately 10% of metallic Mg in the reactively deposited film [30].

Table I summarizes the structural, thermodynamic and electrical properties expected for the Mg-based compounds that are considered relevant for the current work.

1.4.2 Magnesium nickel hydride

Magnesium nickel hydride (Mg_2NiH_4) is another well-known metal hydride. It is considered for hydrogen storage because it can store 3.6 wt% H reversibly and the hydrogenation-dehydrogenation reactions are faster and can be operated at lower temperatures than MgH_2 [27]. Still, the hydride in its pure form is considered too stable to be useful in reversible hydrogen storage applications. In 2001, Richardson et al. demonstrated that this hydride also could be suitable for application in smart windows [31].

Table I – Key parameters at standard conditions of relevant Mg-based compounds

	Magnesium	**Magnesium hydride**	**Magnesium oxide**	**Magnesium hydroxide**
Formula	Mg	MgH_2	MgO	$Mg(OH)_2$
Crystal structure	Hexagonal $P6_3/mmc$ a = 3.21 Å c = 5.21 Å [32]	Tetragonal $P4_2/mnm$ a = 4.52 Å c = 3.02 Å [33]	Cubic Fm-3m a = 4.21 Å [34]	Trigonal $P3m1$ a = 3.14 Å c = 4.77 Å [34]
Formation enthalpy [kJ/mole Mg]	0	-75 [35]	-602 [35]	-925 [35]
Electronic state, E_g	Metallic	Insulating, 5.6 eV [29]	Insulating, 7.8 eV [36]	Insulating, 6 eV [37]

Crystalline Mg_2NiH_4 is found in two different structures: The low-temperature (LT) structure is monoclinic [38]. It is often divided into two categories, the LT1 and the LT2. The LT2 phase is a modification of the LT1 phase with micro-twinning or stacking faults [38]. It is a minor change in the structure, but there is a large difference in optical and electrical properties of the two phases [39]. If the hydride is heated up to temperatures above 237 ºC, it undergoes a transition to the HT structure. The HT structure is face centered cubic with a lattice parameter of 6.507 Å [40]. Powder samples that are cooled from the HT structure go to the micro-twinned LT2 structure below the transition temperature. The LT1 structure is only obtained for samples that have been hydrogenated and kept below the transition temperature.

Thin films of Mg_2NiH_4 are found to behave slightly different structurally. If synthesized below the transition temperature they exhibit an amorphous structure. Both *in-situ* deposited films [41] and *ex-situ* hydrogenated films [42] are found to be amorphous. Thin-film samples hydrogenated above the transition temperature exhibit a HT cubic structure, and they remain in the HT structure also after cooling to room temperature [39].

There are various reports of the band gap of Mg_2NiH_4, as discussed in Paper VI, but most of the reports are close to the original report of 1.68 eV which was claimed for both the HT and the LT phase by Lupu in 1987 [43]. Paper VI in this thesis discusses the band gap of the two thin-film phases of Mg_2NiH_4 in more detail, and it seems clear that the band gaps of both the crystalline phases and also the amorphous thin-film state are in the range 1.5 – 2.2 eV.

In the discussion of the results in this thesis, it is useful to use the following abbreviations for the various forms of magnesium nickel hydride:

- Mg_2NiH_4: The stoichiometric compound of magnesium nickel hydride with 2.0 Mg and 4.0 H per Ni.
- $Mg_{\sim 2}NiH_{\sim 4}$: Magnesium nickel hydride with any composition yielding a semiconductor with a band gap of 1.5-2.2 eV.
- Mg-Ni-H: Any combination of Mg, Ni and H.
- a-Mg_2NiH_4: Amorphous thin-film Mg_2NiH_4.
- c-Mg_2NiH_4: Crystalline fcc thin-film Mg_2NiH_4.

Table II summarizes the structural, thermodynamic and electrical properties expected for the Mg-Ni-based compounds that are considered relevant for the current work.

Table II - Key parameters at standard conditions of relevant Mg-Ni-based compounds*

	Nickel	**Magnesium nickel**	**LT-magnesium nickel hydride**	**HT-magnesium nickel hydride**
Formula	Ni	Mg_2Ni	Mg_2NiH_4	Mg_2NiH_4
Crystal structure	Cubic *Fm*-3*m* *a* = 3.52 Å [32]	Hexagonal $P6_222$ *a* = 5.19 Å *c* = 13.21 Å [44]	Monoclinic *C*2/*c* *a* = 14.34 Å *b* = 6.40 Å *c* = 6.48 Å *β* = 113.52° [45]	Cubic *Fm*-3*m* *a* = 6.51 Å [40]
Formation enthalpy [kJ/mole Ni]	0	-52 [46]	-52 (2Mg + Ni) + -128 (Mg_2Ni + $2H_2$) [47]	
Electronic state, E_g	Metallic	Metallic	Semiconducting, 1.7 eV [43]	Semiconducting, 2.2 eV [39]

*For magnesium, see Table I.

1.4.3 Yttrium hydride

Yttrium hydride is most well-known from the invention of the metal hydride-based switchable window [26] (see Figure 8, page 27). It is generally considered to belong to the class of the rare-earth metal hydrides [48]. At room temperature and atmospheric pressure, two phases of yttrium hydride can be obtained: The dihydride (YH_2) and the trihydride (YH_3). Whereas the Y metal as well as YH_2 is conductive and non-transparent, YH_3 is a semiconductor with a band gap of 2.6 eV and therefore partly transparent to visible light [26]. When prepared in thin-film form capped by a thin layer of Pd, the H can be loaded and unloaded re-

versibly and the optical state of the YH_x film can be controlled by regulating the H_2 pressure in the environment of the sample.

During the H loading process, YH_x films go through two structural transitions. Y metal has a hcp lattice, YH_2 has a fcc lattice and YH_3 has a hcp lattice again. Through this loading process, also the optical and electrical properties are dramatically changed. The structural, optical and electrical properties have been analyzed to great detail in a paper of van Gogh et al. [49]. The very similar hydride of La does not demonstrate such a structural change when going from LaH_2 to LaH_3, although the optical and electrical change corresponds to what is observed for Y. It has also been shown that Y films doped with quantities of Mg ([Mg]/[Y] $\geq$ 0.1) demonstrate an optical change without the fcc-hcp structural transition [50]. It therefore appears that the optical transition is not necessarily related to the structural transition in YH_x.

In the discussion of the results on yttrium hydride, it proves useful to define the following terms:

- YH_x: Yttrium hydride. Any combination of Y and H. In the discussion this also includes combinations where O is incorporated.
- B-YH_x: Black YH_x. Yttrium hydride samples that are in the low-reflective and metallic state that is typically observed for YH_2.
- T-YH_x: Transparent YH_x. Yttrium hydride samples with a band gap close to 2.6 eV. The amount of O incorporated in the sample can be substantial[6], but the crystal structure and optical and electrical properties resemble that of YH_3 rather than that of Y_2O_3 or $Y(OH)_3$.

[6] In Paper IV, this type of sample is referred to as «oxygen-containing yttrium hydride».

Table III summarizes the structural, thermodynamic and electrical properties obtained from literature for the Y-based compounds that are considered relevant for the current work.

Table III - Key parameters at standard conditions of relevant Y-based compounds

	Yttrium	**Yttrium dihydride**	**Yttrium trihydride**	**Yttrium oxide**	**Yttrium hydroxide**
Formula	Y	YH_2	YH_3	Y_2O_3	$Y(OH)_3$
Crystal structure	Hexagonal *P*63/*mmc* *a* = 3.65 Å *c* = 5.73 Å [51]	Cubic *Fm*-3*m* *a* = 5.21 Å [48]	Hexagonal *P*63/*mmc* *a* = 3.67 Å [48]	Cubic *Ia*3 *a* = 10.60 Å [52]	Hexagonal *P*63/*m* *a* = 6.25 Å *c* = 3.54 Å [53]
Formation enthalpy [kJ/mole Y]	0	-228 [48]	-228 ($Y + H_2$) + -40 ($Y + \frac{1}{2}H_2$) [54]	-953 [35]	-1472.3 [55]
Electronic state, E_g	Metallic	Metallic	Semiconducting, 2.6 eV [49]	Insulating, 5.6 eV [56]	Semiconducting, 3.05 eV [57]

1.5 The synthesis method – reactive sputter deposition

Magnetron sputter deposition is a method that is widely applied in materials science and industry for deposition of a range of different thin films. The method is suitable for large area deposition and can be incorporated in industrial production lines. The chamber in a magnetron sputter is during deposition filled with argon gas at low pressures, typically 0.1-10 Pa.

When a certain electric field is applied over the gas, it will ionize and form a plasma. The charged Ar+ ions will then be accelerated by the electric field and collide with the surface of the target sputter away atoms from the target which can be deposited on an opposite surface.

When a gas that is capable of reacting with the sputtered atoms from the target is added to the Ar gas in the deposition chamber it is called reactive sputtering. Addition of a reactive gas during the deposition can give substantial changes to the chemical and physical processes in the chamber. A review of the reactive sputtering process and a few commonly deposited materials is given in the book "Reactive sputter deposition" edited by Depla and Mahieu [58]. The most well-known example of reactive sputtering is the addition of O_2 gas to the chamber in order to obtain metal oxide films from metallic targets. This way, for example stoichiometric films of Al_2O_3 can be obtained by sputtering from an Al target [59]. Reactive sputtering with H_2 is less common, but is routinely applied for example in deposition of hydrogenated amorphous silicon and microcrystalline silicon [60] and has been demonstrated for several metal hydrides (see page 21).

Metal hydrides can be synthesized in a range of different ways. The most common synthesis techniques produce powders of metal hydrides. Thin-film metal hydrides have received comparatively little attention. The standard synthesis method for thin-film metal hydrides is by hydrogenation of Pd-capped metal films, as demonstrated in Figure 6(a). This method was suggested by Pick et al. in 1979 [61]. Also uncovered metal films can be hydrogenated, but might require high temperatures and long loading times. Long loading times have indeed been found necessary to form Mg_2NiH_4 films in this way [39], [42]. On the other hand, rare-earth

dihydrides form readily even when no H_2 gas is intentionally added, as observed for early studies of thin-film deposition of rare-earth elements [62] and more recently under deposition of Y using pulsed laser deposition (PLD) [63].

In this work we preferred to avoid the Pd cap because of two reasons. Firstly it complicates electrical and optical measurements because of the high electrical conductivity and high optical opacity of Pd, and secondly because Pd is a precious metal that should be avoided in the context of low-cost solar energy technology.

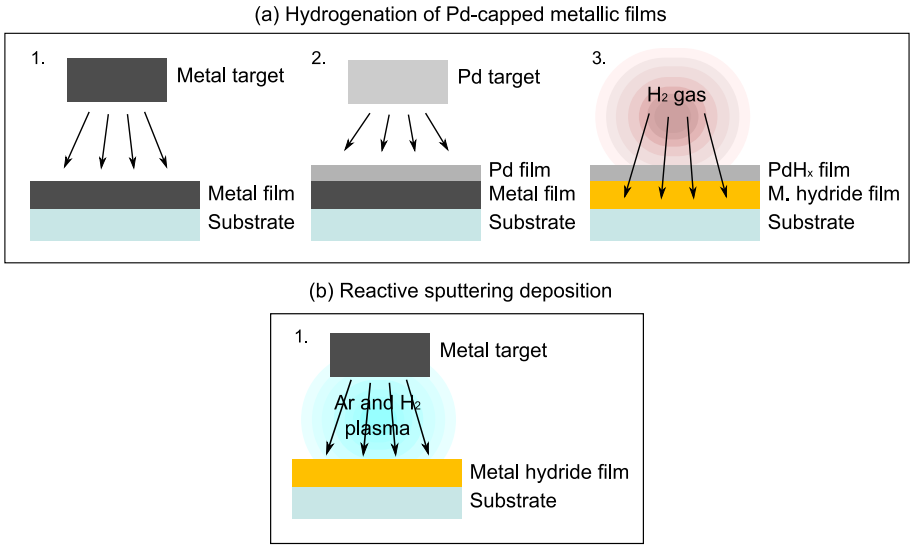

Figure 6 – Conceptual drawings demonstrating synthesis methods for metal hydride films. (a) The commonly applied synthesis method of hydrogenation of Pd-capped metallic films. (b) Single step formation of metal hydride films by reactive sputter deposition.

There are mainly two methods for *in-situ* deposition of metal hydrides avoiding the Pd cap layer: reactive evaporation and reactive sput-

tering. Reactive evaporation is the deposition of metals from a metallic evaporation cell in a reactive gas atmosphere. Under *activated* reactive evaporation, a source of atomic H [64] is used to increase the reaction rate with H. Activated reactive evaporation has been demonstrated for MgH_2 [30] and Mg_2NiH_4 [41], whereas reactive evaporation with molecular H_2 has been demonstrated for TiH_2 [65] and single-crystalline YH_2 films grown on W(110) substrates [66].

The concept of direct *in-situ* formation of metal hydride films by reactive sputter deposition is demonstrated in Figure 6(b). Reactive sputter deposition to achieve direct growth of metal hydride films *in-situ* has been relatively little explored. The earliest reports of reactive sputter deposition of metal hydrides was in the 1990's, for TiH_x [67–69] and LiH [70]. More recently there have been reports of reactive sputter deposition of $GdMgH_5$ [71], $NaAlH_4$ [72], CaH_2 [73] and NaH [73]. There have also been recent reports of reactive sputter deposition of MgH_2 [74], [75]. ErH_3 films have been synthesized by a similar technique, reactive ion beam sputter deposition, using a plasma source to generate atomic H [76]. Reactive sputter deposition of Mg_2NiH_4 or YH_x had not been reported of before the publication of Paper V and Paper III in this thesis.

In the reports of reactive sputter deposition of metal hydrides, a H_2 mixing ratio of 10-50% in the Ar process gas is generally used to obtain growth of hydride films. O contamination of films is a common issue with films deposited by this method, reported for TiH_x [68], LiH [70] and MgH_x [75] films. Another issue is the presence of metallic particles in the hydride matrix of the films, specifically observed for MgH_x [74], [75] and $NaAlH_4$ [72]. It has also been reported that stoichiometric TiH_2 films are difficult to obtain [69].

1.6 Metal hydrides for solar energy applications

Several applications of metal hydride films with regards to solar energy have been suggested, but no technological application has yet been commercialized. The exception is the use of PV solar panels to charge nickel-metal hydride batteries, which cannot be considered relevant in the context of this thesis.

1.6.1 Semiconducting metal hydrides for solar cells

Since the discovery of the metal hydrides, it has been known that the electrical properties of a metal hydride generally are very different from that of the metal itself. Many of the metal hydrides are now known to be semiconducting. However, it was not until in 2007 that hydride-based semiconductor electronics was suggested [77–79]. Semiconductors are the core of modern electronics and many different classes of semiconducting compounds[7] have been developed for different purposes, but metal hydride semiconductors had received little attention. There might be many reasons for that, the most important may be that metal hydrides are generally found to be chemically unstable under normal conditions and thus difficult to work with.

For pure metal hydrides in powder form, one can have an idea about the electrical properties just by visual observation. Hydride powders with white appearance are insulators. Yellow, orange, red or brown powders are semiconducting with a band gap in the visible range of light. Black or silvery powders are metallic or low-band gap semiconductors.

Insulating or semiconducting metal hydrides can be called non-metallic, which sounds contradicting, but here "non-metallic" refers to

[7] Comprising oxides, nitrides, sulfides, etc. See e.g. the book "Oxide and nitride semiconductors" (2009) by Yao and Hong.

the electronic state and not to the chemical composition of the compound. There is a long list of hydrides that are non-metallic. Karazhanov et al. has given a survey that demonstrate the band gap found by density functional theory (DFT) for 72 such hydrides [80], which may be candidates for so-called *hydride electronics*. Considering all possible alloys that form hydrides, the complete list of non-metallic hydrides is probably substantially longer. Several non-metallic metal hydrides are probably not even thought of yet.

The idea of hydride electronics is to use semiconducting metal hydrides as the active layer in semiconducting electronics. In a PV solar cell, this would mean to use films of semiconducting metal hydrides e.g. as light absorbing materials that generate electricity through separation of excited electron-hole pairs. Figure 7 gives a simple demonstration such a structure.

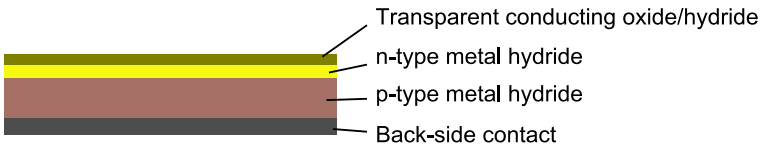

Figure 7 – A concept sketch of a metal-hydride based solar cell.

Requirements for PV materials

A material for PV solar cells has to be semiconducting with a band gap close to 1.4 eV (see Figure 4), it has to have suitable electrical transport characteristics and it should be stable in operation in a PV device under realistic conditions for more than 20 years. Depending on the type of device, it should also be possible to control the doping of the material by incorporating controlled levels of impurities acting as p- or n-type doping. Regarding these requirements, there is relatively little information

available in the literature concerning metal hydrides. Generally, the most well-known of these parameters are the band gap and the chemical stability in vacuum. Based on the available information in literature, we therefore decided to work on Mg_2NiH_4. This hydride has a band gap within the range that is interesting for solar cells, and the chemical stability is reasonably high. DFT studies earlier performed in our group had also showed that the electronic band structure of Mg_2NiH_4 is similar to that of Si [81], which was considered promising with regards to the electronic transport mechanisms. However, there might well be metal hydrides that are semiconducting and have even more suitable characteristics than Mg_2NiH_4, but are rarely discussed because of low relevance for hydrogen storage and smart windows. For example the closely related hydrides Mg_2CoH_5 and Mg_2FeH_6 have demonstrated optical properties [82] which suggest that the band gaps of these hydrides are within the range that is interesting for solar cells.

There is relatively little information available on the electrical properties of semiconducting metal hydrides. However, the invention of the metal-hydride based smart window spurred some attention on electrical properties of thin-film metal hydrides that are relevant for PV applications. In addition to band gap estimations by optical methods, the electrical conduction mechanisms of YH_x [83] and Mg_2NiH_x [84] films have been investigated by measurements of the Hall effect. n-type conductivity was reported for both these hydrides, where H vacancies appear to act as electron donors. Interestingly, an early report on the conductivity mechanisms in CeH_x reported of p-type conductivity [85].

Why metal hydrides for solar cells?

Many materials are already demonstrated to work well in PV applications. However, as already mentioned, there are some concerns with the commercial PV technologies of today. For thin-film solar cells there is an issue with the limited availability of the constituent elements In and Te. Si, on the other hand, is abundantly available in the Earth's crust and there is no practical limitation on the extraction rate. However, wafer-based Si solar cells are at present priced higher than thin-film solar modules. So, if low-cost thin-film solar cells with high efficiency could be manufactured from abundantly available materials based on e.g. Mg, Ni and H, that would present very high interest for future developments in solar cells for electricity generation.

In a longer perspective, it is probable that more sophisticated technologies with higher efficiency will emerge on the solar cell market. The most promising technology is the multi-junction solar cell [86], which depends on having suitable materials with different band gaps. If reasonable solar cell efficiencies in metal-hydride based solar cells can be demonstrated, the wide range of band gaps available within the class of metal hydrides might open up new opportunities of such high-efficiency technologies. It is also demonstrated that the band gap of metal hydrides can be engineered by controlling stoichiometry and crystal structure: For Y-La trihydride alloys, the band gap can be controlled by the La:Y ratio, going from 1.9 eV for pure LaH_3 to 2.6 eV for pure YH_3 [49]. For Mg_2NiH_4, the band gap is determined by the crystal structure, the crystal structure can be controlled by synthesis temperature [39], [42] and, for powder samples, by mechanical pressure [87]. The band gap of Mg_2NiH_4

can also be controlled by the Mg:Ni ratio, for which band gap tuning from 1.5 eV to 2.0 eV has been reported earlier [88].

Surface passivation of Si

In Si solar cells, H is known to be able to passivate electronically active defects and impurities in the bulk of a Si crystal [89]. H also plays a role in chemical passivation of the interface of the Si wafer with the surrounding materials as e.g. SiO_2 [90]. Good passivation provides longer lifetime of excited charge carriers, a solution to one of the main challenges for Si solar cells [91]. Therefore, it might be beneficial to combine Si with metal hydrides as pure passivation layers. The abundance of H in metal hydrides might also be beneficial in applications where one combine Si with other semiconductors, as in multi-junction or hetero-junction solar cells.

1.6.2 Chromogenic metal hydrides

In 1996, Huiberts et al. reported a fascinating optical transition in Pd-capped Y and La films that were exposed to H_2 gas [26]. The H_2 gas dissociated at the surface of the catalyzing Pd cap-layer, and diffused into the Y or La film which when going from dihydride to trihydride went through a metal-insulator transition. The visual appearances of the three optical states are displayed in Figure 8. The optical state of the film could be controlled and varied from metallic reflecting to transparent by variation of the H_2 pressure in the surrounding container. In the following years, substantial work on the properties of YH_x and LaH_x films and the electronic structure of the compounds was done by many research groups.

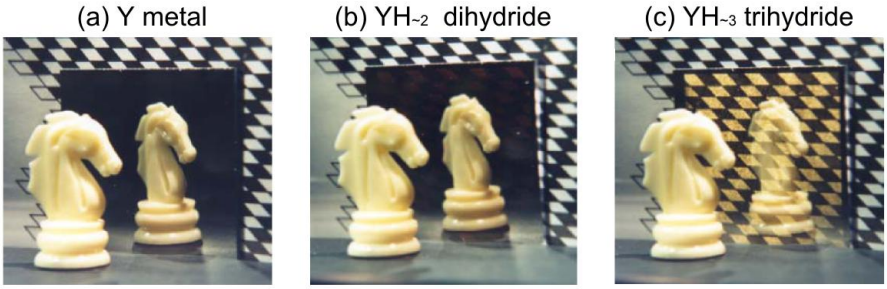

Figure 8 – The H_2-induced optical transition of Pd-capped YH_x films: (a) The reflecting metallic Y film prior to hydrogenation, (b) the dihydride state (c) the transparent trihydride state. Pictures from Huiberts et al., 1996 [26].

In 2001, Richardson et al. demonstrated that the optical switching could also be obtained with Mg-Ni films capped by Pd [31]. This was considered an advantage as Mg and Ni are more abundant elements than the rare earths, and it extended the material choice for further development of the metal-hydride-based smart windows.

The gasochromic reaction with H_2 gas being unpractical for commercial applications, solid-state alternatives were later developed. All-solid-state smart window devices have been demonstrated both for rare-earth-based hydrides [71] and Mg-Ni hydrides [92]. Presently, the metal-hydride smart window research gravitates around the group of K. Yoshimura at AIST in Japan, where they are developing new alloys [93], [94] and testing the materials under realistic conditions [95], [96]. There is also current interest in utilizing the optical switching of metal hydrides in optical H_2 sensors [97], [98].

Photochromism in yttrium hydride

In a high-pressure experiment reported in 2007, Ohmura et al. reported on the observation of a photochromic reaction in transparent YH_x samples at high pressures [99]. The effect was seen at pressure of 5.8 GPa (57000 × atmospheric pressure), and a coexistence of fcc and hcp YH_x was observed at this pressure. No photochromic effect was observed for the pure hcp YH_x at lower pressures. The light used to trigger the photochromic reaction was a laser with a wavelength of 488 nm, and a few seconds of illumination was sufficient to cause a pronounced change in the optical properties of the sample. The intensity of the laser at the sample was estimated to 10^5 W/cm^2, corresponding to one million times the typical intensity of solar illumination. They reported of a 0.11% lattice contraction of the fcc phase during the photochromic reaction.

A relevant finding, which was not directly presented as a photochromic effect, was the persistent photoconductivity as a result of UV illumination that was observed and reported by Hoekstra et al. [100]. They reported that UV illumination at temperatures < 1 K increased the electric conductivity of hcp YH_x samples, and the increased conductivity persisted at temperatures of up to 200 K.

1.6.3 Other solar energy applications of metal hydrides

This thesis focuses on the development of metal hydrides for solar energy applications in smart windows and PV solar cells, but there have been some other suggestions that are worth to mention in the context of metal hydrides and solar energy:

- *Smart solar collectors*: For many metal hydride film systems, three main optical states exist: Reflective for low H content, optically absorbing and black in appearance for intermediate H content and

transparent for high H content. In a paper published by Borsa et al. in 2006, it was suggested to take advantage of the reflective to black switching in Mg-Ti-H films with low and intermediate H content in order to regulate the temperature in solar thermal collectors [101]. Such a regulation mechanism could allow the use of materials with low heat stability such as plastics in the solar collector.

- *Energy storage*: It is obviously relevant to deploy metal hydrides in energy storage for PV solar cells using Ni-MH batteries and eventually metal-hydride-based H_2 storage. As mentioned earlier, this is not considered relevant for this thesis. More relevant is the report of Licht et al. from 1999, of a highly inventive concept of combining a AlGaAs/Si/metal hydride multi-junction solar cell with an integrated metal hydride energy storage layer [102], [103]. A schematic representation of the device is presented in Figure 9. Such a device would be able to deliver electricity even under dark conditions, depending on the energy deposited in the metal hydride layer. An overall conversion efficiency of 18.2 % was reported for this type of device.
- *Transparent conducting films*: Transparent conducting films are used as transparent electrodes in an increasing number of technological applications such as displays and thin-film PV solar cells. It has been suggested that wide band gap metal hydrides could have a potential as transparent conducting films, and the case of Si-doped AlH_3 has been studied in a DFT simulation study [78]. A transparent conducting material based on $Mg(OH)_2$ with large amounts of C has been reported recently in an experimental study [104]. This

material is possibly the first non-oxide transparent conducting compound that has been demonstrated [105].

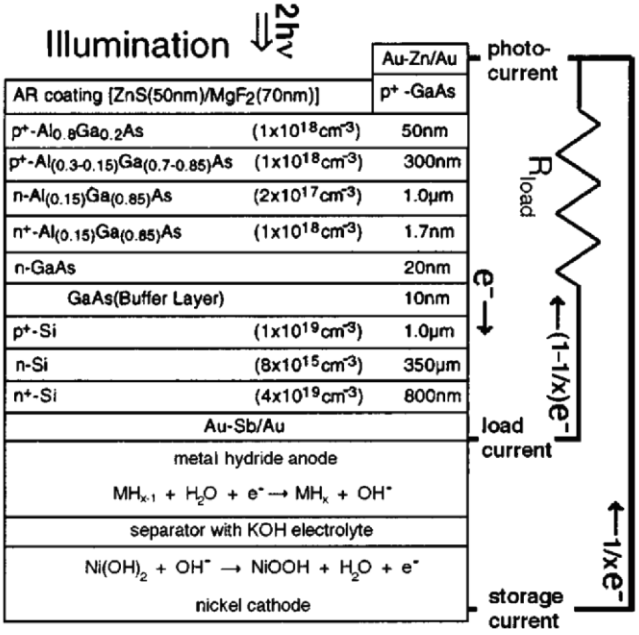

Figure 9 – Schematic representation of the AlGaAs/Si/metal hydride multijunction solar cell synthesized by Licht et al. Figure obtained from [102].

2 Experimental techniques

The work reported in this thesis is based on a set of experiments performed at IFE and other institutes and universities.

2.1 Sample synthesis

The samples were synthesized at IFE using a Leybold Optics A550V7, a large, in-line sputtering system. The system is optimized for industrial production on large area substrates, with high deposition rates and high throughput.

Metallic targets of Y, Mg and Ni were used for the deposition of metal hydride films. The purity of the targets was 99.99%, 99.5% and 99.8%, respectively. The targets had surface area of 600 × 125 mm^2. The distance from the targets to the substrate was 116 mm.

The sputtering system had four target positions, of which three were DC power operated and one was RF power operated. Figure 10 shows a picture and an outline of the system. The RF gun and one of the DC guns were situated beside each other, and could be put at an angle to enhance co-sputtering. In all experiments, the Mg target was operated from the RF power position, the Ni target from the DC power co-sputtering position and the Y target was operated with pulsed DC power. A pulse frequency of 70 kHz (T = 14.2 μs) with a reverse cycle of 4 μs was used. The power used on the targets was in the range 100-1000 W. The average power density on the target at 1000 W was 1.3 W/cm^2. The typical deposition rate for metallic films was ~50 nm/min for 1000W target power.

The purity of gases used was 99.999% for Ar and 99.9999% for H_2. The base pressure of the chamber was 10^{-4} Pa, and the depositions were

done at pressures of 0.1 to 1 Pa. Total gas flow rates of 200 sccm were used in all depositions, with gas mixtures going from pure Ar up to 50% (flow rate) H_2. 100 sccm H_2 means a molecular flow of 8.91×10^{-3} mole/min. This is in the same range of magnitude as the total molar deposition rate. For Y, a deposition rate of 50 nm/min over a 600×125 mm^2 surface gives a total molar deposition rate of 1.88×10^{-4} mole/min.

In most cases, it was chosen to operate the substrate carrier in stationary mode. The alternative is oscillating carrier mode, with the substrate carrier moving back and forth (as demonstrated with double-pointed arrow in Figure 10(b)) in front of the targets. Oscillating carrier is preferred when uniform thickness is important and is used to avoid gradients in the chemical composition under co-sputtering. Stationary mode was selected because it reduces the material consumption and it provides better understanding of how the material parameters vary over the deposition zone.

Under co-sputtering, the RF and DC targets on the left side of Figure 10(b) were operated simultaneously. The targets were set at an angle against each other as indicated, to enhance the co-deposition. The center-to-center distance between the targets was 210 mm. The power applied to each target could be adjusted independently to adjust the chemical composition of the deposited film.

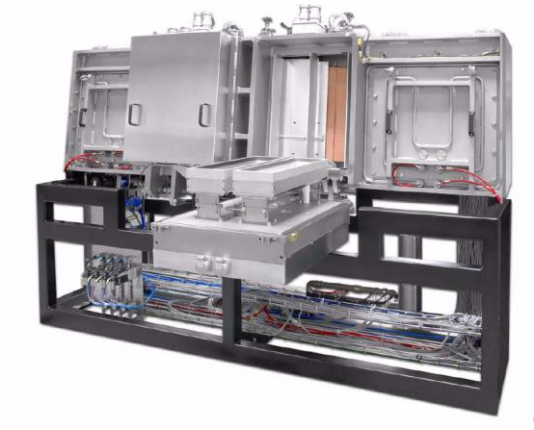

(a)

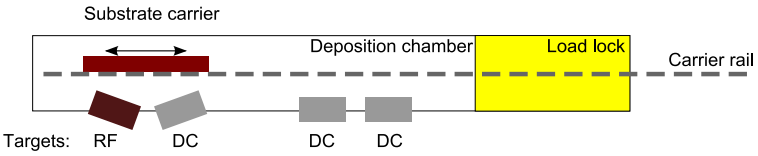

(b)

Figure 10 – The sputtering system used. (a) A photo of the system with one of the target loading doors open [106]. (b) A bird's-eye view of the system and its main parts.

Generally, glass substrates (Menzel-Gläser microscope slides, 76×26×1 mm^3) were used for deposition of the film samples. The substrates were pre-cleaned by 15 minutes ultrasound bath in de-ionized water and then blow-dried by pressurized N_2 gas. Pre-cleaning of the glass with acetone and methanol was also done, but no substantial difference in the film quality was observed as a result of this. The glass substrates were used for optical, electrical and structural (XRD) measurements. Fused quartz substrates (Suprasil, 10×10×1 mm^3) were used for better optical measurements in the UV range, because of the high optical absorption in normal glass for wavelengths below 300 nm. Monocrystalline silicon substrates were used for optical measurements, TEM

and neutron reflectometry. For the RBS characterization, glassy carbon substrates (SIGRADUR G plates) were utilized.

In addition to the depositions done with the Leybold Optics system at IFE, depositions were done with an AJA systems sputter deposition unit at TU Delft. The system had a base pressure of 10^{-5} Pa, and a residual gas analyzer (RGA) for monitoring the gases in the chamber during deposition.

2.2 Thin-film characterization

2.2.1 Thickness and density

The thickness of the deposited films was measured with a Tencor AS-200 profilometer. The accuracy of the measurements was in the order of ±20 nm. It was satisfying for the purpose of estimating deposition rates when films of a few hundred nm were produced. On transparent films, optical ellipsometry could be used for estimating the thickness more accurately.

The density of the resulting films could be measured by direct weighing of the substrates before and after the deposition. The typical mass of a film of ~1 μm thickness deposited on a microscope slide was 2-10 mg, and the accuracy of the scale was ~0.1 mg.

2.2.2 Optical measurements

The optical transmission and reflection of the films were measured with an Ocean Optics QE65000 diffractive spectrometer for the ultraviolet and visible range, and with an Ocean Optics NIRQUEST spectrometer for the IR range (900-1600 nm). The probe light was provided by a halogen light source with a deuterium lamp for enhanced signal in the UV range. The reflection measurements were calibrated with a specular Mg film depos-

ited on a glass substrate and optical data for Mg [107]. The transmission measurements were calibrated with 100% transmission in air. All reported measurements were done with the probe light hitting the sample on the film side of the sample. The reflected or transmitted light was collected in an integrating sphere in order to account for both diffuse scattering and specular reflection or transmission.

Optical ellipsometry was also applied. A Woollam variable angle spectroscopic ellipsometer was used to acquire the data, and the data were analyzed in the J. A. Woollam WVASE32 software package. The ellipsometer measures the changes in polarization upon reflection on the sample. The data can be used to estimate thickness of one or multiple layers when the refractive index is known, and by careful modeling the refractive index can also be determined. For T-YH_x, a Cauchy model was fitted to the ellipsometry data obtained in the wavelength range above the band gap ($\lambda > 500$ nm). This model could then be used to estimate the thickness of films by ellipsometry or by fitting of optical transmission data. The simple optical modeling software Optical[8] was used to simulate the optical transmission and reflection of T-YH_x samples, and it was also used to estimate the optical absorption, which the Cauchy model does not apply for. In a more thorough optical analysis of Mg-Ni-H (Paper VI), we used ellipsometry to adapt a general oscillator model in order to obtain the dielectric functions of Mg-Ni-H films.

In the analysis of the photochromic effect in T-YH_x, a solar simulator at IFE was used. This was a relevant light source to work with in relation to possible utilization of the effect in smart window technology, and

[8] Optical is available for free download at *http://www.raysolar.com/optical/optical.html*

the light from the solar simulator gave a reasonably strong and fast photochromic effect on the samples. The intensity of the solar simulator was approximately 0.1 W/cm^2, the light mainly distributed over the wavelengths from 400 to 1000 nm. One way of characterizing the photochromic effect was to measure the optical transmission and reflection of a sample before and after illumination of a certain time by the solar simulator. This was a fairly simple procedure, but as the relaxation is rather fast in the first few seconds after illumination, this method does not capture the most extreme state of the sample. It is also an error source that the sample has to be moved from the spectrometer to the solar simulator and back again, as small non-uniformities in thickness could give changes in the optical transmission and reflection due to the thin-film interference. Therefore, time-resolved measurements of the optical transmission under illumination were also performed, simultaneously measuring the electrical resistivity response. These measurements were performed as demonstrated in Figure 11. The measurements were after data collection corrected for the stray light from the solar simulator. The solar simulator is a much stronger light source than the probe light, and the stray light strongly affected the results even when care was taken to avoid the stray light. The results are reported in Paper IV.

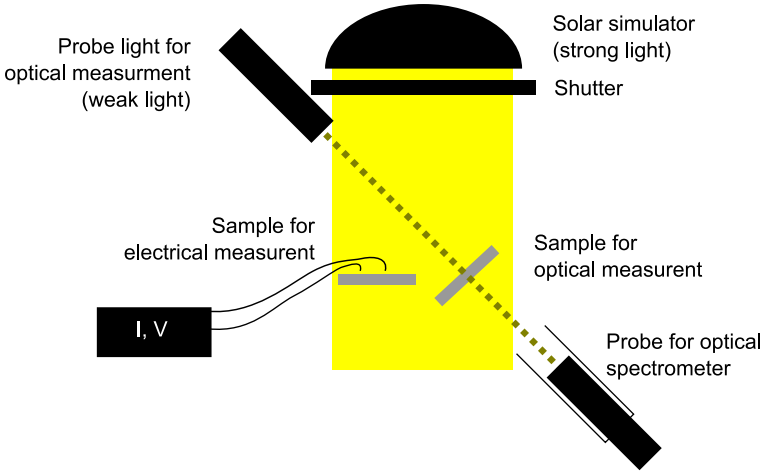

Figure 11 – The measurement setup to do time-resolved measurements of optical transmission and simultaneously electrical measurements for the photochromic T-YH$_x$ films.

2.2.3 Electrical measurements

The electrical resistivity of the samples was measured by a collinear 4-point-probe [108] with a probe spacing of 1.5875 mm, using a Keithley 197 Autoranging Microvolt DMM multimeter. For compositional gradient Mg-Ni-H samples (Paper V) the probes were placed along the perpendicular direction to the gradient, so all the probes were touching the area with the same composition. Measurements were taken every 5 mm on gradient samples, corresponding to a certain difference in the composition as discussed in Paper V.

For the photochromic T-YH$_x$ films, simultaneous measurements of the optical transmission and the electrical resistivity were carried out. These measurements were done using the setup demonstrated in Figure 11, locating a sample for measurements of the electrical resistivity in the light from the solar simulator. The electrical resistivity was in this case measured by a two-probe configuration with two rectangular aluminum

pads separated by a gap of approximately 20 μm, upon which a film was deposited. This sample geometry was chosen because of the high resistivity of the sample (in the order of 10^5 Ωcm), and to allow illumination of the sample at the same time as it was subject to measurements. The resistance over the two pads was measured by applying a constant voltage of 24 V and measuring the current using a National Instruments USB multimeter. Although the resistivity of the material could in principle have been calculated from the resistance measured and the sample geometry, there were too many uncertainties in the experiment for this to be reasonable and thus only the measured resistance over the probes is shown in this thesis.

Hall measurements of Mg-Ni-H were also done, in order to estimate the polarity, carrier concentration and mobility of the carriers of the material. A variable temperature Hall effect measurement system from MMR Technologies was utilized. The Hall effect results were not conclusive and they thus have not been presented explicitly in this thesis. However, a set of temperature-dependent measurements of resistivity are displayed in Chapter 4, as a demonstration of the data that can be obtained with this method.

2.2.4 Structural investigation

X-ray diffraction (XRD) was done in order to determine the crystal structure of the samples and identify crystalline metal hydride and metallic phases. XRD was carried out using several different diffractometers. The first diffractometer used (in Papers I and III) was the diffractometer at IFE, a Bruker AXS D8 Advance instrument with a Göbel mirror mono-

chromator and a 1D Lynxeye detector. θ – 2θ scans were performed on this instrument in a parallel-beam geometry.

θ – 2θ scans are not always best suited for diffraction experiments on thin films. A grazing incidence diffraction experiment (GI-XRD) is better suited because it causes the X-ray beam to interact with a larger amount of the thin-film material. Thus the diffraction experiment can be carried out faster because of a better signal to noise ratio. Also one can avoid or greatly reduce the background scattering from the substrate, which in our case was (non-crystalline) glass. GI-XRD was performed at Uppsala University by using a Bruker-Siemens D5000 diffractometer (Paper II) and at SMN, University of Oslo, using a Bruker D8 Discover instrument (Paper IV and V).

All the diffraction instruments used Cu-Kα radiation with a wavelength of $\lambda_{Cu\text{-}K\alpha}$ = 1.5418 Å. In Paper II and III, the diffraction data has been analyzed by the Rietveld whole-profile refinement method [109]. The analysis was done using the General Structure Analysis System (GSAS) software[9].

In addition to XRD, electron diffraction patterns were obtained using the TEM setup described in Section 2.2.7 (data in Paper V).

A detailed structural analysis of photochromic T-YH_x comprising a texture analysis and a time-resolved study of the lattice under the photochromic reaction was performed through a series of experiments at the Swiss-Norwegian Beamline (SNBL) at the European Synchrotron Radiation Facility (ESRF) in Grenoble, France. The experiments were carried out at BM1A, using a Kuma KM6-CH multipurpose diffractometer and a

[9] GSAS is available for free download at *http://www.ccp14.ac.uk/solution/gsas/*

2D solid-state detector. Data analysis was done with the programs Fit2D[10], Maud[11] and GSAS. This work is still in progress and, apart from results showed in Chapter 3, a detailed report and analysis will be the subject of a forthcoming paper that is not included in this thesis.

2.2.5 Methods for compositional analysis

Several methods were pursued in order to investigate and quantify the chemical composition of the samples. The most important was to estimate the amount of H and O in the samples, and to determine the Mg-Ni ratio in the Mg-Ni-H samples.

Energy dispersive x-ray spectroscopy (EDS)

EDS is a method for estimation of the amount of elements present in a sample. EDS was performed on the Mg-Ni-H samples in order to estimate the Mg-Ni ratio (Paper V and VI). It was also attempted to use the method to estimate the O content in T-YH_x samples, but the results were ambiguous in this case. EDS is not well suited for quantification of O and lighter elements. For H, there is no sensitivity at all, because the method depends on the excitation of inner shell electrons which H does not possess. The EDS spectra were collected in the SEM equipment described in Section 2.2.7, using a Noran System SIX detector and the data were analyzed in the software NSS 3.0.

[10] Fit2D is available for free download at *http://www.esrf.eu/computing/scientific/FIT2D/*

[11] Maud is available for free download at *http://www.ing.unitn.it/~maud/*, and an excellent tutorial on how to use the program for a texture analysis using radial diffraction files can be found at *http://merkel.zoneo.net/RDX/*.

Rutherford back-scattering (RBS)

RBS is a method that can be used for obtaining depth-dependent information of the composition of a sample, well-suited for the study of thin films [110]. The sensitivity is low for light elements, but one can achieve a satisfying quantification of the elements as low in weight as O. It is for a thin film, however, an advantage for the sensitivity that the substrate is made of a lighter element than the elements present in the film. Since C is lighter than O, carbon substrates are chosen when O is important. RBS was employed to estimate the Mg-Ni ratio and the O concentration of Mg-Ni-H samples (Paper V and VI). It was also used on YH_x samples for estimating the O content, but low adhesion of T-YH_x to the sample put limitations on the measurements that could be performed, as described in further detail in Chapter 3.

The RBS measurements were carried out at the Tandem Accelerator Laboratory at Uppsala University. The data were analyzed in the SIMNRA software [111].

Nuclear reaction analysis (NRA)

Depth-resolved information about the H content in a thin film can be obtained by nuclear reaction analysis (NRA) [112]. The method is based on the resonant nuclear reaction between a beam of ^{15}N ions and the H atoms in the film. The reaction between ^{15}N and ^{1}H has a resonance at a kinetic energy of 6.385 MeV of the incoming ^{15}N ions, resulting in the emission of an α particle and a γ ray with an energy of 4.43 MeV. The emission rate of γ rays depends on the amount of H in the sample and the stopping power of the compound, and the detection of the γ rays can therefore yield the H concentration of the sample. The depth resolved

information is obtained by variation of the energy of the ^{15}N beam. If the energy is higher than the resonant energy of 6.385 MeV, the energy of the ions will be reduced as it traverses the sample and the resonant reaction will take place deeper in the film. In the NRA results displayed in Paper VI, the energy was varied from 6.40 MeV to 6.64 MeV in steps of 0.02 MeV in order to obtain depth dependent information from the surface and in to a depth of approximately 100 nm in the sample. If the measurements are compared to that of a well-known standard, the absolute concentration of H can be determined. At the point of writing this thesis we have not been able to do such a measurement due to the lack of a well-known standard, and the data displayed in Paper VI are therefore only a qualitative comparison between an amorphous and a crystalline film, and a demonstration of the depth dependence of the H content.

The NRA measurements were performed in the setup of the Materials Physics group in the Tandem Accelerator Laboratory at Uppsala University.

Thermal desorption spectroscopy

Thermal desorption spectroscopy (TDS) is a method that is well known in the field of metal hydride research. It is used to obtain information on the chemical properties of metal hydrides and to estimate the H content of a sample. It is based on monitoring the pressure of a container holding the sample during controlled heating from room temperature and up to the temperature where release of the H bound in the sample takes place. In this way one can find the desorption temperature of the hydride and also the amount of H that is contained in the hydride. TDS was performed on Mg-Ni-H samples, the data are presented in Paper V. The

TDS measurements were performed in a setup available at IFE. The set-up was optimized for samples of a few g, whereas the thin-film samples we investigated had a mass of 1-5 mg. We were therefore not able to establish a quantitative measure on the H content of the sample, but the desorption temperatures for the samples are clearly visible in the data.

2.2.6 Neutron and X-ray reflectometry

Neutron reflectometry (NR) and X-ray reflectometry (XRR) are methods capable of determining the thickness and density of films with thickness in the range of 5-100 nm. The setup of a typical reflectometry experiment is demonstrated in Figure 12. The principles and more details about the methods can be found in a book edited by Daillant and Gibaud [113]. Whereas XRR is sensitive to the electron density[12], NR is sensitive to the coherent neutron scattering length density (n-SLD). The n-SLD depends on the composition and density of the film, where the elements contribute with a specific scattering length. The interesting point with regards to metal hydride films is that H is one of the few elements that has a negative scattering length. Neutron reflectometry is therefore very sensitive to H. The advantage of NR and the negative scattering length of H are further discussed in Paper VII.

[12] Sometimes XRR is presented as a method that finds the mass density of a sample. This is true in the rough generalization where each electron corresponds to two nuclear particles (protons or neutrons), and is e.g. not valid for H (1 electron per 1 nuclear particle) or Y (1 electron per 2.28 nuclear particles).

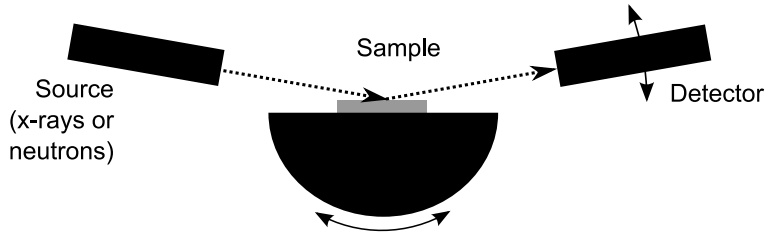

Figure 12 - The typical geometry of a reflectometry experiment

NR was carried out at the EROS reflectometer [114] at the Laboratoire Leon Brillouin[13], Saclay, France. The NR data was analyzed with the EROS data treatment package[14].

XRR was done in the Bruker D8 Discover instrument described in Section 2.2.4. Analysis of XRR data was done using the GENX software[15]. No XRR data are explicitly presented in this thesis.

2.2.7 Microscopy

The films were investigated using several different microscopy methods. Optical microscopy was done to study the structure of delaminated and laser treated samples, and the photochromic effect of T-YH_x was discovered using the optical microscope. However, no optical microscope images are included in this thesis.

Electron microscopy in some form was used for characterization of all types of samples prepared in this work. The SEM apparatus used was

[13] LLB has a neutron source – a nuclear reactor where the neutrons that are generated from the uranium fission reaction – devoted to experiments for materials science. IFE has a similar neutron source, but there is currently no reflectometer at IFE.

[14] The software can be downloaded for free at *http://www-llb.cea.fr/menl/softs_p.php*.

[15] GENX is available for free download at *http://genx.sourceforge.net/*.

a Hitachi S-4800, available at IFE. Paper II displays scanning electron microscopy (SEM) images of the surface morphology of MgH_x films, and a cross-section of a YH_x film can be seen in Chapter 3. For Mg-Ni-H films, the surface morphology was too flat to yield any distinguishable features on the SEM images, but the apparatus was important in the measurement of composition, using the integrated EDS instrument (see Section 2.2.5).

Transmission electron microscopy (TEM) was done on a sample of Mg-Ni-H for assessing the nanostructure (Paper V). The TEM was done at UiO, using a 200 keV JEOL 2010 F microscope.

Atomic force microscopy (AFM) was used to determine the surface roughness of the YH_x samples that were to be investigated by NR. An AFM setup from Surface Imaging Systems available at IFE was utilized. The AFM measurements were performed in air.

3 Reactive sputter deposition of metal hydrides

The Papers I-II, III and V of this thesis deal with reactive sputter deposition of metal hydride films and the effect of the deposition parameters, for respectively MgH_x, YH_x and Mg-Ni-H films. In this chapter, some more details and general observations on the deposition process and the properties of the resulting films are presented and discussed.

3.1 General observations on process parameters and film growth

Operating voltage

Two main types of electric fields are used for sputter deposition; radio-frequency (RF) and direct-current (DC). RF sputtering is suitable for deposition from insulating targets, because the oscillating electric field does not cause electric charge to build up on the surface of the target. DC sputtering gives higher deposition rates and is usually preferable for deposition of metals. Under reactive DC sputtering of metallic targets, pulsing of the DC power is generally applied. This is important if the reaction product of the target material and the reactive gas is insulating (as for example $2Al + 3/2\ O_2 \rightarrow Al_2O_3$), as the surface of the target can become covered by an insulating layer that cause arcing from the charge that is built up on the surface of the insulating layer. A metallic target with an insulating surface layer formed under reactive sputtering is called a *poisoned* target. A poisoned target also yields substantially lower deposition rates. A way to enhance the deposition during reactive sputtering is to

apply a small reverse voltage to remove the surface charge under reactive sputtering [115]. In this work, pulsed DC was applied under reactive sputtering with Y. The pulsing was observed to reduce the rate of arcing on the target.

Reactive gas flow

The H_2 partial pressure was found to be important in all cases. The partial pressure was adjusted by the H_2 flow rate relative to the Ar flow rate, from 0% up to 67% of the total flow rate. Our system did not have an RGA, so we could not directly monitor the partial pressure of H_2. While smaller amounts of H_2 added to the process gas resulted in solid solution of H in the metal phase, 10-20% and higher H_2 levels resulted in the direct growth of metal hydride films for all the compounds studied (MgH_x, YH_x and Mg-Ni-H). The exception was $Mg_yNi_{1-y}H_x$ with $y < 0.33$, which did not form hydride under any of the applied sets of parameters.

Target poisoning

The signs of target poisoning typically observed for reactive sputter deposition with O_2 are arcing, decrease in the deposition rate and changes in the cathode voltage. The cathode voltage is normally monitored from the control unit of a sputtering machine. The change in cathode voltage during reactive sputtering depends on the ion induced secondary electron emission, and can be positive or negative for depending on the metal and the reactive gas [116]. Figure 13(a) demonstrates data obtained for the development of the cathode voltage for reactive sputter deposition of Al with O_2 as a reactive gas, with a pronounced fall in the cathode voltage at a flow of 16% reactive O_2. There is also a hysteresis: the poisoned state of the target persists to lower O_2 partial pressures when the reactive gas

flow is reduced. This is typical for reactive sputtering of e.g. Al, Mg and Y in O_2, while some other metals, e.g. the noble metals Au and Pt, give a smaller and positive change in the cathode voltage under similar conditions [116]. For reactive sputtering of Y with H_2 gas, there is a slight increase in the cathode voltage at 13 % H_2 (Figure 13(b)), and there is a corresponding reduction in the deposition rate at the same flow rate (Figure 13(c)). This change might be related to a poisoned state of the target, but since the change is quite small and gradual, it may be questioned if there really is a poisoned state of Y under H_2 reactive sputtering.

Deposition temperature

The temperature during deposition is another parameter that greatly affects the film growth. The deposition chamber at IFE was, however, not well equipped for experimenting with the deposition temperature. Heaters were installed in the load lock to pre-heat the carrier and in the deposition chamber to keep the temperature high during deposition, but there was no monitoring of the actual substrate temperature. In some instances (Paper I and II), we used temperature-sensitive stickers as an indicator for the maximum temperature achieved during processing. Additionally, the heating of the substrate was purely radiative, which resulted in lengthy pre-heating processes to achieve a stable substrate temperature. However, some temperature variation was done in the case of MgH_x and Mg-Ni-H. The results were higher crystallinity and slower oxidation in ambient conditions for MgH_x (Paper I & II) and higher resistivity and optical transparency for Mg-Ni-H (Paper V).

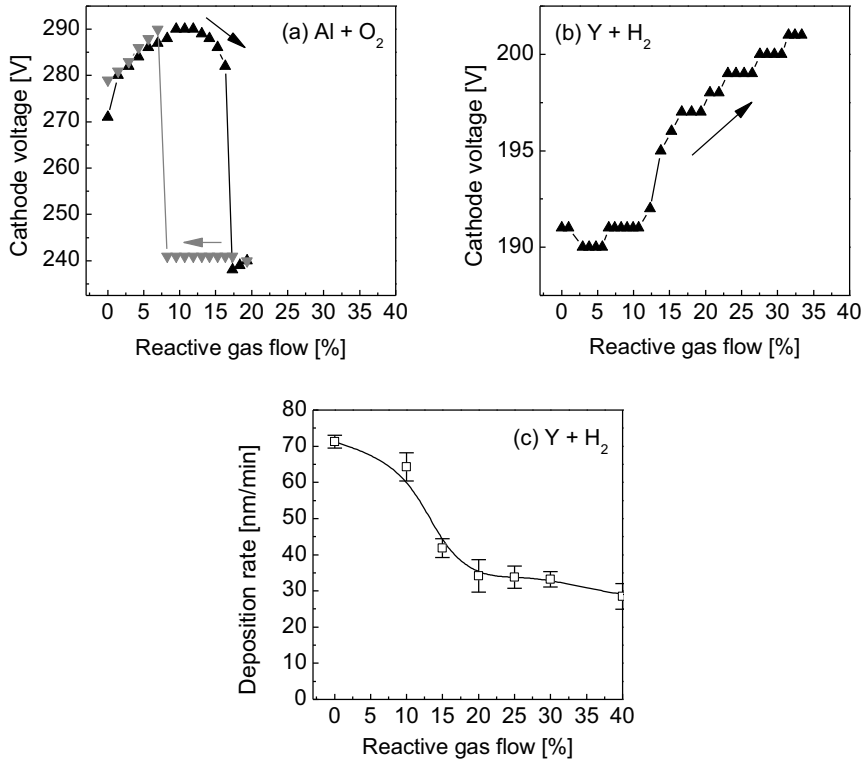

Figure 13 – Reactive sputter deposition and signs of poisoning of the target. (a) Cathode voltage on Al target, demonstrating poisoning of Al target when sputtering with reactive O_2. There is a hysteresis in the effect illustrated by the extension of the poisoned state when lowering the O_2 flow rate. (b) Cathode voltage on Y target when increasing the flow of reactive H_2. Contrary to the Al-O_2 case, the cathode voltage is increased. Hysteresis curves were not measured. (c) Deposition rate of Y-H films in the center of the deposition zone, as a function of H_2 flow. The line is a guide to the eye.

Surface morphology

The surface structure of the metal hydride films was investigated by SEM and AFM. In Paper II, SEM images of the surface of MgH_x films demonstrate porosity and a quite dramatic morphology with features of up to several hundred nm. For YH_x and Mg-Ni-H films, no such surface morphology was found. The films were flat; no surface structures could be identified by SEM. AFM and NR measurements of the roughness gave RMS roughness in the order of 1-5 nm for YH_x and Mg-Ni-H.

Phase separation

For MgH_x films, phase separation of crystalline MgH_2 and Mg was observed by XRD. For YH_x there was no such sign of phase separation, whereas for Mg-Ni-H films there were signs of phase separation in the eutectic regions and in the case of Mg-rich films where both crystalline Mg metal and MgH_2 was observed.

Oxidation and oxygen content

The post-deposition oxidation and the O content of the films were highly different for the different metal hydrides. MgH_x films seemed to have little O content in the as-deposited state[16], but XRD proved formation of $Mg(OH)_2$ after a certain time of exposure to ambient conditions. YH_x films were found to have a substantial amount of O even in the as-deposited state, and observations of changes in the optical properties suggest that even more O is absorbed in the films also after exposure to

[16] The MgH_x films were not investigated by RBS so the O content was not actually measured. In a study of similar samples, X-ray photoelectron spectroscopy (XPS) revealed large amounts of O also in the as-deposited state of MgH_x films [75].

air. On the other hand, $Mg_{\sim 2}NiH_{\sim 4}$ films contained little O in the as-deposited state, and the films were found to be resistant against oxidation also when exposed to air for longer periods of time.

3.2 Magnesium hydride

Paper I and II deal with the deposition and characterization of MgH_x films. The H/Ar ratio and the deposition temperature were varied in an attempt to produce single-phase MgH_2 using reactive RF sputter deposition. However, as mentioned above, the resulting films for all the attempted deposition conditions resulted having an amount of crystalline metallic Mg. This is in accordance with reported findings on MgH_x films deposited by reactive sputtering [74], [75] and by the very similar process of activated reactive evaporation [30].

The Papers I and II give a thorough report of the optical, electrical and structural properties of the MgH_x films.

3.3 Magnesium nickel and magnesium nickel hydride

The Papers V and VI deal with the deposition and characterization of Mg-Ni-H films. Co-sputtering of Mg and Ni was used. Due to the geometry of the deposition chamber (see Figure 10), a sample with a compositional gradient was obtained. This was beneficial, as a film with a compositional range from almost pure $Mg(H_x)$ to almost pure Ni resulted from every deposition, as demonstrated in Figure 14. Hydride films were observed to form for all compositions with more than 33% Mg (ignoring the H content), but single phase hydride films was only observed for compositions close to $Mg_{\sim 2}NiH_{\sim 4}$.

The Papers V-VI gives a good description of the structural, optical and electrical properties. However, some more details on the deposition rates and the composition of the resulting films are presented in here.

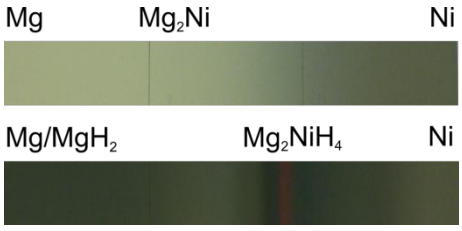

(a)

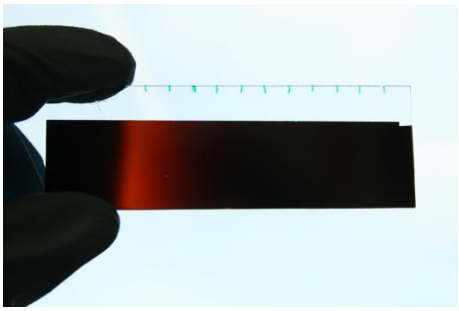

(b)

Figure 14 - Visual appearance of the metallic and hydride gradients of Mg-Ni(-H) resulting from reactive co-sputtering. (a) A photograph of the reflection of metallic and metal hydride gradients and (b) a photograph of the optical transmission of $Mg_{\sim 2}NiH_{\sim 4}$ gradient with white light in the background.

Deposition rates

Measurement of the thickness of the deposited films and thereby the *volumetric deposition rate* is not always the best measure of deposition. The volumetric deposition rate in the case of co-sputtering and reactive sputtering can be misleading because the volume of a compound film is not necessarily the same volume as the sum of the volume the constituents in the case of single target or non-reactive deposition. Figure 15 demon-

strates an example of how the volumetric deposition rate increases while the *gravimetric deposition rate* decreases, when 30 % H_2 is introduced in the Ar process gas under Mg sputter deposition. The density of the deposited material is important, as is also the porosity in the sample. The gravimetric deposition rate is a more direct measure of the amount of material in the sample, which is why weighing of the samples was used in addition to thickness measurements to estimate the deposition rates.

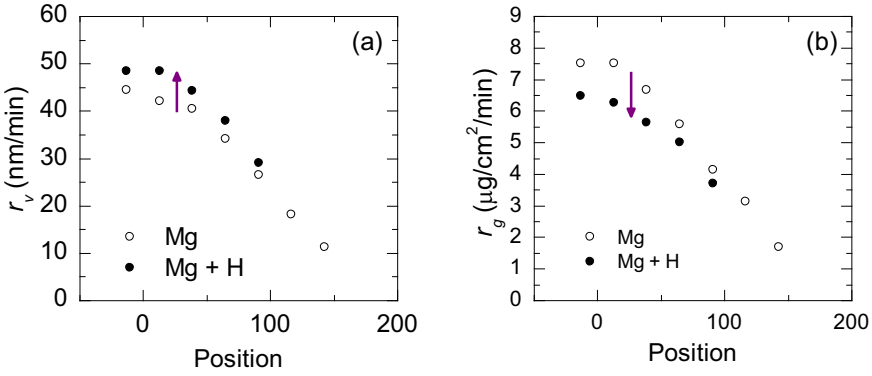

Figure 15 – (a) Volumetric and (b) gravimetric deposition rates as a function of position for Mg sputter deposition with and without reactive H_2. The center of the deposition zone is approximately at position 0.

Composition

In the case of co-sputtering Mg-Ni films without reactive H_2, measurement of the deposition rates gave a good estimation of the composition at each point in the compositional gradient. The underlying assumption is that the deposition rates are not changed under co-sputtering with respect to the case of single-target deposition. This assumption is often used in co-sputtering of metallic Mg-Ni films [39], [117]. Measurements of the gravimetric deposition rates supported this, and separate measurements

of the local composition using EDS confirmed that the use of single-target deposition rates for estimation of the composition of films deposited by co-sputtering gives satisfying accuracy (Figure 16).

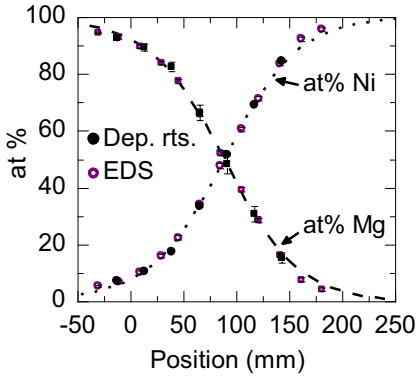

Figure 16 – Estimation of the composition of Mg-Ni films as a function of position in the deposition zone from gravimetric deposition rates, compared to EDS measurements of the local composition. The figure demonstrates data for co-sputter deposition of Mg and Ni without reactive H_2. The broken lines are guides to the eye.

For Mg-Ni-H films deposited with reactive Mg-Ni, it was found that the single-target deposition rates could not be used for estimation of the composition. That was because a collapse in the partial deposition rate of Mg was observed under reactive co-sputtering of Mg (see Paper V). The composition of Mg-Ni-H films was measured by EDS and RBS. The data in Figure 17 demonstrates that the two methods coincide in the quantification of the Mg and Ni content.

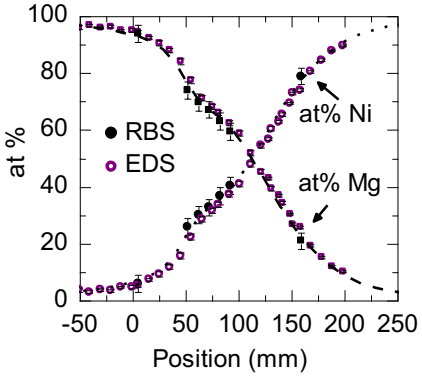

Figure 17 – Comparison of data from EDS and RBS for measurement of composition on Mg-Ni-H compositional gradient samples. The figure demonstrates data for co-sputter deposition of Mg and Ni with reactive H_2. H is ignored in the calculation of the at%. The lines are guides to the eye.

Oxygen content

Reliable measurements of the O content could not be done by EDS. RBS did, on the other hand, give information about the O content, and also depth-dependent information about the O content in the samples was obtained. It is demonstrated in the Papers V and VI that the O content is relatively low, in the case of $Mg_{\sim 2}NiH_{\sim 4}$ it is close to or less than 1%. This means that little O is incorporated during the deposition process and that the samples do not oxidize substantially in air. The samples were exposed to ambient conditions for several weeks between the deposition and the measurement. Figure 18 shows the RBS data, also presented in the Papers V and VI, demonstrating the O content for eight different samples of Mg-Ni-H with different Mg:Ni ratio, denoted here as z in Mg_zNiH_x. For all samples there is most O on the upper and lower interfaces of the films and relatively low O content in the bulk. The bulk O

content is especially low for the compositions where z is between 2 and 3. This is exactly where we can observe the semiconducting state of Mg-Ni-H, and this observation is thus very positive regarding the chemical stability of $Mg_{\sim 2}NiH_{\sim 4}$ and its potential application in PV technology.

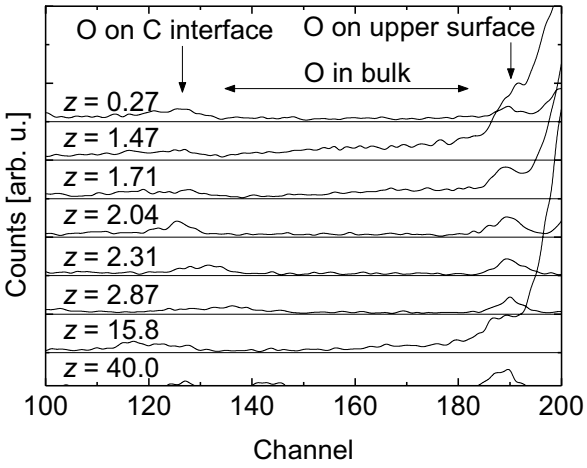

Figure 18 – RBS data showing the O content in a set of samples with different composition Mg_zNiH_x.

Hydrogen content

The H content of the samples has not been quantified. Considering the high resistivity and the high transparency of the $Mg_{\sim 2}NiH_{\sim 4}$ films, it is probable that they consist of a close to stoichiometric hydride. It is not clear from literature what H content is to be expected for fully hydrogenated samples where $z > 2$ in Mg_zNiH_x, but it seems reasonable that there are 2 H atoms per Mg atom if the compound is a combination of Mg_2NiH_4 and MgH_2. Paper VI shows NRA data with a comparison of the H content of an as-deposited and a crystallized Mg_2NiH_4 film, which demonstrates that the H is evenly distributed through the thickness of the

film and that the H content is similar for both of the samples. Unfortunately there was no suitable calibration sample available at the time of the NRA measurement, so the data could not be used to quantify the H content.

Density

The density of a film can be calculated from the measured area, thickness and total mass. Table IV gives a summary of the densities found for various Mg-Ni-H compounds in the form of thin films.

Table IV – Measured density of Mg-Ni-H samples

Compound	Measured density [g/cm^3]	Density of bulk compound* [g/cm^3]
Mg	1.79 ± 0.1	1.73
Ni	8.37 ± 0.9	8.9
MgH_x	1.41 ± 0.04	MgH_2: 1.45
Mg_2NiH_4	2.82 ± 0.2	2.69

*Calculated from known crystal structure (See Table II)

3.4 Yttrium hydride

Paper III reports deposition of YH_x by reactive sputtering. In this paper, the optical, electrical and structural properties of optically transparent and black samples (T-YH_x and B-YH_x) are presented and compared with data for Y and Y_2O_3. The most interesting in this paper, apart from giving the first report on reactive sputter deposition of these compounds, is the fact that the films of T-YH_x has an fcc structure whereas transparent

samples of YH_3 normally are found in a hcp structure (see Table III). Paper III constitutes the background for Paper IV, where in the latter the photochromic effect in T-YH_x is reported. Paper VII demonstrates a NR study on B-YH_x and T-YH_x films, examining especially the surface oxide that forms on unprotected samples.

In this section, more details about the deposition and the properties of the resulting films will be given. A discussion of the O content of the YH_x samples is also presented.

Deposition zone

In Paper III, we have stated "*For zero or low hydrogen flow, metallic α-phase yttrium films were obtained. For higher hydrogen flow ratios, black or transparent films were formed.*" Due to limitations on the length of the paper, we had to leave out the complete explanation about under what conditions B-YH_x and T-YH_x preferentially forms. Considering that the B-YH_x appears optically similar to the known YH_2 phase and T-YH_x appears similar to YH_3, it is intuitive that B-YH_x forms for intermediate H_2 flow rates and T-YH_x forms for higher H_2 flow ratios. It is, however, not so straight-forward. The fact is that both phases formed in the same process, only at different positions in the deposition zone.

Figure 19(a) displays the appearance of the deposition zone with areas of T-YH_x (yellow) and B-YH_x on the carrier (grey). The red rectangle demonstrates the position of the Y target in relation to the deposition zone. The area where B-YH_x is deposited corresponds to what is known as the racetrack-region on the target. The racetrack region is the rounded shape on which the etching of the target happens, visible on a photo of the target displayed in Figure 19(b).

The region where B-YH_x is formed is reduced if the H_2 flow rate is increased or if the total process pressure is increased. The appearance of the deposition zone demonstrated in Figure 19(a) is typical for a 20% H_2 in the process gas and a process pressure of 0.4 Pa. One might believe that this peculiar result is related to the sputtering setup used, but using the sputtering setup available at our collaborators at TU Delft, we obtained similar results. A comparison of a sample from IFE and TU Delft is showed in Figure 20.

We have not determined why the two phases form in this way, under such similar conditions. As discussed in Paper III, the crystal structures of the two phases are similar, but with a slightly shorter lattice parameter for the B-YH_x phase. Additionally, it seems that the T-YH_x has higher concentration of O, and results presented in the following suggest that the O mainly is incorporated during the deposition of the film.

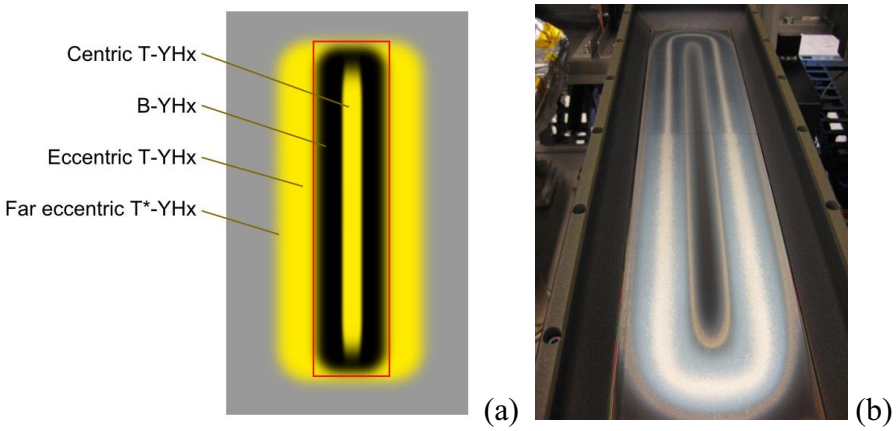

Figure 19 – (a) A demonstration of the appearance of the deposition zone with typical distribution of T-YH_x and B-YH_x. (b) A photo of the Y target after reactive deposition, showing the racetrack region on the target.

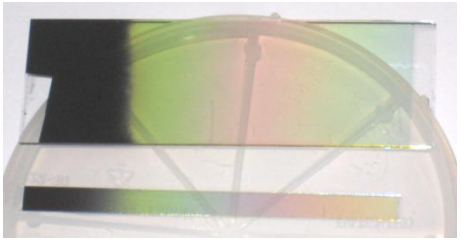

Figure 20 – Photo of sample prepared at IFE (upper) and sample prepared at TU Delft (lower) exhibiting regions of both B-YH_x and T-YH_x. The upper sample is deposited on a microscope slide (76 × 26 mm^2), the lower on a quartz strip. The color variation visible in the T-YH_x region is due to optical interference effects in the thin film.

Oxygen content

For O content estimations of film samples by RBS, the samples should preferably be deposited on C substrates so that the noise from the substrate does not interfere with the signal from the film. Preparation of a sample of T-YH_x on a C substrate was, however, not so straight-forward. The adhesion of T-YH_x on the polished glassy C substrate was very poor, and samples delaminated from the substrate within short time after the deposition. There was no problem with the adhesion to the C substrates for any other kind of compound investigated in this work.

The adhesion obstacle of T-YH_x was solved by depositing a buffer layer and an overlying protection layer, both consisting of a 10 nm thick film of Mo. The over-layer was applied *in-situ* without exposing the sample to air, and was intended to protect the sample from oxidation. Figure 21 shows the layout of the sample and the data obtained by RBS. Two important conclusions can be drawn from this data: Firstly, the amount of O in the film is substantial. There is more than one O atom per Y atom in the structure, the O concentration was estimated to x_O =

[O]/[Y] = 1.1. Secondly, the constant signal over the channels ~100-170, accounting for the signal from O, demonstrates that the O in the film is evenly distributed through the thickness of the film. The even distribution and the fact that the O was found even though a protecting metallic Mo layer has been applied, suggests that the O originated from the deposition process, and not from post-deposition oxidation of the sample in air.

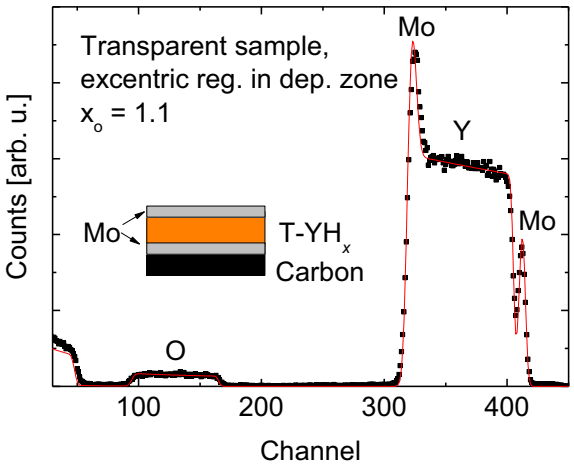

Figure 21 – RBS spectra for T-YH_x with data (black squares) and simulation (red line), as well as a sketch of the sample of T-YH_x used for quantification of the O content.

It might be timely to ask whether it is right to call this compound a hydride when it is shown to contain such high levels of O. The O content of stoichiometric Y_2O_3 would be $x_O = 1.5$, not far from the value found for the T-YH_x in the data demonstrated in Figure 21. However, considering the crystal structure, the optical properties and the electrical properties, which are all closer to what is normally observed for YH_2 and YH_3, it still seems correct to refer to this as a hydride. The compound known

as yttrium hydroxide, $Y(OH)_3$, has a crystal structure that is completely different from that which is found for T-YHx, and it also has a much higher O content.

Figure 22 shows RBS data for different films of unprotected yttrium metal, YH_x and Y_2O_3. Figure 22(a) displays data for a metallic Y film deposited without any reactive H_2 added to the plasma. The O content of the film is relatively low, and the O is mainly located on the upper and lower interface of the film. Figure 22(b) displays data for a B-YH_x film. There is definitely some O in the bulk of the film, and there appears to be a surface oxide with higher levels of O. The total O content in this B-YH_x film is estimated to $x_O = 0.13$, substantially lower than the O content of the T-YH_x film for which data is displayed in Figure 21. As a reference, an Y_2O_3 film was prepared by annealing a metallic yttrium film at 400 ºC for 1h in air, similarly as the Y_2O_3 reference presented in the XRD study in Paper III. The data for this oxide film, presented in Figure 22(c), demonstrate an O content $x_O = 1.55$, close to the 1.5 expected for stoichiometric Y_2O_3. In Figure 22(d), data for a T-YH_x sample from the *far eccentric deposition zone* (see Figure 19(a)) is presented, from here on referred to as T*-YHx. The sample is collected from far away from the center of the deposition zone, where the deposition rate is very low. The O content of this sample ($x_O = 1.67$) is even higher than expected for the stoichiometric Y_2O_3. The crystal structure of this sample exact sample was not investigated, but XRD studies on similar samples showed that even this type of sample exhibited the fcc T-YH_x structure with a lattice parameter $a = 5.35$ Å.

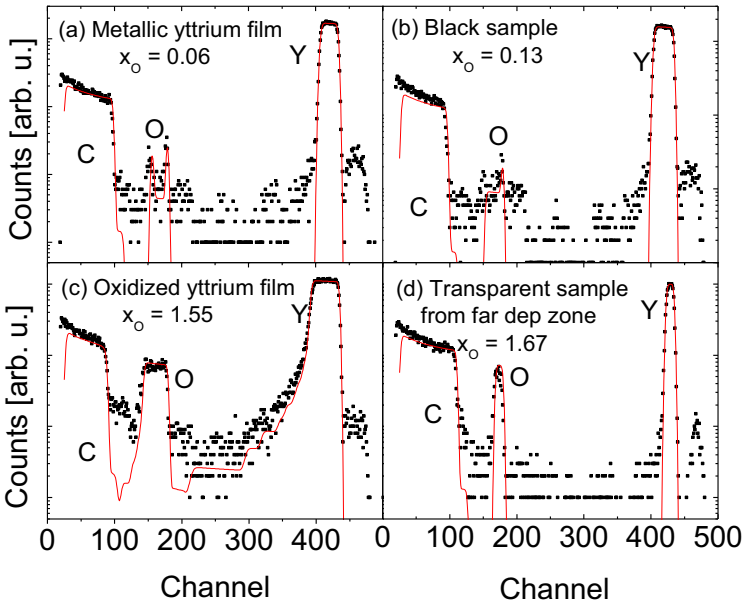

Figure 22 – RBS spectra obtained for different samples. The origins of the signal for the different peaks (C, O and Y) have been indicated. Data is represented by black squares, whereas the result of the simulation is shown as a red line. Not that the counts are shown on a logarithmic scale, in opposition to the scale of Figure 21, to enhance the visibility of the O signal which is relatively low for (a) and (b).

Paper VII presents a study of the YH_x samples, with a focus on the surface oxide layer. It demonstrates that T-YH_x and B-YH_x samples that are unprotected against oxidation have surface oxides of 5-10 nm, and that below this oxide the composition is relatively uniform. This is in agreement with the findings of the RBS on the B-YH_x sample in Figure 22(b), which demonstrates a peak in the O signal at the upper surface. RBS on unprotected T-YH_x samples could not be performed due to the

problem with adhesion of T-YH_x to the C substrate. The findings of surface oxide on unprotected samples indicate that the formation of such a surface oxide protects the sample from further oxidation.

Figure 23 shows NR data collected for a Mo-protected film of T*-YHx from the far eccentric deposition zone. This data was not included in Paper VII because it did not demonstrate any more details about the surface oxide layer which was the subject of the paper. The change in the plateau of total reflection, the *pseudo-plateau*, was not observed for the B-YH_x and T-YH_x samples discussed in Paper VII. The observation of such a pseudo-plateau gives an unambiguous proof that this type of sample has a higher SLD than the Si sample. The SLD of the film is close to 3×10^{-6} Å^{-2}, whereas the expected SLD for pure YH_3 and Y_2O_3 is -0.88×10^{-6} Å^{-2} and 4.42×10^{-6} Å^{-2}, respectively. In other words, the composition of this T*-YHx sample seems to be closer to Y_2O_3, but there is still a considerable difference between the SLD of Y_2O_3 and the investigated sample. If the O content of this sample is $x_O = 1.6$ (as found for as similar sample by RBS, see Figure 22) and the sample has no porosity, the H content can be estimated to $x_H = [H]/[Y] = 1.5$. The samples should however be further investigated to firmly determine the composition.

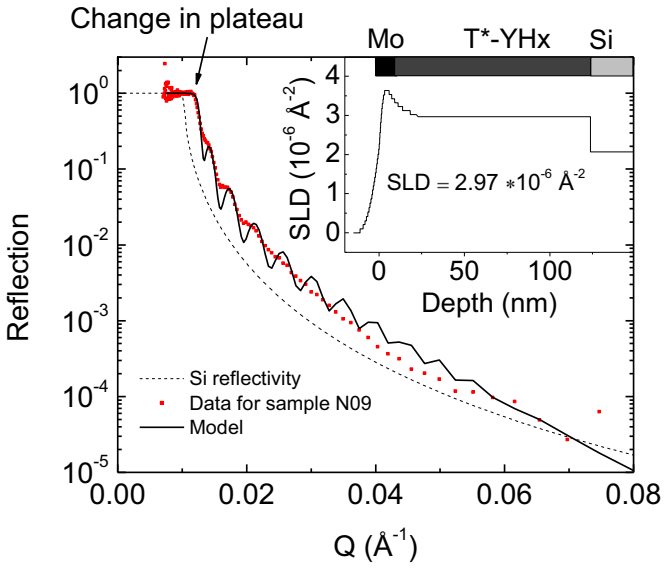

Figure 23 – NR data, model and corresponding SLD profile (SLD) for T-YH_x sample from the far excentric deposition zone.

The even distribution of O through the thickness of the films, the O content of Mo-protected films, and the different O content at different positions in the deposition zone indicate that most of the O is incorporated in the films during the deposition process. However, no reactive O_2 gas is used, and the purity of the gases is too high for the process gases to be the source of the O. It should also be noted that the O content of Y films deposited *without* reactive H_2 is relatively low. To add to the confusion, Mg-Ni-H films deposited *with* reactive H_2 contains very low levels of O. Under the deposition of YH_x films using the sputtering machine at TU Delft, which was equipped with an RGA, substantial amounts of H_2O was observed to form when introducing H_2 gas in the plasma. The source of the H_2O might be the chamber walls, as reactive H^+ ions from the plasma might react with adsorbed O on the walls. However, there is so far no conclusive evidence on the origin of the O in the T-YH_x films.

Mass density

The mass density of both the T-YH_x and B-YH_x films was found by weighing and thickness estimation to be in the range 4.0-4.5 g/cm^3. XRR analyses gave similar results. The mass density of the stoichiometric compounds in the known crystal structure (see Table III) is for YH_2, YH_3 and Y_2O_3 respectively 4.30 g/cm^3, 3.87 g/cm^3 and 5.04 g/cm^3.

Structure and morphology

In Paper III, the crystal structures of T-YH_x and B-YH_x samples are discussed. We found that both these compounds exhibited an fcc structure with space group *Fm*-3*m*. This structure is the same as that of YH_2, where the lattice parameter is known to be 5.20 Å [49]. In our work, B-YH_x and T-YH_x films were found to have a lattice parameter of 5.26 Å and 5.35 Å, respectively. In Paper III, the difference in the intensities of the diffraction peaks have been attributed to film texture with preferred orientation of the (1 1 1) plane parallel to the substrate plane for B-YH_x and correspondingly preferred orientation of the (1 0 0) plane for T-YH_x. This type of orientation was later confirmed in a yet unpublished texture study of the two types of films. Figure 24 demonstrates a reconstructed pole plot showing the highly preferential growth of T-YH_x samples, which explains the high intensity obtained for the (2 0 0) reflection in the θ - 2θ geometry applied in the XRD study of Paper III.

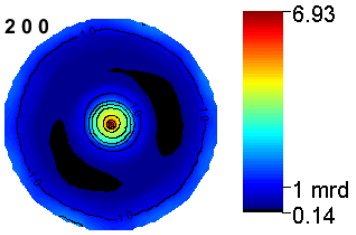

Figure 24 – Reconstructed pole plot for the (2 0 0) reflection for a T-YH_x sample. The unit [mrd] stands for multiples of random distribution.

The microstructure of the YH_x films has not been reported in any of the papers. Figure 25(a) shows an AFM image of the surface of a 540 nm thick B-YH_x film deposited on glass. The surface shows features with as size in the order of 50-200 nm, which corresponds well to the crystallite size obtained from the width of the reflection peaks in XRD. Figure 25(b) demonstrates a SEM image of a cross-section of a ~1000 nm thick T-YH_x sample. The cross-section was exposed by breakage of the film and the crystalline Si substrate, and the cross-section interface demonstrates a quite rough breakage. Columnar structures in the film can clearly be seen, as well as an increase in size of the crystalline grains towards the upper surface of the film. On the top surface one can also discern a similar surface structure as the one demonstrated in the AFM image of Figure 25(a).

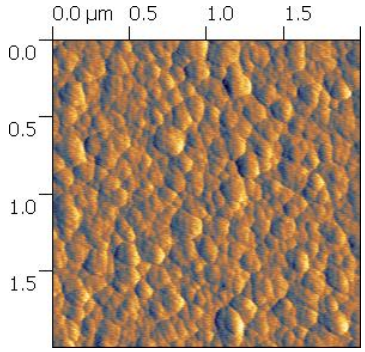

(a)

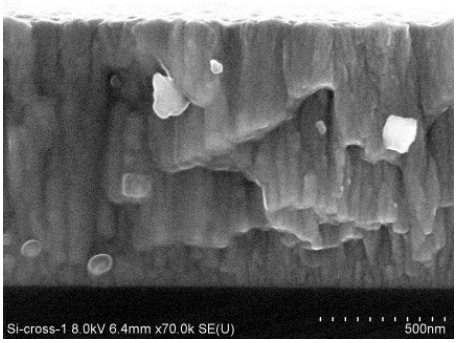

(b)

Figure 25 – Microstructure of the reactively deposited YH_x samples. (a) Surface morphology studied by AFM. The surface RMS roughness for this image is 4.9 nm. (b) Cross-section of sample on a crystalline Si wafer studied by SEM.

4 Magnesium nickel hydride films for PV applications

Films of semiconducting $Mg_{\sim 2}NiH_{\sim 4}$ were obtained using reactive sputter deposition. As discussed in Paper V and VI, as well as in Chapter 3, the films showed high purity as compared to the experiments with MgH_x and YH_x, with no observable presence of metallic particles and low O content. The results are promising with regards to using $Mg_{\sim 2}NiH_{\sim 4}$ as a material for semiconductor devices as e.g. PV solar cells.

Paper V and VI deal with the deposition and characterization of Mg-Ni-H films. Reactive sputtering had, before the publication of Paper V, not been reported earlier in literature as a synthesis method for $Mg_{\sim 2}NiH_{\sim 4}$. Westerwaal and his coworkers had published a paper on a similar synthesis method; activated reactive evaporation [41]. The most common synthesis method for $Mg_{\sim 2}NiH_{\sim 4}$ films is hydrogenation of Pd-capped $Mg_{\sim 2}Ni$ films [31]. We chose to develop reactive sputtering as a synthesis method because it is a more industrially relevant method, being a single step synthesis method and because there is no need for use of the rare metal Pd. It also greatly simplifies measurements to avoid the Pd capping, because the metallic Pd layer would complicate electrical and optical measurements. In the end it is also an advantage to avoid the Pd cap layer with regards to stability, as the Pd catalyst makes H desorption from Mg_2NiH_4 films happen in vacuum or at ambient conditions [41].

4.1 Structural properties

The reactively deposited films of $Mg_{\sim 2}NiH_{\sim 4}$ were found to be amorphous when investigated with XRD, while the other compositions of Mg-

Ni-H formed crystalline material. This is in accordance with what had been found for activated reactive evaporation [41] and hydrogenation of Pd-capped metallic films [118]. However, in this work we also found that by a post-deposition heat treatment, the films could be crystallized in the high-temperature structure. Crystalline films in this structure had been prepared earlier, but then by doing the actual synthesis of the films by hydrogenation of metallic films at high temperatures [39]. Figure 26 shows the visual appearance of a $Mg_yNi_{1-y}H_x$ compositional gradient sample before and after crystallization. Paper VI demonstrates typical XRD patterns for different compositions of the film in the amorphous and crystalline form.

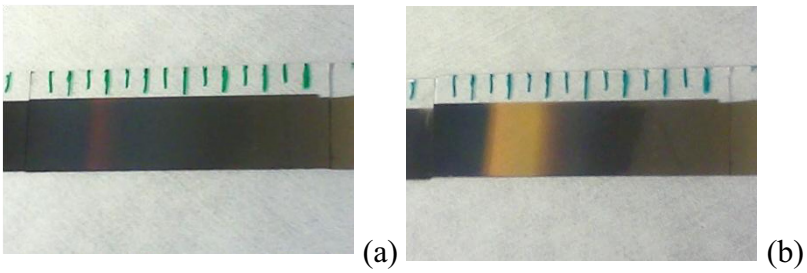

Figure 26 – Appearance at room temperature of a compositional gradient film (a) before and (b) after crystallization treatment (30 min at 523 K, in air). The sample is more Ni-rich on the right side, with composition $Mg_{\sim 2}NiH_{\sim 4}$ in the region which is red-transparent in (a) and orange-transparent in (b).

4.2 Optical properties

Optically, the as-deposited films of $Mg_{\sim 2}NiH_{\sim 4}$ were found to have high transmission above the band gap, suggesting low presence of metallic particles in the films. The geometry of a single film on a substrate is

more accessible for optical investigation than films covered by Pd-capping because the measurements are not hampered by the high reflection and low transmission of the Pd metal. Therefore, we found it worthwhile to perform a more in-depth optical analysis, using optical ellipsometry as a method to determine the dielectric functions of the samples. The results are reported in Paper VI. The dielectric functions were obtained from a general oscillator fit to the ellipsometry data. The dielectric functions were used to find the optical band gap of the films. The band gap of Mg-Ni-H depends on the Mg:Ni ratio of the sample, and increases with the Mg content. For Mg_2NiH_4 in the amorphous and crystalline form we found band gaps of 1.6 eV and 2.1 eV, respectively.

4.3 Electrical properties

In Paper V, we reported a resistivity of up to 10 Ωcm for $Mg_{\sim 2}NiH_{\sim 4}$ samples deposited at room temperature, and 400 Ωcm for samples deposited at ~100 ºC. Resistivity in the order of of 10^5 Ωcm was later measured for $Mg_{\sim 2}NiH_{\sim 4}$ samples prepared at room temperature by reactive sputtering using the sputtering equipment at TU Delft. The resistivity found in this work is thus much higher than earlier reported for Mg_2NiH_4 films. Enache et al. reported a maximum value of 12.5 mΩcm for Pd-capped Mg_2NiH_4 samples, whereas Westerwaal et al. found a resistivity of up to 0.34 Ωcm for samples deposited by activated reactive evaporation. The deviations reflect that the resistivity of a semiconductor is highly dependent on subtle variations in the material. Vacancies, interstitials, defects and impurities may act as donors or traps and one can therefore not expect reproducibility for the resistivity values when working with different deposition methods. One can also discuss the effect that the Pd cap

layer in the work of Enache et al. had on the measurements of electrical properties (see Paper V). We also observed that the resistivity and the band gap were changed when the samples were annealed at temperatures of 100-200 ºC *ex-situ* after the deposition. The crystalline films in the fcc HT structure had high resistivity, outside of the measurement range of the four point probe setup used for resistivity measurements.

Temperature-dependent measurements of electrical properties

In addition to the resistivity measurements reported in Paper V, temperature-dependent Hall and resistivity measurements were done. Measurements were first done on a sample deposited at IFE, and later on samples deposited at TU Delft. Even though the composition, appearance, optical properties and stability of the IFE and TU Delft samples were similar, the results of the electrical measurements were different. The room temperature resistivity of the samples from Delft was in the range 10^3-10^5 Ωcm.

The temperature dependence of the resistivity of one of the samples from TU Delft can be seen in Figure 27. This temperature dependence was typical for all the samples from Delft, showing a logarithmic increase in resistivity as the temperature decreases. The IFE sample investigated had a different temperature-dependence of the resistivity, with a slight and almost linear increase in the resistivity as a function of increasing temperature in the range 100-400K. At 400-450 K, both types of samples showed an irreversible reduction in the resistivity, probably related to the onset of dehydrogenation of the sample in the vacuum of the measurement chamber. Hall measurements on the samples were not conclusive. On the sample from IFE, the Hall coefficient appeared to be neg-

ative, with a value of about -0.03 cm^2/C at 300K. A negative Hall coefficient had been reported by Enache et al., who through Hall effect measurements on Pd-capped Mg_2NiH_4 found that H vacancies act as n-type doping in Mg_2NiH_4 [84]. However, Hall analysis of amorphous materials is known to be very difficult [119]. Taking this into consideration, there is therefore not enough evidence to conclude about the conduction mechanisms and the polarity of amorphous Mg_2NiH_4 films.

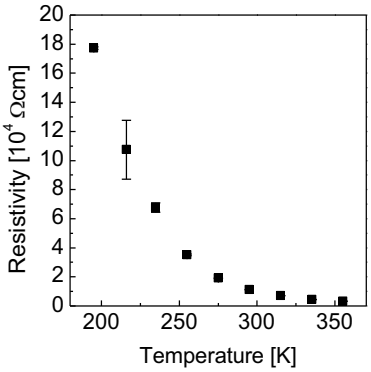

Figure 27 – Temperature dependence of resistivity for a thin film of $Mg_{2.17}NiH_x$ prepared by reactive sputtering at TU Delft.

4.4 Chemical stability under ambient conditions

The films of Mg-Ni-H were found to be stable under ambient conditions. Chapter 3 (Figure 18) and the Papers V and VI demonstrate RBS measurements on films that had been stored unprotected at ambient conditions. The measurements showed that not much more than 1% O was present in the bulk of the film in the case of $Mg_{\sim 2}NiH_{\sim 4}$. The films were also surprisingly resistant towards heat treatment, as demonstrated by the possibility to crystallize the films in air under heating of up to 250 ºC, apparently with little loss of H. If further heated, dehydrogenation was

triggered around 300 ºC in air. In vacuum, $Mg_{\sim 2}NiH_{\sim 4}$ films were found to dehydrogenate at 200-240 ºC. However, even though the films do not completely oxidize or decompose at temperatures below 200 ºC, permanent changes in the optical and electrical properties were observed even for treatment at lower temperatures of only 50 ºC. This has to be taken into consideration if the material is to be used as a semiconductor in technological applications.

4.5 The prospects of $Mg_{\sim 2}NiH_{\sim 4}$ for PV applications

Thin-film solar cells based on Mg-Ni-H would constitute an alternative technology to the thin-film solar cells of today's market, free of scarce elements as In and Te. It has unfortunately not been possible in this work to demonstrate a working PV device based on Mg_2NiH_4. However, the experiments that have been carried out within the project have not revealed any concrete barriers with regards to this application of the material.

On one hand, our experiments have showed that it is relatively simple to obtain Mg-Ni-H films with a band gap that is interesting for utilization in a single band gap solar cell. The band gap we have found (1.6 eV for Mg_2NiH_4) is close to the optimal value for a single-band-gap solar cell (see Figure 4). The optical and electrical properties discussed in Paper V and VI are also promising, due to strong optical absorption and reasonable electrical resistivity. It is possible to deposit Mg_2NiH_4 using reactive sputtering, a method which is suitable for industrial large area processing. The resulting films are found to be stable against oxidation at ambient conditions, and no phase segregation was observed for $Mg_{\sim 2}NiH_{\sim 4}$ by XRD. Phase segregation is a well-known problem in other alternative semiconductor materials for solar cells, as e. g. in CZTS [120]

and CuO [121]. All these factors are promising with regards to the application of $Mg_{\sim 2}NiH_{\sim 4}$ for solar cells.

On the other hand, we do still not have control over the electrical properties. We do not know the polarity and doping of the as-deposited material, or how to modify the electrical properties by impurities. The fact that the compound is amorphous in the as-deposited form might be a draw-back, but not necessarily. The crystalline form that can be obtained by annealing the samples has a too high band gap to be interesting as an absorber material for PV applications.

With the current information, we can therefore not make any estimations about the feasibility and possible ultimate performance of a $Mg_{\sim 2}NiH_{\sim 4}$-based PV device. This would depend on material characteristics that have not yet been examined, and the type of device to be made. There are many options for making a PV device, including for example homo-junction and hetero-junction devices, as demonstrated in Figure 3 (page 7) for two existing PV technologies.

In sum, there still remains substantial work in order to understand and control the electrical properties and design a working PV device based on $Mg_{\sim 2}NiH_{\sim 4}$.

5 Photochromism in yttrium hydride

Our discovery of photochromic effect in T-YH_x films introduced something new in metal hydride science. It has also given a new contribution to the limited number of known inorganic photochromic materials.

Photochromism – the change of color upon illumination of a material – was actually reported for YH_x in 2007, in a high-pressure experiment performed by Ohmura and his coworkers at the Japanese Synchrotron Radiation Center [99]. Another relevant finding was that of the group of Rosenbaum at the University of Chicago, who found persistent photoconductivity in YH_x at temperatures of up to 10 K [100]. The work of these two groups put our findings in a context and provide a background for the discussion of the phenomenon (see Section 1.6.2 for more details). The discovery of photochromism of thin T-YH_x films at ambient conditions and with moderate light intensity has brought the phenomenon closer to technological relevance and eases the study of the effect, avoiding high pressure and cryogenic temperatures.

5.1 Optical properties of the transparent state

The optical properties of the non-illuminated, transparent state of T-YH_x were investigated by optical ellipsometry. The real part n of the complex refractive index, $\tilde{n} = n + ik$, was found by fitting the obtained optical constants to a Cauchy model for the dielectric function. The complex part k was later estimated by fitting optical transmission and reflection data using the n obtained from ellipsometry. The refractive index obtained for T-YH_x is displayed in Figure 28. The Cauchy model is weaker than the general oscillator model fit done for $Mg_{\sim 2}NiH_{\sim 4}$ in Paper VI, and especially the refraction index for wavelengths below the band gap at ~477

nm (2.6 eV) should be considered slightly speculative. However, the refractive index obtained by this method gives a reasonable fit for the optical transmission and reflection for T-YH_x films, as demonstrated for two different samples in Figure 28.

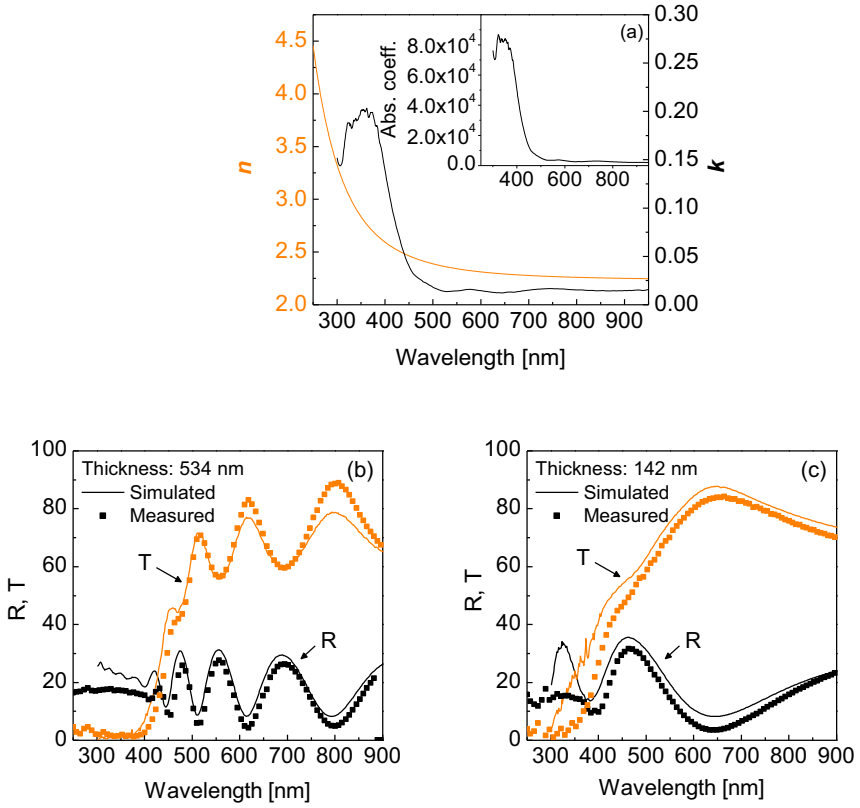

Figure 28 – Optical properties of the transparent state of T-YH_x. (a) The refractive index. (b) and (c) show the fit of the optical reflection and transmission of two T-YH_x samples with thickness of respectively 534 nm and 142 nm, using the refractive index in (a).

5.2 Properties of the photochromic reaction

The photochromic reaction in T-YH_x is described in Paper IV. When a thin film of T-YH_x is illuminated by visible or UV light, it becomes dark-

er, the optical transmission is reduced by up to ~50% after one hour in solar illumination. The reaction is reversible, so the sample will return to its initial transparency if it is left in the dark. The time it takes for complete relaxation depends on the strength and time of the illumination, the temperature of the sample and the sample itself.

The photochromic darkening is accompanied by a decrease in resistivity, as visible in Figure 29. Figure 29 displays the optical transmission and the changes in electrical resistivity for a film illuminated by light from a solar simulator light source. Each illumination cycle of 30 s reduces the optical transmission by approximately 10%. The electrical resistivity is reduced by approximately one order of magnitude by the first illumination, and then by ~75% for each of the following cycles. The relaxation that happens in the dark part of the cycle is substantial, but not complete. Especially for the electrical resistivity one can see that it takes longer time to relax back than it takes to reduce the resistivity under illumination.

The strength and kinetics of the photochromic reaction depends on the light that illuminates the sample. It also depends on the external conditions, as also observed by the earlier reports at high pressure [99] and low temperature [100]. In our experiments, we observed that especially the temperature was central; the relaxation speed was greatly increased by heating to moderate temperatures of 40-50 ºC. For other inorganic photochromic materials, the chemical ambient is also of great importance for the photochromic reaction. Gavrilyuk et al. have e.g. reported on the effect of air humidity on the photochromic response of MoO_3 films [122]. The effect of chemical environment has not been thoroughly studied for T-YH_x films in this work.

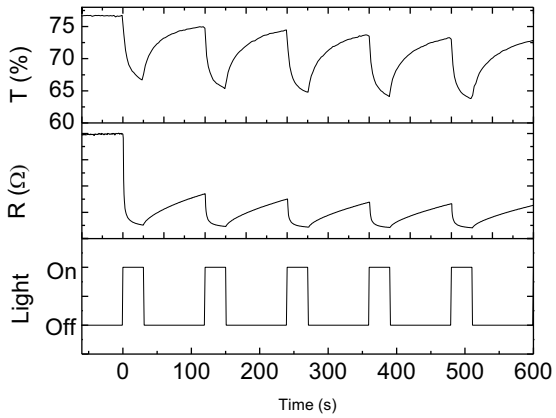

Figure 29 – Optical transmission and changes in electrical resistivity for a thin film of 500 thick sample of T-YH_x exposed to light from the solar simulator.

In addition to the external factors, the nature of the sample itself plays a large role for the kinetics and strength of the photochromic reaction. The film thickness and O content are important parameters. The time after deposition and the illumination history of the sample also affects the photochromic reaction. A conclusive study of how these different factors affect the photochromic reaction has not yet been performed.

The role of oxygen and the fcc crystal structure

As discussed in Paper III, the crystal structure of the T-YH_x films differed from the hcp structure which is normally expected for transparent YH_3. We believe that the O that is incorporated during deposition in the reactive sputtering process (see Chapter 3) is important for the photochromic reaction. Whether the role of the O is primary, as an active species in the electronic change of the material, or only secondary, as a stabilizer of the fcc lattice, is not known. Anyway, it is a fact that photo-

chromic reaction at ambient conditions never has been observed in films of low-O YH_3 in the hcp structure.

Figure 30 shows the transmission spectra before and after illumination for 30 minutes by a strong light probe, for a film deposited at IFE and films prepared by hydrogenation of Pd-capped Y and by reactive sputtering at TU Delft. It shows that while photochromism was observed for both of the reactively deposited samples, the hydrogenated sample did not show any significant change in the transmission. There is also a large difference in the reaction strength between the reactively deposited samples from IFE and TU Delft, which might have to do with the large difference in thickness and a potential difference in the O content. While the reactively deposited samples exhibited an fcc lattice, the hydrogenated is

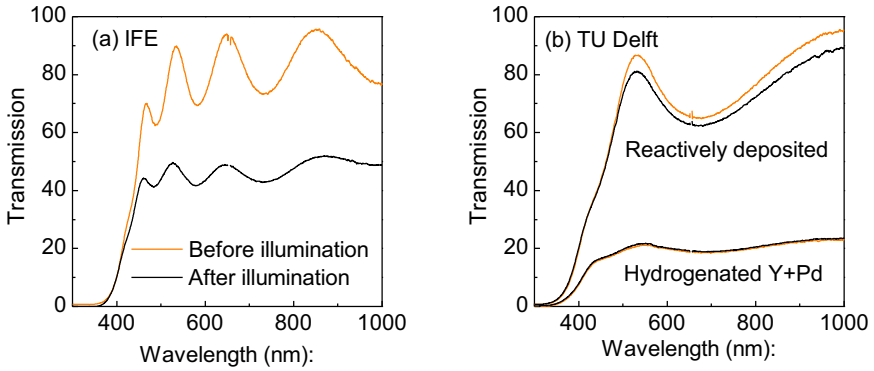

Figure 30 – Optical transmission spectra before and after 30 minutes of illumination. The illumination used here is the same as the light probe used for transmission measurements. (a) For a ~600 nm thick sample prepared at IFE. (b) For samples prepared at TU Delft; a ~230 nm thick reactively deposited sample and a ~200 nm thick hydrogenated Y sample with ~10 nm Pd capping.

assumed to exhibit the hcp structure as the synthesis method is well known and so far only hcp-YH_3 has been reported to form by using this method[17].

The physical mechanisms

The possible physical mechanisms of the photochromic reaction have been discussed in section 3.3 of Paper IV. At present, the mechanism is still unknown. It is obvious to compare with the gasochromic transition of YH_x films between transparent and opaque [26], but it seems improbable that there should be a reversible exchange of H with the ambient at normal conditions, especially with an oxide layer protecting the film from the external environment (as demonstrated in Paper VII). Another parallel that could be discussed is the photochromism of other compounds in thin films, as the transition metal oxides WO_3 and MoO_3. The mechanisms in these compounds have been studied thoroughly, and are reasonably well understood [21], [123]. However, the reaction characteristics of T-YH_x differs from that of the transition metal oxides in many aspects, so there is little reason to believe that the same mechanisms are active in T-YH_x.

In a recent and yet unpublished study, we performed time-resolved synchrotron diffraction under illumination of T-YH_x films at the SNBL at ESRF in Grenoble. We found a contraction of the lattice, as a response to both the X-ray beam itself and the illumination applied. Figure 31 demonstrates the volume change in as a result of the lattice contraction observed for a sample of T-YH_x exposed to illumination and the X-ray

[17] There is one exception: Hydrogenated films of Pd-capped Y-Mg have been found to exhibit the fcc structure [50].

beam for 3 hours. A lattice contraction was also reported by Ohmura et al. in the finding of photochromism of YH_x at high pressure [99].

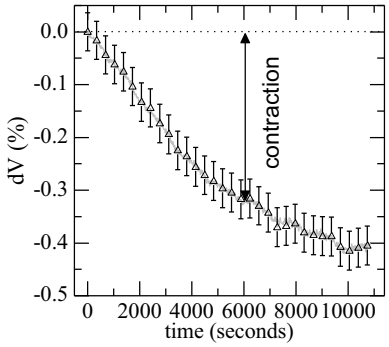

Figure 31 – Lattice contraction of T-YH_x under illumination, studied by time-resolved XRD at the SNBL in Grenoble.

5.3 Smart windows based on photochromic T-YH_x

In the context of solar energy, it is relevant to consider the application of films of T-YH_x in energy-saving smart windows. Films of T-YH_x has a photochromic response to sunlight that reduces the optical transmission, and could therefore be suitable in a window technology for reducing the need for cooling in areas where sunlight gives excessive heating of buildings during daytime (see Section 1.3). The fact that the reduction in transmission is relatively uniform over the visible and near infrared light spectrum is favorable for such applications. It is also reversible and the window would return to the maximum transparency during night or low light conditions. Deposition of films of T-YH_x on large area as in a window is no problem; deposition on large area glass has been demonstrated in this work, as displayed in Figure 32.

There are, however, some important drawbacks of the application of T-YH_x for photochromic windows. One is that the band gap of T-YH_x is within the visible spectrum (~2.6 eV, or ~480 nm, corresponding to blue light), giving the films have a yellow appearance. That could reduce the comfort for users of the building and might limit the application of such windows to areas where such a tint would be desirable as a part of the architecture. This problem could be solved by applying very thin films that absorb less light and are therefore more color neutral. Another solution could be to produce an alloy with Mg, as the introduction of Mg in YH_3 has been observed to increase the band gap of the hydride [50]. Increasing the O content is another way to increase the band gap of rare-earth hydride, as has been reported for O-containing GdH_x films [124].

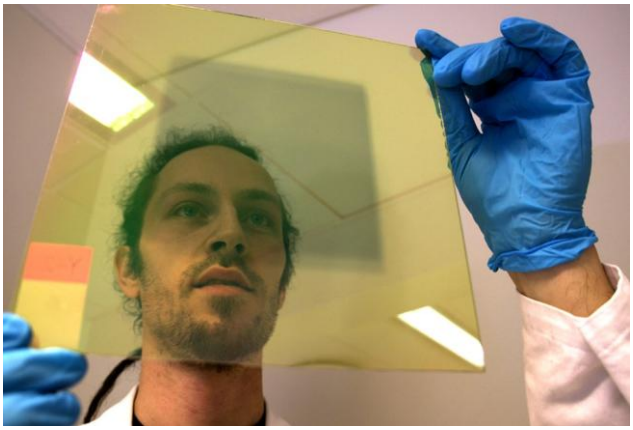

Figure 32 – The author with a sample of a photochromic film of T-YH_x on large area substrate for demonstration of smart photochromic window based on T-YH_x. The dark quadratic field in the center of the sample is a result of 1 h illumination of the corresponding area with the solar simulator. Photo: Arnfinn Christensen/Forskning.no [125].

Another drawback is the speed of the reaction. The darkening of a typical film is not saturated even after several hours of illumination, and the relaxation reaction back to the transparent state could take many hours. Relaxation times of even up to several days were observed for some samples after a day of natural sunlight illumination.

The effect on the energy balance of a building due to a photochromic window with the properties of T-YH_x has not been analyzed in this work. It would be interesting to do an analysis of how such a window would work under typical conditions in a climate where cooling of buildings is a necessity. Together with an assessment of the extra cost that the introduction of a T-YH_x film would give on the fabrication of windows, such an analysis could provide an indication of whether a commercialization of the technology would be feasible.

6 Conclusions

While research on metal hydrides recently has focused mainly on hydrogen storage, battery technology and smart windows, this work demonstrates that other applications of metal hydrides are viable. Many interesting effects and possible applications of these compounds are yet to be revealed. This thesis signals some directions that might be pursued in future research on metal hydrides, with emphasis on applications of thin films in solar energy technology.

Thin-film metal hydride synthesis by reactive sputtering

Reactive sputtering has so far been a relatively unexplored way of synthesizing metal hydrides. This thesis provides a reference point for future work with similar materials. For the different materials synthesized, the following are the most important findings:

- MgH_2 films were deposited by RF reactive sputter deposition, but the formation of some amount of metallic Mg particles could not be avoided.
- Mg-Ni-H films were deposited by reactive co-sputtering of Mg and Ni targets, the resulting films having relatively high purity in the case of $Mg_{\sim 2}NiH_{\sim 4}$. The high purity was demonstrated by high optical transmission for energies below the band gap and the relatively high resistivity. Low content of O was also confirmed by measurements. Films with higher Ni content than $MgNi_2H_x$ did not react with H, and films with more Mg than Mg_3NiH_x formed a mixture of metal hydride and metallic Mg particles. It was observed that the deposition rate of Mg was severely changed by both the introduction of H_2 in the chamber during deposition and the co-deposition

of Ni using H_2-containing gas. On the other hand, the Ni deposition rate was relatively unaffected by both reactive H_2 and co-deposition.

- YH_x films can be synthesized in two very different electronic states, one conducting and optically black state (B-YHx) and one insulating and optically transparent state (T-YH_x). The two states resemble earlier reported results for YH_2 and YH_3, respectively, but it was found that the samples hold a substantial amount of O. The O content was especially high, up to ~1 O atom per Y, for the T-YH_x samples, which also had a different crystal structure than what is known for YH_3. There was no sign of phase segregation in the XRD patterns for any of the YH_x films deposited.

Semiconducting films of magnesium nickel hydride for PV applications

The results obtained here demonstrate that metal hydride films with material properties that are promising for PV applications can be synthesized. Using reactive sputter deposition, we have been able to obtain amorphous $Mg_{\sim 2}NiH_{\sim 4}$ films with a band gap that is suitable for solar cells. Optical measurements by ellipsometry and spectrophotometry showed band gaps in the range 1.5 – 1.8 eV depending on the Mg:Ni ratio in the samples. The electrical properties can be manipulated not only by the Mg:Ni ratio but also by temperature treatment and by changing the temperature or the H_2:Ar ratio during the deposition process. However, at the time of writing this thesis, no proof of a working metal hydride-based solar cell has yet been demonstrated.

The photochromic effect in T-YH$_x$

Films of T-YH$_x$ showed a strong photochromic effect accompanied by persistent changes in the conductivity of the material. The material responds to visible and UV light, but the reaction is strongest for light with photon energy above the band gap (~2.6 eV). The photochromic response gives a uniform reduction in the optical transmission over visible and IR wavelengths. The photochromic reaction is reversible; the material relaxes back to its initial transparent state when left in dark. This is the first report of such an effect in metal hydride films at ambient conditions, even though similar phenomena have been observed earlier at low temperatures and high pressures. Evidence suggests that the fcc crystal structure and/or the O content is essential for the photochromic effect. The physical mechanism of the optical and electrical response has not been resolved, but the properties and the nature of the reaction make it relevant for applications in technology related to e. g. smart windows to regulate solar heating and daylight illumination in buildings.

7 Future work

This thesis has demonstrated two new directions in experimental metal hydride science, focusing on thin-film semiconducting metal hydrides. The results are promising, but the knowledge of the materials is still too scarce to assess the feasibility and performance of metal hydrides in semiconductor devices as solar cells, or in windows or other products incorporating photochromic metal hydrides.

The experience from synthesis and characterization of semiconducting $Mg_{\sim 2}NiH_{\sim 4}$ should be built upon with more detailed studies of the electrical properties of such films. It is central to understand the conduction mechanisms and be able to control them e.g. by impurity doping. When a certain level of control and understanding of the material is achieved, semiconductor devices can be suggested and tested experimentally.

The photochromic effect in T-YH_x should be further pursued in order to understand the physical origin of the photochromic reaction. A good physical understanding might enable us to tune the kinetics and strength of the photochromism and thereby tailor the material for different technological applications. With respect to the application of T-YH_x in photochromic windows, an energy balance study should be carried out to investigate the performance of such technology with respect to relevant alternatives. The feasibility of T-YHx photochromic windows should also be analyzed, in the light of the cost of the production methods and the cost and availability of the raw materials.

There are also important questions remaining with regards to the reactive sputter deposition process. The most puzzling is the O in the T-

YH_x films and which is the source of this O in the reactive sputtering process. Further, the room for variation of gases, pressure and deposition temperature open many opportunities with regards to thin-film metal hydride deposition, of which only a small number of combinations has been investigated in this work. Results have shown that the electrical properties of Mg-Ni-H films are highly dependent on the process, but the relation of the electrical properties with the H and O content and the microstructure of the films has not yet been investigated.

Finally, I would like encourage future studies of reactive sputter deposition of metal hydrides, by investigating the reactive deposition of other hydrides. The material class of the metal hydrides is vast, and most metal hydrides been little investigated in their thin-film form. These materials might demonstrate properties that are highly relevant for application in technologies for PV applications, smart windows or applications that are yet unthought-of.

References

[1] J. Diamond, *Collapse: How Societies Choose to Fail or Succeed*. London: Penguin Books Ltd, 2011, pp. 79-119.

[2] P. M. Vitousek, "Beyond global warming: Ecology and global change," *Ecology*, vol. 75, no. 7, pp. 1861-1876, 1994.

[3] A. Maddison, *Contours of the world economy 1-2030 AD*. Oxford University Press, 2007.

[4] F. Krausmann, S. Gingrich, N. Eisenmenger, K.-H. Erb, H. Haberl, and M. Fischer-Kowalski, "Growth in global materials use, GDP and population during the 20th century," *Ecological Economics*, vol. 68, no. 10, pp. 2696-2705, 2009.

[5] "CDIAC: Online trends - A compendium of data on global change." [Online]. Available: http://cdiac.esd.ornl.gov/trends/co2/contents.htm. [Accessed: 04-May-2012].

[6] F. Fanebust, *Selvbedraget*. Oslo: Pax forlag, 2010.

[7] N. Adger et al., "Summary for Policymakers," in *Climate Change 2007: Impacts, Adaptation and Vulnerability. Contribution of Working Group II to the Fourth Assessment Report of the Intergovernmental Panel on Climate Change*, M. L. Parry, O. F. Canziani, P. J. Palutikof, P. J. van der Linden, and C. E. Hanson, Eds. Cambridge: Cambridge University Press, 2007, pp. 7-22.

[8] S. Solomon et al., Eds., *Climate Change 2007: The Physical Science Basis. Contribution of Working Group I to the Fourth Assessment Report of the Intergovernmental Panel on Climate Change*. Cambridge, UK: Cambridge University Press, 2007.

[9] M. Parry, O. Canziani, J. Palutikof, P. van der Linden, and C. Hanson, Eds., *Climate Change 2007: Impacts, Adaptation and Vulnerability. Contribution of Working Group II to the Fourth Assessment Report of the Intergovernmental Panel on Climate Change*. Cambridge, UK: Cambridge University Press, 2007.

[10] "IEA: Key World Energy Statistics," 2011.

[11] "Wikimedia commons: Rendered spectrum." [Online]. Available: http://commons.wikimedia.org/wiki/File:Rendered_Spectrum.png. [Accessed: 04-May-2012].

[12] T. Markvart and L. Castaner, *Solar cells: materials, manufacture and operation*. Elsevier, 2004.

[13] "First solar passes $1 per watt industry milestone," 2009. [Online]. Available: http://investor.firstsolar.com/releasedetail.cfm?ReleaseID=571539 . [Accessed: 22-Mar-2012].

[14] V. Fthenakis, "Sustainability of photovoltaics: The case for thin-film solar cells," *Renewable and Sustainable Energy Reviews*, vol. 13, no. 9, pp. 2746-2750, 2009.

[15] M. A. Green, K. Emery, Y. Hishikawa, W. Warta, and E. D. Dunlop, "Solar cell efficiency tables (version 39)," *Progress in photovoltaics*, vol. 20, pp. 12-20, 2012.

[16] W. Shockley and H. J. Queisser, "Detailed balance limit of efficiency of p-n junction solar cells," *Journal of Applied Physics*, vol. 32, no. 3, pp. 510-519, 1961.

[17] M. A. Green, *Solar cells*. Longman Higher Education, 1982.

[18] L. Pérez-Lombard, J. Ortiz, and C. Pout, "A review on buildings energy consumption information," *Energy and Buildings*, vol. 40, no. 3, pp. 394-398, 2008.

[19] C. G. Granqvist, S. Green, G. A. Niklasson, N. R. Mlyuka, S. von Kræmer, and P. Georén, "Advances in chromogenic materials and devices," *Thin Solid Films*, vol. 518, no. 11, pp. 3046-3053, 2010.

[20] S. S. Kanu and R. Binions, "Thin films for solar control applications," *Proceedings of the Royal Society A: Mathematical, Physical and Engineering Sciences*, vol. 466, no. 2113, pp. 19-44, 2010.

[21] C. G. Granqvist, *Handbook of electrochromic materials*. Amsterdam: Elsevier, 1995.

[22] V. Wittwer, M. Datz, J. Ell, A. Georg, W. Graf, and G. Walze, "Gasochromic windows," *Solar Energy Materials and Solar Cells*, vol. 84, no. 1–4, pp. 305-314, 2004.

[23] L. Schlapbach and A. Züttel, "Hydrogen-storage materials for mobile applications," *Nature*, vol. 414, pp. 353-358, 2001.

[24] B. Sakintuna, F. Lamaridarkrim, and M. Hirscher, "Metal hydride materials for solid hydrogen storage: A review," *International Journal of Hydrogen Energy*, vol. 32, no. 9, pp. 1121-1140, 2007.

[25] E. M. Gray, C. J. Webb, J. Andrews, B. Shabani, P. J. Tsai, and S. L. I. Chan, "Hydrogen storage for off-grid power supply," *International Journal of Hydrogen Energy*, vol. 36, no. 1, pp. 654-663, 2011.

[26] J. N. Huiberts et al., "Yttrium and lanthanum hydride films with switchable optical properties," *Nature*, vol. 380, pp. 231-234, 1996.

[27] I. P. Jain, C. Lal, and A. Jain, "Hydrogen storage in Mg: A most promising material," *International Journal of Hydrogen Energy*, vol. 35, no. 10, pp. 5133-5144, 2010.

[28] "McPhy Energy - The technology." [Online]. Available: http://www.mcphy.com/en/hydrogen-storage/mcphy-technology.php. [Accessed: 18-May-2012].

[29] J. Isidorsson, I. A. M. E. Giebels, H. Arwin, and R. Griessen, "Optical properties of MgH2 measured in situ by ellipsometry and spectrophotometry," *Physical Review B*, vol. 68, p. 115112, 2003.

[30] R. J. Westerwaal, C. P. Broedersz, R. Gremaud, M. Slaman, A. Borgschulte, and W. Lohstroh, "Study of the hydride forming process of in-situ grown MgH2 thin films by activated reactive evaporation," *Thin Solid Films*, vol. 516, pp. 4351 - 4359, 2008.

[31] T. Richardson, J. L. Slack, R. D. Armitage, R. Kostecki, B. Farangis, and M. D. Rubin, "Switchable mirrors based on nickel–magnesium films," *Applied Physics Letters*, vol. 78, no. 20, p. 3047, 2001.

[32] H. W. King, "Crystal structures and lattice parameters of allotropes of the elements," in *CRC Handbook of Chemistry and Physics*, 92nd–Inter ed., W. M. Haynes, Ed. 2011.

[33] F. Ellinger et al., "The preparation and some properties of Magnesium Hydride," *Journal of the American Chemical Society*, vol. 77, p. 2647, 1955.

[34] "Springer Materials - The Landolt-Börnstein database." [Online]. Available: www.springermaterials.com.

[35] G. Aylward and T. Findlay, *SI Chemical Data*, 5th ed. John Wiley and Sons Australia, 2002.

[36] O. E. Taurian, M. Springborg, and N. E. Christensen, "Self-consistent electronic structures of MgO and SrO," *Solid State Communications*, vol. 55, no. 4, pp. 351-355, 1985.

[37] L. Kumari, W. Z. Li, C. H. Vannoy, R. M. Leblanc, and D. Z. Wang, "Synthesis, characterization and optical properties of Mg(OH)2 micro-/nanostructure and its conversion to MgO," *Ceramics International*, vol. 35, no. 8, pp. 3355-3364, 2009.

[38] D. Noreus and L. Kihlborg, "Twinning at the unit cell level in the low temperature phase of Mg2NiH4 studied by electron microscopy," *Journal of the Less Common Metals*, vol. 123, no. 1–2, pp. 233-239, 1986.

[39] M. Lelis et al., "A mechanically switchable metal–insulator transition in Mg2NiH4 discovers a strain sensitive, nanoscale modulated resistivity connected to a stacking fault," *Journal of Alloys and Compounds*, vol. 496, no. 1–2, pp. 81-86, 2010.

[40] K. Yvon, J. Schefer, and F. Stucki, “Structural studies of the Hydrogen Storage Material Mg2NiH4. 1. Cubic High-Temperature Structure,” *Inorganic Chemistry*, vol. 20, pp. 2776-2778, 1981.

[41] R. J. Westerwaal et al., “Optical, structural, and electrical properties of Mg2NiH4 thin films in situ grown by activated reactive evaporation,” *Journal of Applied Physics*, vol. 100, p. 063518, 2006.

[42] H. Zhang, X. L. Wang, Y. Q. Qiao, X. H. Xia, and J. P. Tu, “Microstructure, hydrogenation and optical behavior of Mg–Ni multilayer films deposited by magnetron sputtering,” *Applied Surface Science*, vol. 257, no. 13, pp. 5759-5765, 2011.

[43] D. Lupu, R. Sârbu, and A. Biriş, “Semiconducting properties of Mg2NiH4,” *International Journal of Hydrogen Energy*, vol. 12, no. 6, pp. 425-426, 1987.

[44] T. Hirata, T. Matsumoto, M. Amano, and Y. Sasaki, “In situ X-ray diffractometry study of the hydride in the intermetallic compound Mg2Ni,” *Journal of Physics F*, vol. 11, pp. 521-529, 1981.

[45] P. Zolliker, K. Yvon, J. D. Jorgensen, and F. J. Rotella, “Structural studies of the hydrogen storage material Mg2NiH4. 2. Monoclinic low-temperature structure,” *Inorganic Chemistry*, vol. 25, pp. 3590-3593, 1986.

[46] M. Y. Song, “Phase separation of Mg2Ni by hydriding–dehydriding cycling,” *Journal of Alloys and Compounds*, vol. 282, pp. 297-301, 1999.

[47] J. J. Reilly and R. H. Wiswall, “The reaction of hydrogen with alloys of magnesium and nickel and the formation of Mg2NiH4,” *Inorganic Chemistry*, vol. 7, no. 11, pp. 2254-2256, 1968.

[48] P. Vadja, “Hydrogen in rare-earth metals, including RH(2+x) phases,” in *Handbook on the Physics and Chemistry of Rare Earths*, 20th ed., K. A. Gschneider and L. Eyring, Eds. North-Holland, 1995, p. 207.

[49] A. T. M. van Gogh et al., "Structural , electrical , and optical properties of La(1-z)Y(z)H(x) switchable mirrors," *Physical Review B*, vol. 63, p. 195105, 2001.

[50] S. J. van der Molen et al., "Insulating fcc YH(3-δ) stabilized by MgH2," *Physical Review B*, vol. 63, no. 23, p. 235116, 2001.

[51] F. H. Spedding, A. H. Daane, and K. W. Herrmann, "The crystal structures and lattice parameters of high-purity scandium, yttrium and the rare earth metals," *Acta Crystallographica*, vol. 9, pp. 559-563, 1956.

[52] Y. Xu, "Electronic, structural, and optical properties of crystalline yttria," *Physical Review B*, vol. 56, no. 23, pp. 993-1000, 1997.

[53] G. W. Beall, W. O. Milligan, and H. A. Wolcott, "Structural trends in the lanthanide trihydroxides," *Journal of Inorganic and Nuclear Chemistry*, vol. 39, no. 1, pp. 65-70, 1977.

[54] E. S. Kooij, A. T. M. V. Gogh, D. G. Nagengast, N. J. Koeman, and R. Griessen, "Hysteresis and the single-phase metal-insulator transition in switchable YH x films," *Physical Review B*, vol. 62, no. 15, pp. 10088-10100, 2000.

[55] I. I. Diakonov, "Standard thermodynamic properties and heat capacity equations of rare earth hydroxides : and Y-hydroxides . Comparison of thermochemical and solubility data," 1998.

[56] S. Zhang and R. Xiao, "Yttrium oxide films prepared by pulsed laser deposition," *Journal of Applied Physics*, vol. 83, no. 7, p. 3842, 1998.

[57] F. D. Quarto, M. C. Romano, M. Santamaria, S. Piazza, and C. Sunseri, "A semiempirical correlation between the optical band gap of hydroxides and the electronegativity of their constituents," *Russian Journal of Electrochemistery*, vol. 36, no. 11, pp. 1358-1364, 2000.

[58] D. Depla and S. Mahieu, *Reactive Sputter Deposition*. Berlin Heidelberg: Springer-Verlag Berlin Heidelberg, 2008.

[59] K. Koski, J. Hölsä, and P. Juliet, "Properties of aluminium oxide thin films deposited by reactive magnetron sputtering," *Thin Solid Films*, vol. 339, pp. 240-248, 1999.

[60] J. E. Gerbi and J. R. Abelson, "Deposition of microcrystalline silicon: Direct evidence for hydrogen-induced surface mobility of Si adspecies," *Journal of Applied Physics*, vol. 89, no. 2, p. 1463, 2001.

[61] M. A. Pick, J. W. Davenport, M. Strongin, and G. J. Dienes, "Enhancement of hydrogen uptake rates for Nb and Ta by thin surface overlayers," *Physical Review Letters*, vol. 43, no. 4, pp. 286-289, 1979.

[62] A. E. Curzon and O. Singh, "Thin film studies of yttrium, yttrium hydrides and yttrium oxide," *Journal of Physics F*, vol. 8, no. 8, p. 1619, 1978.

[63] B. Dam, A. C. Lokhorst, A. Remhof, J. H. Rector, D. Borsa, and J. W. J. Kerssemakers, "In situ preparation of YH2 thin films by PLD for switchable devices," *Journal of Alloys and Compounds*, vol. 356–357, pp. 526-529, 2003.

[64] C. Eibl, G. Lackner, and A. Winkler, "Quantitative characterization of a highly effective atomic hydrogen doser," *Journal of Vacuum Science Technology A Vacuum Surfaces and Films*, vol. 16, no. 5, pp. 2979-2989, 1998.

[65] H. Chatbi, M. Vergnat, and G. Marchal, "Thermal stability of titanium hydride thin films," *Applied Physics Letters*, vol. 64, no. 10, p. 1210, 1994.

[66] J. Hayoz et al., "Preparation and characterization of clean, single-crystalline YHx," *Journal of Vacuum Science and Technology A*, vol. 18, no. 5, pp. 2417-2431, 2000.

[67] M. Mâaza, B. Farnoux, and F. Samuel, "Study of the hydrogen diffusion in superlattices by grazing angle neutron reflectometry," *Physics Letters A*, vol. 181, pp. 245-250, 1993.

[68] S. Nakao et al., “Preparation and optical transmittance of titanium hydride (deuteride) films by rf reactive sputtering,” *Thin Solid Films*, vol. 343–344, pp. 195-198, 1999.

[69] G. Meunier, J. Manaud, and P. Grall, “Synthesis and characterization of titanium hydride thin films obtained by reactive cathodic sputtering,” *Materials Science and Engineering: B*, vol. 18, no. 3, pp. 303-307, 1993.

[70] G. B. Thompson and D. D. Allred, “Reactive gas magnetron sputtering of lithium hydride and lithium fluoride thin films,” *Journal of X-ray science and technology*, vol. 7, no. 2, pp. 159-170, 1997.

[71] P. V. D. Sluis and V. M. M. Mercier, “Solid state Gd-Mg electrochromic devices with ZrO2Hx electrolyte,” *Electrochimica Acta*, vol. 46, pp. 2167- 2171, 2001.

[72] M. Filippi, J. H. Rector, M. J. V. Setten, B. Dam, R. Gremaud, and M. J. van Setten, “Lightweight sodium alanate thin films grown by reactive sputtering,” *Applied Physics Letters*, vol. 95, no. 12, p. 121904, 2009.

[73] M. Gonzalez-Silveira et al., “In-situ deposition of alkali and alkaline earth hydride thin films to investigate the formation of reactive hydride composites,” *Journal of Physical Chemistery C*, vol. 114, pp. 13895-13901, 2010.

[74] S. Singh, S. W. H. Eijt, M. W. Zandbergen, W. J. Legerstee, and V. L. Svetchnikov, “Nanoscale structure and the hydrogenation of Pd-capped magnesium thin films prepared by plasma sputter and pulsed laser deposition,” *Journal of Alloys and Compounds*, vol. 441, pp. 344-351, 2007.

[75] I. J. T. Jensen et al., “X-ray photoelectron spectroscopy study of MgH2 thin films grown by reactive sputtering,” *Surface and Interface Analysis*, vol. 42, no. 6–7, pp. 1140-1143, 2010.

[76] D. P. Adams, J. A. Romero, M. A. Rodriguez, J. A. Floro, and P. G. Kotula, “SAND2002-1466 Microstructures, phase formation, and stress of reactively-deposited metal hydride thin films,” 2002.

[77] S. Z. Karazhanov, A. G. Ulyashin, P. Ravindran, and P. Vajeeston, "Semiconducting hydrides," *EPL*, vol. 82, p. 17006, 2008.

[78] S. Z. Karazhanov, P. Ravindran, P. Vajeeston, and A. G. Ulyashin, "Hydride electronics," *Physica Status Solidi A*, vol. 204, no. 10, pp. 3538 - 3544, 2007.

[79] A. G. Ulayshin, S. Z. Karazhanov, and A. Holt, "Semiconducting component," U.S. Patent US 2010/0319760 A12010.

[80] S. Z. Karazhanov, A. G. Ulyashin, P. Vajeeston, and P. Ravindran, "Hydrides as materials for semiconductor electronics," *Philosophical Magazine*, vol. 88, pp. 2461-2476, 2008.

[81] S. Z. Karazhanov and A. G. Ulyashin, "Similarity of electronic structure and optical properties of Mg2NiH4 and Si," *EPL*, vol. 82, p. 48004, 2008.

[82] A. C. Lokhorst, "Reflections on Switchable Mirror Devices," Vrije Universiteit, Amsterdam, 2006.

[83] J. N. Huiberts et al., "Synthesis of yttriumtrihydride films for ex-situ measurements," *Journal of Alloys and Compounds*, vol. 239, pp. 158-171, 1996.

[84] S. Enache, W. Lohstroh, and R. Griessen, "Temperature dependence of magnetoresistance and Hall effect in Mg2NiHx films," *Physical Review B*, vol. 69, no. 11, p. 115326, 2004.

[85] R. C. Heckmann, "Conductivity and Hall effect in cerium dihydride," *Journal of Chemical Physics*, vol. 46, no. 6, pp. 2158-2161, 1967.

[86] G. F. Brown and J. Wu, "Third generation photovoltaics," *Laser & Photonics Review*, vol. 3, no. 4, pp. 394-405, 2009.

[87] H. Blomqvist and D. Noreus, "Mechanically reversible conductor–insulator transition in Mg2NiH4," *Journal of Applied Physics*, vol. 91, no. 8, p. 5141, 2002.

[88] R. Gremaud, J. L. M. V. Mechelen, H. Schreuders, M. Slaman, B. Dam, and R. Griessen, "Structural and optical properties of Mg(y)N(1–y)H(x) gradient thin films in relation to the as-deposited metallic state," *International Journal of Hydrogen Energy*, vol. 34, pp. 8951-8957, 2009.

[89] B. Sopori et al., "Hydrogen in silicon: A discussion of diffusion and passivation mechanisms," *Solar Energy Materials and Solar Cells*, vol. 41–42, pp. 159-169, 1996.

[90] C. G. van de Walle and J. Neugebauer, "Hydrogen in semiconductors," *Annual Review of Materials Research*, vol. 36, no. 1, pp. 179-198, 2006.

[91] J. Nelson, *The Physics of Solar Cells*. Imperial College Press, 2003, pp. 190-193.

[92] K. Tajima, Y. Yamada, S. Bao, M. Okada, and K. Yoshimura, "Optical switching properties of all-solid-state switchable mirror glass based on magnesium–nickel thin film for environmental temperature," *Solar Energy Materials and Solar Cells*, vol. 94, no. 2, pp. 227-231, 2010.

[93] Y. Yamada, H. Sasaki, K. Tajima, M. Okada, and K. Yoshimura, "Optical switching properties of switchable mirrors based on Mg alloyed with alkaline-earth metals," *Solar Energy Materials and Solar Cells*, pp. 1-3, 2011.

[94] S. Bao, Y. Yamada, K. Tajima, P. Jin, M. Okada, and K. Yoshimura, "Switchable mirror based on Mg – Zr – H thin films," *Journal of Alloys and Compounds*, vol. 513, pp. 495-498, 2012.

[95] K. Yoshimura, K. Tajima, Y. Yamada, and M. Okada, "Stress in switchable mirror thin film resulting from gasochromic switching," *Japanese Journal of Applied Physics*, vol. 49, no. 7, p. 075701, 2010.

[96] K. Tajima, H. Hotta, Y. Yamada, M. Okada, and K. Yoshimura, "Accelerated test on electrochromic switchable mirror based on magnesium alloy thin film in simulated environment of various

relative humidities," *Solar Energy Materials and Solar Cells*, vol. 99, pp. 76-83, 2012.

[97] R. J. Westerwaal et al., "Thin film based sensors for a continuous monitoring of hydrogen concentrations," *Sensors and Actuators B: Chemical*, vol. 165, no. 1, pp. 88-96, 2012.

[98] K. Yoshimura, Y. Yamada, M. Okada, M. Tazawa, and P. Jin, "Room-temperature hydrogen sensor based on Pd-capped Mg2Ni thin film," *Japanese Journal of Applied Physics*, vol. 43, no. No. 4B, p. L507-L509, 2004.

[99] A. Ohmura, A. Machida, T. Watanuki, K. Aoki, S. Nakano, and K. Takemura, "Photochromism in yttrium hydride," *Applied Physics Letters*, vol. 91, p. 151904, 2007.

[100] A. F. T. Hoekstra, A. S. Roy, T. F. Rosenbaum, R. Griessen, R. J. Wijngaarden, and N. J. Koeman, "Light-induced metal-insulator transition in a switchable mirror," *Physical Review Letters*, vol. 86, no. 23, pp. 5349-5352, 2001.

[101] D. Borsa et al., "Mg–Ti–H thin films for smart solar collectors," *Applied Physics Letters*, vol. 88, no. 24, p. 241910, 2006.

[102] S. Licht, B. Wang, T. Soga, and M. Umeno, "Light invariant, efficient, multiple band gap AlGaAs/Si/metal hydride solar cell," *Applied Physics Letters*, vol. 74, no. 26, p. 4055, 1999.

[103] B. Wang, S. Licht, T. Soga, and M. Umeno, "Stable cycling behavior of the light invariant AlGaAs / Si / metal hydride solar cell," *Solar Energy Materials and Solar Cells*, vol. 64, pp. 311-320, 2000.

[104] T. Kuji, T. Honjo, M. Chiba, T. Nobuki, and J.-C. Crivello, "Development of new transparent conductive material of Mg(OH)2-C," *e-Journal of Surface Science and Nanotechnology*, vol. 6, pp. 15-16, 2008.

[105] T. Honjo, M. Chiba, T. Nobuki, and T. Kuji, "Development of transparent conductive material of Mg(OH)2-C by magnetron

sputtering," in *Supplemental proceedings: Volume 3: General paper selections (The Minerals, Metals & Materials Society 2011)*, 2011, vol. 29, no. 9, pp. 532-536.

[106] "Operating instructions - A550V7," 2008.

[107] E. Palik, *Handbook of optical constants of solids*. Elsevier, 1998.

[108] D. K. Schroeder, *Materials characterization*. Hoboken, New Jersey: John Wiley and Sons, 2006, pp. 2-9.

[109] H. M. Rietveld, "A profile refinement method for nuclear and magnetic structures," *Journal of Applied Crystallography*, vol. 2, no. 2, pp. 65-71, 1969.

[110] T. Sajavaara and K. Arstila, "Thin film characterization using MeV ion beams," in *Ion beams in nanoscience and technology*, R. Hellborg, H. J. Whitlow, and Y. Zhang, Eds. Berlin, Heidelberg: Springer Berlin Heidelberg, 2010, pp. 171-183.

[111] M. Mayer, "SIMNRA User's Guide (Report IPP 9/113)," Garching, Germany, 1997.

[112] W. A. Lanford, H. P. Trautvetter, J. F. Ziegler, and J. Keller, "New precision technique for measuring the concentration versus depth of hydrogen in solids," *Applied Physics Letters*, vol. 28, pp. 566-568, 1976.

[113] J. Daillant and A. Gibaud, Eds., *X-ray and neutron reflectivity*. Springer-Verlag Berlin Heidelberg, 2009.

[114] F. Cousin, F. Ott, F. Gibert, and A. Menelle, "EROS II: A boosted time-of-flight reflectometer for multi-purposes applications at the Laboratoire Léon Brillouin," *The European Physical Journal Plus*, vol. 126, no. 11, 2011.

[115] W. D. Sproul, D. J. Christie, and D. C. Carter, "Control of reactive sputtering processes," *Thin Solid Films*, vol. 491, pp. 1 - 17, 2005.

[116] D. Depla, S. Heirwegh, S. Mahieu, J. Haemers, and R. De Gryse, "Understanding the discharge voltage behavior during reactive sputtering of oxides," *Journal of Applied Physics*, vol. 101, no. 1, p. 013301, 2007.

[117] R. Gremaud, "Hydrogenography," Vrije University Amsterdam, 2008.

[118] T. Richardson et al., "X-Ray absorption spectroscopy of transition metal–magnesium hydride thin films," *Journal of Alloys and Compounds*, vol. 356–357, pp. 204-207, 2003.

[119] R. A. Street, *Hydrogenated amorphous silicon*. Cambridge: Cambridge University Press, 1991, pp. 245-246.

[120] C. Platzer-Björkman, J. Scragg, H. Flammersberger, T. Kubart, and M. Edoff, "Influence of precursor sulfur content on film formation and compositional changes in Cu2ZnSnS4 films and solar cells," *Solar Energy Materials and Solar Cells*, vol. 98, pp. 110-117, 2012.

[121] V. F. Drobny and D. L. Pulfrey, "Properties of reactively-sputtered copper oxide thin films," *Thin Solid Films*, vol. 61, pp. 89-98, 1979.

[122] A. Gavrilyuk, U. Tritthart, and W. Gey, "The nature of the photochromism arising in the nanosized MoO3 films," *Solar Energy Materials and Solar Cells*, vol. 95, no. 7, pp. 1846-1851, 2011.

[123] T. He and J. N. Yao, "Photochromism of molybdenum oxide," *Journal of Photochemistry and Photobiology C: Photochemistry Reviews*, vol. 4, no. 2, pp. 125-143, 2003.

[124] A. Miniotas, B. Hjörvarsson, L. Douysset, and P. Nostell, "Gigantic resistivity and band gap changes in GdO(y)H(x) thin films," *Applied Physics Letters*, vol. 76, no. 15, p. 2056, 2000.

[125] A. Christensen, “Forskning.no > Formørknings-mysteriet.” [Online].
Available: http://www.forskning.no/artikler/2012/februar/314552.
[Accessed: 28-Feb-2012].

Paper I

Reactive sputtering of magnesium hydride thin films for photovoltaic applications

Popular summary

How can MgH_2 be utilized in solar cells? MgH_2 is an insulator which would be transparent in its pure form, like e.g. glass or ice. Because it is an insulator, it cannot constitute the main part of a solar cell, but can be used as a transparent layer in a solar cell device. However, the existence of metallic particles in the deposited films makes the films appear only partly transparent. In this paper, usage of MgH_2 as a surface passivation film for silicon solar cells is explored. The hydrogen in the films could possibly be beneficial for the silicon material, resulting in higher efficiency of silicon solar cells. Our experiments did however not show any proof of such positive effects on the silicon material.

Context

This was the first paper of our group concerning an experimental study on metal hydride films. We chose to start with MgH_2 because it is a simple, well-known and reasonably stable compound. In this phase of the work we were concentrating on the deposition process and it was not at all certain that we would be able to make magnesium hydride films by using reactive sputtering. We were therefore pleased to observe that MgH_2 indeed did form.

Mater. Res. Soc. Symp. Proc. Vol. 1210 © 2010 Materials Research Society 1210-Q03-15

Reactive sputtering of magnesium hydride thin films for photovoltaic applications

C. Platzer-Björkman[1,2], T. Mongstad[1], S. Karazhanov[1], J.P. Mæhlen[1], E. Marstein[1], and A. Holt[1]

[1]Institute for Energy Technology, NO-2027 Kjeller, Norway
[2]Uppsala University, Solid State Electronics, Box 534, SE-751 21 Uppsala
Ph: +47-63606463, email: charlotte.platzer@angstrom.uu.se

ABSTRACT

Deposition of MgH_x (MgH_2 + Mg) thin films is performed using RF reactive sputtering in argon-hydrogen plasma. Films are characterized using x-ray diffraction (XRD), scanning electron microscopy, optical and resistivity measurements. Formation of crystalline MgH_2 is confirmed by XRD, but the formation of some metallic Mg in the films could not be avoided. Increased H/Mg ratio by deposition at high hydrogen flow or high total pressure gives films that oxidize within days or weeks. Deposition at elevated substrate temperature results in improved crystallinity and stability. Initial studies of MgH_x for silicon surface passivation are presented.

INTRODUCTION

Metal hydride materials have been thoroughly studied for hydrogen storage, battery and switchable windows applications. In these cases low stability is an important requirement, as it enables hydrogenation/ dehydrogenation at reasonable temperatures and pressures. Due to the insulating or semiconducting nature of many metal hydrides, they were recently proposed for application in photovoltaic devices [1]. The high hydrogen content in these materials could possibly be beneficial for passivation in silicon-based devices and also used as antireflective coating. Another possibility, based on the suitable and large span of band gap energies for the metal hydride material group, could be hydride-based multijunction devices. Both applications would require stable materials as well as favorable electrical and optical properties.

MgH_2 is an insulator with a band gap of 5.6 eV [2] that has been studied for hydrogen storage purposes due to the light weight, high hydrogen content and large availability of Mg. However, the hydrogenation and dehydrogenation processes are slow, in particular for large particle sizes [3]. Thin films of MgH_2 have been prepared by hydrogenation of Pd capped Mg films, and by activated reactive evaporation. In the case of hydrogenation of metallic Mg with a thin palladium cap, completely transparent films with surprisingly low resistivity are obtained [4]. In-situ deposition of MgH_2 was reported using activated reactive evaporation of magnesium with an atomic hydrogen source [5]. In that case, insulating, amorphous films with a brown/transparent appearance were obtained. By modeling the optical properties using effective medium theory it was concluded that the films consisted of metallic magnesium particles in magnesium hydride. About 10 vol.% of metallic Mg could not be prevented for in-situ grown films. In this work we present initial experimental studies of in-situ deposition of metal hydride thin films using RF sputtering of magnesium in a hydrogen containing plasma. Since the aim is to investigate the possibility for using MgH_2 or other metal hydrides in photovoltaic applications, special attention is given to stability and passivation issues.

EXPERIMENTAL

Depositions are performed in a Leybold Optics A550V7 inline sputtering system using a metallic Mg target (99.95%). Both stationary and oscillating substrate carrier is used. The maximum power of the RF generator is 1000 W. Parameters such as RF power, working pressure, Ar/H_2 flow ratio and substrate temperature are varied. Films are deposited on glass substrates (microscope slides) and monocrystalline silicon wafers. Characterization includes x-ray diffraction (XRD) using a Bruker-Siemens D5000 diffractometer in Bragg-Brentano geometry, scanning electron microscopy (SEM), transmittance and reflectance measurements, resistivity using four-point-probe and thickness using an alpha-step profilometer.

For studies of silicon surface passivation, monocrystalline, double side polished silicon wafers (1-3 Ωcm, p-type cz-Si, Siltronix, 300 μm, (100) oriented) were etched in a Piranha etch for 8 minutes followed by a 2 minute dip in HF and subsequently loaded into a PECVD chamber for single side deposition of about 40 nm a-Si at 230 ˚C. After unloading, samples were dipped in HF again before loading into the sputter chamber for deposition of MgH_x on the opposite side. One sample was passivated with PECVD a-Si on both sides as a reference. The effective minority carrier lifetime was measured using a Semilab microwave photoconductance decay (μW-PCD) setup.

RESULTS AND DISCUSSION

Depositions on glass

The influence of different process parameters on the properties of MgH_x films was investigated. In the first experimental series, the power was fixed at 600 W and the working pressure at 3.8 x 10^{-3} mbar, while the flow rates of Ar and H_2 were varied according to table 1. For increasing hydrogen content in the plasma the film resistivity increases and the optical properties change from metallic to dark. This optically black state of MgH_x is well known in literature [4]. Thinner films appear brown and partly transparent while thicker films deposited under the same conditions appear black. X-ray diffractograms of films deposited with different Ar:H_2 flow are shown in figure 1. Peaks corresponding to tetragonal MgH_2 can be observed in sample B and D, together with peaks from metallic Mg. For increasing H_2/Ar flow, the intensity of the Mg peaks decrease and that of the MgH_2 peaks increase. The large background is due to the amorphous glass substrate. Thinner films with Ar:H_2 flow of 160:40 (sample C) appear amorphous in θ-2θ scans.

Table 1: Influence of varying Ar/H_2 gas flow ratio for constant power (600W) and working pressure (3.8x10^{-3} mbar).

Sample	Gas flow Ar (sccm)	Gas flow H_2 (sccm)	Thickness (nm)	Appearance	Resistivity (Ωcm)
A	200	0	210	Metallic	7.4x10^{-6}
B	180	20	285	Dark	9.5x10^{-4}
C	160	40	140	Transparent/brown	Too high
D	160	40	680	Black	Too high
E	140	60	130	Transparent/brown	Too high

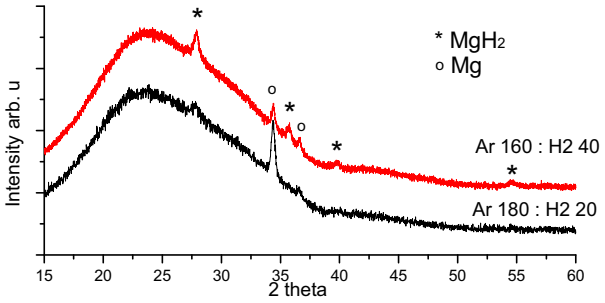

Figure 1: Sample D (red, above) and B (black, below) from table 1. Peaks related to MgH_2 and Mg are observed in both samples. The large background is due to the amorphous glass substrate.

In another experimental series, the power was varied while keeping the Ar: H_2 flow at 160 : 40 sccm and the total pressure at 3.8e-3 mbar. This gave transparent/brown films in all cases but with lower resistivity (7.0×10^{-3} Ωcm) for a 100 nm thick film deposited at low power (300 W). For higher power (600 and 900 W) and for 300 nm thick films deposited at 300 W, the resistivity was too high to be measured by our four point probe set-up. Decreased power results in decreased Mg sputtering rate and could be expected to increase the probability for formation of the insulating hydride phase. The decreased resistivity could be due to a different microstructure where metallic Mg particles are connected in a conductive network rather than isolated within the hydride [5]. The high resistivity for the thick, low power film indicates that increased deposition time and/or thickness could cause increased hydrogenation of the deposited film.

A number of depositions were performed where the pressure was increased to 10^{-2} mbar. In all these cases, the as-deposited films were in the optically black state but shifted to completely transparent after exposure to air, as discussed below.

In the last experimental series the substrate temperature was increased (200, 250 and 300 ˚C) while keeping all other process parameters constant (power 600 W, pressure 3.8e-3 mbar, Ar:H_2 flow 160:40 sccm). The intensity of the diffraction peaks increases slightly with increasing substrate temperature for films with similar thickness (660-740 nm). Peaks corresponding to both Mg and MgH_2 increase. From SEM images, the microstructure appears very similar for samples deposited at varying substrate temperature, except for a slightly larger crystal size at higher temperature. All samples in this series showed pronounced porous structure.

The trends presented briefly above results in a trade off when trying to deposit stable and dense films with high hydrogen content. To maximize formation of the hydride phase, large H/Mg ratio (low power) and high H pressure is expected to be beneficial. However, this leads to porous films that easily oxidize. Post-treatments of films in H-plasma could be a way to further hydrogenate films while avoiding the porous structure. Continued investigations of MgH_x deposition will be presented in future work.

Stability

Stability of the deposited films was investigated as a function of storage in air, annealing in air and light exposure under a solar simulator. Changes were monitored by XRD, transmittance and resistivity measurements. The change in transmittance of films annealed in air at different temperatures is shown in figure 2. The sputtering parameters in this case was Ar : H_2 flow 140 : 60 sccm, power 600 W and pressure 3.8e-3mbar. Annealing was performed in a belt furnace for 30 minutes with the hot zone set at 200, 300 or 400 ˚C. The transmittance increases slightly for annealing at 200 ˚C and significantly for 300 and 400 ˚C. For the highest temperature, the increase in transmittance of the bulk film is accompanied by formation of bubbles or holes in the film. For the film annealed at 400 ˚C, XRD θ-2θ scans show a weak and broad peak at 43º that probably corresponds to MgO. The low transmittance around 400 nm is accompanied by low reflectance, i.e. high absorption. This was also observed for films deposited by activated reactive evaporation [5] and attributed to metallic particles embedded in the MgH_2 film. Annealing under the conditions mentioned above does not remove this absorption. In the case of annealing at 400 ˚C, above the upper limit for decomposition of about 290 ˚C at 1 bar ($MgH_2 \leftrightarrow Mg + H_2$) [6], we hypothesize that MgH_2 is replaced by MgO but that metallic Mg remains.

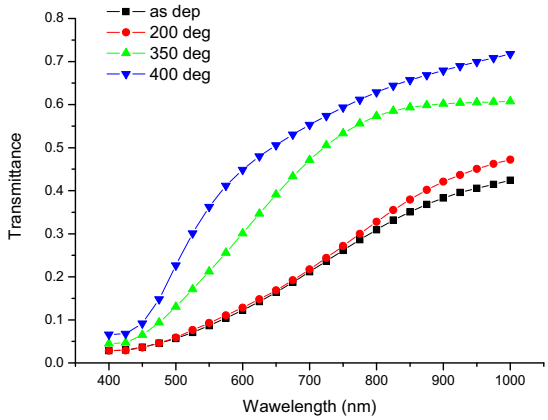

Figure 2: Transmittance of films deposited at 600W, Ar:H_2 flow 160:40 sccm and working pressure 3.8e-3 mbar as a function of annealing 30 minutes in air at different temperatures.

Some samples changed during storage in air, from partly transparent / brown to completely transparent after between one day and several months. The samples that did switch had been deposited with high hydrogen flow, high total pressure and in one case low power. XRD θ-2θ scans show low-intensity peaks at 18.5˚ and 59˚ for a sample that had switched to transparent. These peaks correspond well to $Mg(OH)_2$ [7]. The transparent films are insulating as measured by our four point probe. In some samples, the switching progressed slowly over the sample and the onset could be observed to be in the center. It was also observed that the transparent films grew in thickness with up to 50% from the as-deposited state to the transparent state. This suggests that the films may take up oxygen and hydrogen from air and water vapor.

Since photodecomposition has been reported for some hydrides [8], stability checks under light soaking were performed. Films deposited in the same run as the samples in figure 2 were exposed to a Xenon lamp calibrated to an intensity of 1000 W/m^2. No substrate cooling was available for the setup, so the samples heated up to about 40-60 ˚C during light exposure. Monitoring of transmittance as a function of light soaking time showed negligible increase in transmittance for exposures of up to one hour. However, since both MgH_2 and MgO have very large band gap, oxidation of MgH_2 would not be detected.

Silicon surface passivation

One of the objectives for investigation of metal hydrides in relation to photovoltaics is the possibility to utilize the hydride for passivation of defects in bulk silicon materials, as well as defects at the silicon wafer surface due to the high hydrogen content. In order to make an initial test of the use of MgH_2 for silicon surface passivation, five samples were prepared as shown in table 2. The average lifetime of the as-deposited reference wafer was 220 µs. For the samples with sputtered MgH_x on one side, the lifetime was around 11 µs. In the standard procedure for surface passivation using PECVD a-Si at IFE, a post deposition anneal at 450 ˚C for 1 minute is used to improve passivation properties. In order to investigate the effect of post annealing on samples with MgH_x layers, one wafer was cut into four parts and were subject to 1 minute annealing at 200 ˚C, 300˚C, 350˚C and 400 ˚C respectively. Parts from a reference wafer were annealed together with each sample. The average lifetime of the reference wafer improved to 356 µs after the 400 ˚C anneal, while that of the MgH_x samples did not change. This low lifetime is even slightly lower than for a one-side passivated wafer (sample 1, table 2). The existence of metallic Mg particles in the MgH_x films is expected to provide efficient recombination sites and contribute to the low lifetime. We conclude that sputtering of MgH_x, at least using the present conditions, does not appear to be useful for silicon surface passivation.

Table 2: Process parameters and average effective lifetime of mono-Si wafers with one-side sputtered MgH_x layers. The backside is passivated with PECVD amorphous-Si.

Sample	Ar : H2 flow (sccm)	Power (W)	Pressure (10^{-3} mbar)	Post anneal (˚C)	Average lifetime (µs)
1	No deposition	-	-	-	14.6
2	160 : 40	300	3.8	-	9.8
3	160 : 40	600	3.8	-	10.9
4	160 : 40	900	3.8	-	10.6
5	100 : 100	600	9.8	-	11.7
6	100 : 100	600	9.8	200	11.2
7	100 : 100	600	9.8	300	11.9
8	100 : 100	600	9.8	350	11.8
9	100 : 100	600	9.8	400	11.8
10	PECVD ref	-	-	-	220
14	PECVD ref	-	-	400	356

CONCLUSIONS

In-situ deposition of magnesium hydride is studied using sputtering in argon-hydrogen plasma. Increased hydrogen content in the argon-hydrogen plasma leads to increased resistivity and a shift from metallic magnesium to black MgH_x. Crystalline MgH_2 is detected by XRD, but metallic Mg could not be avoided. By increasing the hydrogen partial pressure or reducing the power, films that oxidize within days or weeks are obtained. Increased substrate temperature improves the crystallinity and stability. Sputtering of MgH_x, at least using the present conditions, does not appear to be useful for silicon surface passivation. One explanation for the large surface recombination is the existence of metallic Mg particles in the films.

ACKNOWLEDGMENTS

Funding from the Norwegian Research Council through the NANOMAT program is acknowledged as well as from the Swedish Governmental Agency for Innovation Systems through the Vinnmer program.

REFERENCES

[1] S. Karazhanov, A. Ulyashin, P. Vajeeston, et al., Phil. Mag **88**, 2461 (2008).
[2] J. Isidorsson, I. Giebels, H. Arwin, et al., Physical Review B **68**, 115112 (2003).
[3] A. Zaluska, L. Zaluski, and J. Ström-Olsen, Journal of Alloys and Compounds **288**, 217 (1999).
[4] I. Giebels, J. Isidorsson, and R. Griessen, Physical Review B **69**, 205111 (2004).
[5] R. Westerwaal, C. Broedersz, R. Gremaud, et al., Thin Solid Films **516**, 4351 (2008).
[6] K. Zeng, T. Klassen, W. Oelerich, et al., Journal of Alloys and Compounds **283**, 213 (1999).
[7] G. Isetti, Period. Mineral. **34**, 327 (1965).
[8] D. Dougherty and P. Herley, Journal of the Less-Common Metals **73**, 97 (1980).

Paper II

Deposition of magnesium hydride thin films using radio frequency reactive sputtering

Popular summary

In this paper we go into further details about the MgH_2 films that were deposited using reactive sputtering. The synthesis method of reactive sputtering had been relatively little explored before we started our experimental work. Therefore there was limited information available in earlier scientific publications on the material characteristics of this type of hydride film. We here discuss the optical properties, show how the nanostructures of the surfaces look and we assess how much of the Mg in the film that is bound in hydride form and how much is in metallic Mg form.

Context

This paper is the continuation of the work started in Paper I. Gradually we gained more experience and were able to draw more conclusions from the work and understand the results. We continued working with MgH_2 even though it seemed not to have any viable applications in solar cells, in the hope of making pure MgH_2 films without the Mg particles, but also to learn more about the synthesis of metal hydrides and extend the knowledge about metal hydride films deposited by reactive sputtering.

Paper III

Transparent yttrium hydride thin films prepared by reactive sputtering

Popular summary

Yttrium hydride films had been explored thoroughly in the years after 1996, because of the fascinating switchable optical effect of hydrogenated yttrium films. However, the synthesis method of reactive sputtering had not been demonstrated. In this paper, we show that both the opaque and the transparent form of yttrium hydride can be obtained directly using reactive sputtering. Another interesting finding is that the transparent form had a different crystal structure than what is normally found for transparent yttrium hydride. The crystal structure of the transparent and the opaque hydride was almost identical, demonstrating that it is not necessarily the crystal structure that determines the electronic properties and optical appearance of this hydride.

Context

Yttrium hydride was the second material we worked with after starting with magnesium hydride. Even though we knew that yttrium hydride had a too large band gap to be useful as a semiconductor for solar cells, we wanted to do some tests with this hydride because it is a simple and well-known compound with reasonable chemical stability.

Paper IV

A new thin film photochromic material: Oxygen-containing yttrium hydride

Popular summary

The yttrium hydride films described in Paper III concealed a secret. They were photochromic, which means that they change color when they are illuminated. There are several potential applications of photochromism, but the phenomenon has not received much attention in materials science, especially considering inorganic compounds. In a technological aspect, the finding opens up new opportunities for metal hydride films, as this was the first time ever that photochromism at normal conditions had been reported for a metal hydride. In the aspect of more fundamental science, it is of great interest to better understand the physics of the reaction.

Context

It was under the microscope, investigating some defects on the surface of transparent yttrium hydride films, I discovered the photochromic effect in yttrium hydride: The light from the microscope, when highly focused, left small dark spots on the sample corresponding to the areas that had been illuminated. The spots gradually disappeared, and appeared again when if I again put the sample under the microscope. I then took the sample to the solar simulator light source in our laboratory and observed the darkening of the entire sample. The effect was characterized in our laboratories and those of our collaborators at TU Delft.

Paper V

$Mg_yNi_{1-y}(H_x)$ thin films deposited by magnetron sputtering

Popular summary

Magnesium nickel hydride is a promising candidate for utilization as a metal-hydride-semiconductor material for solar cells, because it has a band gap within the acceptable range for PV applications. Another reason is that it is based on the cheap and abundant elements Mg, Ni and H. In this paper, we present our results on the synthesis of the material Mg-Ni-H in the form of thin films, suitable for solar cells and for studies of the optical and electric properties of the material. The method of reactive sputter deposition had not been earlier reported for Mg-Ni-H. The quality of the material was found to be quite high in the compositional range with approximately 2 Mg atoms per Ni, which is the composition for which the semiconducting Mg_2NiH_4 forms. The work therefore demonstrated that the synthesis method of reactive sputtering is promising with respect to the application of Mg_2NiH_4 in solar cells.

Context

Magnesium nickel hydride was the first material that we worked with that actually had direct relevance as a light-absorbing layer in a new hydride-based technology for solar cells. The experience that had been built on synthesis and characterization from working on MgH_2 and YH_x proved extremely useful as a background.

Paper VI

The dielectric functions and optical band gaps of thin films of amorphous and cubic crystalline $Mg_{\sim 2}NiH_{\sim 4}$

Popular summary

In the application of the magnesium nickel hydride in solar cells, it is essential to know the optical properties of the material. In this paper, we show an optical analysis using a strong optical characterization method called ellipsometry, used to obtain the dielectric functions of the materials. The dielectric functions describe the optical performance of the material, they tells us how light moves in the material and how much of it that is absorbed. In this paper we also demonstrate that films that are non-crystalline can be crystallized in a very simple heat treating process, and we compare the optical properties of the non-crystalline and the crystalline material.

Context

This work is based on the materials that were reported in Paper V. We wanted to take advantage of the advanced optical characterization techniques that were available in our laboratory and the expertise on optical characterization and modeling of my colleague J. Selj. With the article we wanted to firmly establish the optical properties of magnesium nickel hydride, and to make a comparison between the amorphous and the crystalline thin-film forms of the hydride.

Paper VII

Surface oxide on thin films of yttrium hydride studied by neutron reflectometry

Popular summary

This paper differs from the others in that it concerns mainly with a characterization method rather than the synthesis method. Neutron reflectometry is a method that is very relevant for metal hydride films, because hydrogen has a very special interaction with neutrons as compared to most other elements. That makes the method suitable for observing hydrogen and finding layers of different hydrogen and oxygen content in thin-film metal hydrides. In this paper, we demonstrate how one can use neutron reflectometry to study the surface oxide that naturally forms on yttrium hydride films that are not protected against oxidation.

Context

During the first year of my Ph.D. work, I attended the "HERCULES" course on the use of large experimental infrastructure in Grenoble and Saclay in France. During a practical demonstration of neutron reflectometry, the beamline scientist F. Cousin was so friendly to let me have some tests on one of my own yttrium hydride samples. The tests gave interesting results, so I later applied for beam time at Saclay and I travelled again, together with two of my colleagues, to do further neutron reflectometry studies on the yttrium hydride films.

Surface oxide on thin films of yttrium hydride studied by neutron reflectometry

T. Mongstad,[1,a)] C. Platzer-Björkman,[2] J. P. Mæhlen,[1] B. C. Hauback,[1] S. Zh. Karazhanov,[1] and F. Cousin[3]
[1]*Institute for Energy Technology, P.O. Box 40, 2027 Kjeller, Norway*
[2]*Uppsala University, Solid State Electronics, Box 534, SE-751 21 Uppsala, Sweden*
[3]*Laboratoire Léon Brillouin, CEA Saclay, F-91191 Gif sur Yvette, France*

(Received 26 March 2012; accepted 23 April 2012; published online 10 May 2012)

The applicability of standard methods for compositional analysis is limited for H-containing films. Neutron reflectometry is a powerful, non-destructive method that is especially suitable for these systems due to the large negative scattering length of H. In this work, we demonstrate how neutron reflectometry can be used to investigate thin films of yttrium hydride. Neutron reflectometry gives a strong contrast between the film and the surface oxide layer, enabling us to estimate the oxide thickness and oxygen penetration depths. A surface oxide layer of 5–10 nm thickness was found for unprotected yttrium hydride films. © *2012 American Institute of Physics*. [http://dx.doi.org/10.1063/1.4714517]

Characterization of the distribution and content of light elements in thin-film systems are difficult using methods based on x-rays, electrons, or ion scattering. Hydrogen, the lightest element, is often considered *invisible* due to its low scattering power and the absence of core electrons. Another issue is the high mobility of the H atoms and the reactivity of oxygen to exposed surfaces, resulting in high risks of the sample being modified during sample preparation and/or by the actual measurement. However, H can be the main constituent in solid materials, e. g. metal hydrides. H impurities and H-containing layers are also important for modulating the electrical properties of semiconductors.[1] It is, therefore, of prime interest to establish methods of investigation for H-containing thin films and their interfaces with other materials.

In this work, we show how the use of neutron reflectometry (NR) enables us to investigate the surface oxide and the O and H distribution in films of yttrium hydride. Surface layers are important for the behavior and chemical stability of thin-film metal hydrides. A Pd cap layer is often used for oxidation protection and to catalyze hydrogen uptake. For samples prepared for optical and electrical measurements, the Pd layer is, however, often so thin that the surface partly oxidizes.[2] The thickness of the oxide layer and distribution of the oxygen in the film are hard to assess using conventional methods for compositional analysis as Rutherford backscattering (RBS).

We have, in this work, investigated unprotected yttrium hydride films by NR. Yttrium hydride appears in two different crystal structures at room temperature and ambient pressure.[3] The two phases have very different electronic states; metallic as YH_2 and optically transparent, semiconducting with a band gap of 2.6 eV, when the stoichiometry approaches YH_3.[4] Yttrium hydride is highly reactive towards O, but unprotected films of YH_x have proven to be surprisingly stable against oxidation under ambient conditions.[5] The unprotected YH_x films have showed interesting effects in the crystal structure[5] and a strong and technologically relevant photochromic effect has been observed.[6]

NR is an efficient way of characterizing thin films, multilayers, and interfaces.[7] In particular, it reveals properties of layers and interfaces that are buried below several other layers. NR is a non-destructive technique where the weak sample interaction of the low energy neutrons (~a few meV) ensures that the sample is not changed by the measurement itself.

NR for characterization of hydrogen in thin films and multilayers of metal hydrides was first reported in 1993 by Mâaza *et al.*[8] Later, Munter *et al.* showed how deuterium absorption could be monitored *in-situ* during loading experiments on thin Pd films.[9,10] More recently, a series of studies has been published by Fritzche *et al.*, showing how NR can be used to investigate the thermodynamics of hydrogen uptake process in Pd-capped metal alloy films.[11–15] NR has also proved an efficient way to characterize deviations in the hydrogen stoichiometry in very thin interface layers[9,16] and can be used to determine inter-diffusion of elements at the interfaces of metal hydride films.[11,12]

NR relies on the difference in the coherent scattering length density (SLD) for neutrons between different layers in a multilayer structure. The SLD of each layer can be calculated using the formula $\rho = \sum N_i\, b_i$, summing over all present elements i, where N_i is the density in atoms/cm^3 of the element and b_i is the coherent scattering length of the element (see Table I). Owing to the negative scattering length density of H, metal hydrides show a large contrast in the SLD with respect to the substrate. O has a positive scattering length density and there is thus also a large difference in the SLD of the hydride film and the surface oxide. The large contrast and large difference in thickness of the layers make NR ideal for studying these systems. Fig. 1 demonstrates calculated ideal SLD of the materials explored here. For comparison, the calculated scattering length density for x-rays is showed in Fig. 1(b). The x-ray SLD is very similar for yttrium oxide and the yttrium hydrides, making the distinction between oxide and hydride difficult in the interpretation of x-ray reflectometry (XRR) data.

[a)]Author to whom correspondence should be addressed. Electronic mail: trygve.mongstad@ife.no.

TABLE I. Coherent scattering lengths for neutrons of the constituent elements.[a]

Element	Scattering length (fm)
H	−3.739
O	5.803
Si	4.1491
Y	7.75
Mo	6.715

[a]Ref. 22.

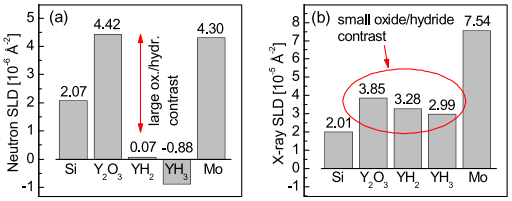

FIG. 1. Calculated neutron and x-ray (Cu Kα) SLD of the materials investigated in this work.

The NR measurements were carried out at the EROS (Ref. 17) time-of-flight reflectometer at Laboratoire Leon-Brillouin, Saclay, France. This reflectometer uses a broad wavelength neutron beam with wavelengths from 3 Å to 25 Å. The typical data collection time was 1 h per sample. The data analysis was done with the EROS reflectivity data analysis software package. The films were deposited on 50 mm Ø, 5 mm thick crystalline Si substrates, and the thickness of the investigated films was in the range of 100–150 nm. The samples were deposited by reactive sputtering (see Ref. 5), using 20% H_2 as reactive gas in the Ar plasma. Two electronic states of YH_x were obtained depending on the deposition parameters: the conductive and black state (B-YH_x) and the optically transparent semiconducting state (T-YH_x).[5] A cap layer of Mo was deposited *in-situ* on some of the samples in order to protect the samples from oxidation in air.

Fig. 2(a) shows the experimental data and the model fit to the NR spectra obtained for a sample of B-YH_x. The calculated reflectivity of a pure silicon substrate is also showed in order to illustrate how the film influences the reflectivity spectrum. The critical scattering vector Q_c is not shifted for the sample with respect to the silicon substrate. This is typically observed for a layer with lower SLD than the substrate. A layer of ∼100 nm thickness with a larger SLD than the substrate would have caused the appearance of a pseudo-plateau, i.e., a shift of the plateau of total reflection towards higher values of the scattering vector Q. The interference fringes visible in the spectrum at higher Q values are known as Kiessig fringes,[18] which constitute the basis for the fit of the SLD profile (inset in Fig. 2(a)). The bulk of the film is found to have an SLD of 1.1×10^{-6} Å^{-2}. This is higher than the expected SLD of YH_2 (see Fig. 1(a)) and can be explained by incorporation of oxygen in the structure and understoichiometry in the hydrogen content. The fit to the NR data in Fig. 2(a) gives a surface oxide and/or hydroxide layer with a thickness of 5 nm, with a maximum SLD of

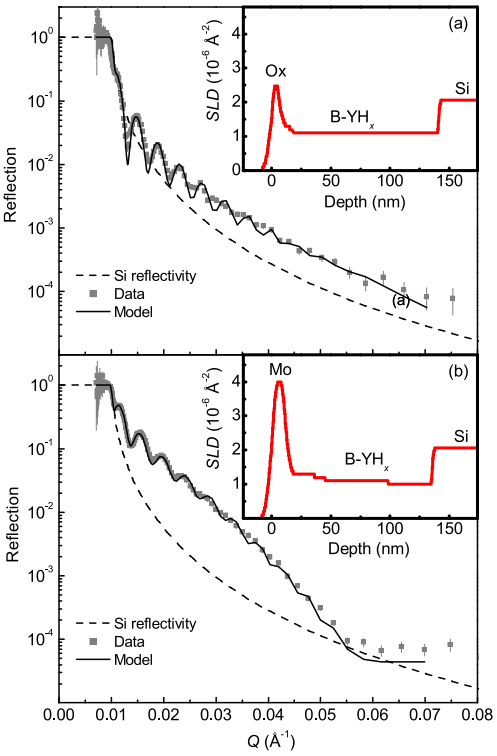

FIG. 2. NR data, model, and corresponding SLD profile (inset) for (a) an unprotected B-YH_x film and (b) a B-YH_x film covered by 10 nm Mo.

2.5×10^{-6} Å^{-2}. The maximum SLD is limited by the fact that the estimated roughness (1.5 nm on the upper surface) is similar to the thickness of the surface layer. In addition, it is probable that the surface layer contains a considerable amount of H, which will also lower the SLD.

Fig. 2(b) shows data and fit for an equivalent film as in Fig. 2(a) but covered with a 10 nm layer of Mo. The presence of the 10 nm capping layer is clearly visible in the NR data as a large Kiessig fringe superimposed on the smaller oscillations. The upper surface is also found to have a roughness of 1.5 nm, and the maximum SLD in the layer is of 4.0×10^{-6} Å^{-2}. To obtain the best fit to the data, a gradient has been incorporated in the SLD profile, going from 1.0×10^{-6} Å^{-2} at the substrate interface to 1.3×10^{-6} Å^{-2} close to the surface oxide. This variation could be a result of the deposition process or O that has penetrated through the Mo layer. It is, however, difficult to get a fully conclusive fit of NR data on such small and non-abrupt changes in the SLD profile. The possible interpretations of such a gradient might not reflect the physical state of the sample. The SLD profile of this geometry is similar to the sample with a surface oxide (Fig. 1(a)), but the NR data are substantially different. This underlines the strength of NR in differentiating between layers with small differences in thickness and SLD.

Fig. 3 displays data and fit for an unprotected film of T-YH_x. The SLD determined for the bulk of the film is

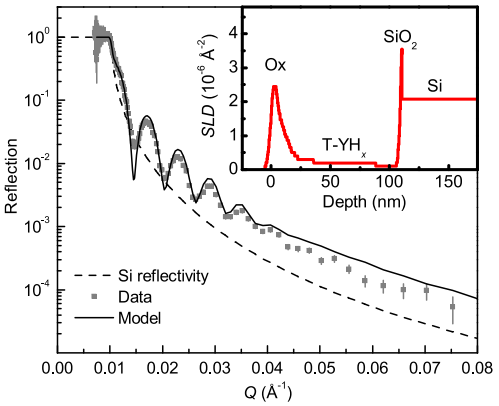

FIG. 3. NR data, model, and corresponding SLD profile (inset) for T-YH$_x$ film.

$\sim 0.2 \times 10^{-6}$ Å^{-2}, which is higher than expected for pure semiconducting YH_3 (see Fig. 1(a)). Again this is related to the O content of the film and understoichiometry in H. The surface oxide/hydroxide layer of this sample is around 10 nm, which is higher than for the conductive YH_x film shown in Fig. 2(b). The oxide also has a tail that penetrates into the bulk of the film. There could be oxide channels growing at the crystal grain borders, as earlier discussed for yttrium hydride[2] and pure yttrium[19] films. For pure yttrium films, we found a surface oxide layer of $\sim$5 nm and a similar oxygen penetration profile. In Fig. 3, there is a layer of SiO_2 with higher SLD present on the substrate interface. The substrate oxide layer is a result of the synthesis of the samples. Because of the poor adhesion of T-YH$_x$ to pure Si, the native surface oxide on the Si substrate was not removed prior to deposition.

Because of the strong sensitivity to H, NR can be used to estimate the H content in a film. The value of the SLD is significantly higher for the B-YH$_x$ (1.1×10^{-6} Å^{-2}, Fig. 2) than for the T-YH$_x$ (0.2×10^{-6} Å^{-2}, Fig. 3). As the samples are prepared in an approximately identical process and has basically the same crystal structure,[5] this provides an unambiguous proof of higher H content in the latter. In principle, the H concentration can be directly calculated from the SLD and the crystal structure. However, a true estimation of the H content requires knowledge of the impurity content, porosity and concentration of interstitials, and vacancies in the sample. For a trustworthy estimation of the H content NR therefore needs to be combined with complementary techniques as x-ray diffraction, XRR, and RBS. Alternatively, one can take advantage of the isotope contrast between hydrogen and deuterium. D has a positive coherent scattering length for neutrons and thereby contributes to an increase in the SLD as opposed to H. If two sets of samples are prepared in the same way but one with H and the other with D, the difference in SLD can give an accurate estimation of the H/D content of the sample. Similarly, NR has been used to study loading/unloading of H in metallic films, where the SLD prior to and post-loading is compared in order to estimate the H concentration.[9,11,13,15,20,21]

In conclusion, NR is highly suitable for the study of oxide layer formation on thin films of metal hydrides, because of the large contrast in SLD between oxide and hydride. NR can similarly also be used for example to investigate H accumulation at interfaces in semiconductors or to study surface oxides on non-hydride films with low SLD.

This work has been made possible through funding from the Norwegian Research Council through the NANOMAT program: Project 181884/S10. The NR measurements were supported by the European Commission under the 7th Framework Programme: Integrated Infrastructure Initiative for Neutron Scattering and Muon Spectroscopy: NMI3/FP7 – Contract No 226507.

[1]C. G. van de Walle and J. Neugebauer, Annu. Rev. Mater. Res. **36**, 179 (2006).
[2]J. N. Huiberts, J. H. Rector, R. J. Wijngaarden, S. Jetten, D. de Groot, B. Dam, N. J. Koeman, R. Griessen, S. Olafsson, and Y. S. Cho, J. Alloys Compd. **239**, 158 (1996).
[3]P. Vajda, *Handbook on the Physics and Chemistry of Rare Earths*, edited by K. A. Gschneider and L. Eyring, 20th ed. (North-Holland, 1995), p. 207.
[4]J. N. Huiberts, R. Griessen, J. H. Rector, R. J. Wijngaarden, J. P. Dekker, D. de Groot, and N. J. Koeman, Nature **380**, 231 (1996).
[5]T. Mongstad, C. Platzer-Björkman, S. Zh. Karazhanov, A. Holt, J. P. Maehlen, and B. C. Hauback, J Alloys Compd **S509**, S812 (2011).
[6]T. Mongstad, C. Platzer-Björkman, J. P. Maehlen, L. P. A. Mooij, Y. Pivak, B. Dam, E. S. Marstein, B. C. Hauback, and S Zh. Karazhanov, Sol. Energy Mater. Sol. Cells **95**, 3596 (2011).
[7]J. Penfold and R. K. Thomas, J. Phys.: Condens. Matter **2**, 1369 (1990).
[8]M. Mâaza, B. Farnoux, and F. Samuel, Phys. Lett. A **181**, 245 (1993).
[9]A. E. Munter and B. J. Heuser, Phys. Rev. B **58**, 678 (1998).
[10]A. E. Munter, B. J. Heuser, and M. W. Ruckmann, Phys. Rev. B **55**, 35 (1997).
[11]H. Fritzsche, M. Saoudi, J. Haagsma, C. Ophus, E. Luber, C. T. Harrower, and D. Mitlin, Appl. Phys. Lett. **92**, 121917 (2008).
[12]H. Fritzsche, M. Saoudi, J. Haagsma, C. Ophus, C. T. Harrower, and D. Mitlin, Nucl. Instrum. Methods Phys. Res. A **600**, 301 (2009).
[13]H. Fritzsche, C. Ophus, C. T. Harrower, E. Luber, and D. Mitlin, Appl. Phys. Lett. **94**, 241901 (2009).
[14]E. Poirier, C. T. Harrower, P. Kalisvaart, A. Bird, A. Teichert, D. Wallacher, N. Grimm, R. Steitz, D. Mitlin, and H. Fritzsche, J. Alloys Compd. **509**, 5466 (2011).
[15]P. Kalisvaart, E. Luber, H. Fritzsche, and D. Mitlin, Chem. Commun. **47**, 4294 (2011).
[16]B. Hjörvarsson, M. Vergnat, J. Birch, J.-E. Sundgren, and B. Rodmacq, Phys. Rev. B **50**, 11223 (1994).
[17]F. Cousin, F. Ott, F. Gibert, and A. Menelle, Eur. Phys. J. Plus **126**, 1 (2011).
[18]H. Kiessig, Ann. Phys. **402**, 769 (1931).
[19]M. Ay, O. Hellwig, H. Becker, B. Hjörvarsson, and H. Zabel, Appl. Surf. Sci. **254**, 3184 (2008).
[20]H. Fritzsche, E. Poirier, J. Haagsma, C. Ophus, E. Luber, C. T. Harrower, and D. Mitlin, Can. J. Phys. **88**, 723 (2010).
[21]C. Harrower, E. Poirier, H. Fritzsche, P. Kalisvaart, S. Satija, B. Akgun, and D. Mitlin, Int. J. Hydrogen Energy **35**, 10343 (2010).
[22]V. F. Sears, Neutron News **3**, 26 (1992).